ON MIXED FINITE ELEMENT FORMULATIONS FOR FLUID-STRUCTURE INTERACTIONS

by

Xiaodong Wang

Bachelor of Science, Shanghai Jiao Tong University, China (1988)
Master of Science, Massachusetts Institute of Technology, U.S.A. (1993)

Submitted to the Department of Ocean Engineering
in partial fulfillment of the requirements
for the degree of

Doctor of Philosophy in Applied Mechanics

at the

MASSACHUSETTS INSTITUTE OF TECHNOLOGY

June 1995

Signature of Author .....
Department of Ocean Engineering
June, 1995

Certified by .....
Klaus-Jürgen Bathe
Professor of Mechanical Engineering
Thesis Supervisor

Accepted by .....
A. Douglas Carmichael
Chairman, Departmental Committee on Graduate Students

ON MIXED FINITE ELEMENT FORMULATIONS
FOR FLUID-STRUCTURE INTERACTIONS

by

Xiaodong Wang

Submitted to the Department of Ocean Engineering
on June, 1995, in partial fulfillment of the
requirements for the degree of
Doctor of Philosophy in Applied Mechanics

Abstract

In this thesis, mixed primitive variable based finite element formulations are developed to solve linear and nonlinear fluid-structure interaction problems involving incompressible (or almost incompressible) fluid models. The mixed elements are used according to the inf-sup condition.

It is pointed out that along the fluid-structure interfaces, different coupling conditions can be used according to different mathematical models or meshing conditions, but the requirements of both mass and momentum conservation must be satisfied on the discretized configuration. In this work, we correct one historical misunderstanding about the causes of the so-called spurious non-zero frequency rotational modes widely reported in the frequency analysis of acoustoelastic/slosh fluid-structure interaction problems. We also discuss mode superposition methods in both primitive variable and potential-based formulations.

In nonlinear fluid-structure interaction analyses involving convection dominated flows, large free surface waves, material nonlinearities, large structural deformations and large fluid-structure interface motions, we apply arbitrary Lagrangian-Eulerian (ALE) descriptions to maintain mesh regularity within the analysis domain. In order to eliminate the spatial oscillations in flow regions with high Reynolds number (or Peclet number), as well as to use high order mixed elements satisfying the inf-sup condition in low Reynolds number (or Peclet number) flow regions, we propose a new upwinding scheme and develop a mixed treatment, i.e. the use of a control volume finite element upwinding formulation for the convective terms and the standard Galerkin formulation for the other terms.

The proposed formulations are implemented experimentally, and various numerical examples are given to demonstrate and confirm the ideas in this thesis.

Thesis Supervisor: Klaus-Jürgen Bathe
Title: Professor of Mechanical Engineering

To my father

Acknowledgments

First, I would like to thank my wife, Jinghua Qian, for her constant encouragement and support. Second, I would like to express my deepest gratitude to my advisor, Professor Klaus-Jürgen Bathe, for his invaluable guidance throughout my Ph.D program at M.I.T.

I am also grateful to other members of my thesis committee, Professor Henrik Schmidt and Professor Eduardo Kausel, for their helpful advice. My appreciation also goes to Professor Koichi Masubuchi, Professor Frank A. McClintock and Professor Tomasz Wierzbicki for helping me at the beginning of my graduate studies at M.I.T.

It is my pleasure to thank the Department of Ocean Engineering and Department of Mechanical Engineering for their hospitality. In particular, I would like to thank my colleagues in the Finite Element Research Group at M.I.T, Chanwut Nitikitpaiboon, Namsua Lee, Dena Hendriana, Daniel Pantuso, Pal-gap Lee, Gunter Gabriel, Himawan Supangkat, Sigit Santosa and Alexander Iosilevich; and the researchers at ADINA, R&D in Watertown, MA, for their help, encouragement and friendship.

My utmost gratitude is due to my mother, whom I have not been able to be with for the past many years, whose love and support during these long years of studying mean the most to me.

Contents

List of Figures

List of Tables

Chapter 1

Introduction

1.1 Overview

Many interaction problems involving different continuous media exist in practical engineering fields. One of them is the so-called fluid-structure interaction problem, where the interaction between fluids and structures can significantly affect the response of the structures and needs to be taken into account properly. Common fluid-structure interaction problems include the analysis of offshore structures, acoustical media, liquid or gas storage tanks, pipeline systems, nuclear reactors and biomechanical systems [1] [2] [3] [4] [5] [6].

For the past two decades, much effort has gone into the application of the existing finite element procedures to areas involving fluid flows and fluid-structure interactions. In addition to the standard Galerkin formulation commonly used in solid mechanics and structural analyses, the streamline upwinding/Petrov-Galerkin (SUPG) formulation, the Galerkin least squares method, the Galerkin method using artificial viscosities, and the skew positive influence coefficient upwinding control volume finite element method (CVFEM) are all currently available, though none is completely satisfactory, in dealing with the convection dominated problems.

A number of finite element formulations have been proposed to model the fluid

for the analysis of fluid-structure interaction problems; namely, the displacement formulation (see Bathe and Hahn [7], Akkas et al [8], Hamdi et al [9], Belytschko and Kennedy [10], Belytschko [3], Olson and Bathe [11]), the displacement potential and pressure formulation (Morand and Ohayon [12]), and the velocity potential formulation (Everstine [13], Olson and Bathe [14], Felippa and Ohayon [6]). For the inviscid and irrotational fluids, the displacement (or the velocity) potential and pressure are often used instead of the displacement or velocity unknowns.

However, the primitive variable formulations have always received considerable attention because they do not require any special interface conditions or new solution strategies (for example, in frequency calculations and response spectrum analysis). Moreover, the true mass and stiffness matrices generated from these formulations provide convenience in solving general coupled problems. With the ever-increasing availability of high speed and large capacity computers, this approach shows great promise in general applications to the solution of a broad range of problems (specifically nonlinear problems). Unfortunately, many difficulties remain unsolved for using primitive variable finite element formulations in analyses involving fluid flows and fluid-structure interactions.

In linear analyses, it has been widely reported that the displacement-based fluid elements employed in frequency or dynamic analyses exhibit spurious *non-zero* frequency circulation modes [15] [9] [11]. Various approaches have been introduced to obtain improved formulations. The penalty method has been applied by Hamdi et al. [9] and has been shown to give good solutions for the cases considered in that reference. Subsequently, Olson and Bathe [11] demonstrated that the method "locks up" in the frequency analysis of a solid vibrating in a fluid cavity and also showed that the reduced integration performed on the penalty formulation yields some improvement in results but does not assure solution convergence in a general case. More recently, Chen and Taylor proposed a 4-node element based on a reduced integration technique together with an element mass matrix projection [16]. The element is used

to solve some example problems, but an analysis or numerical results on whether the element formulation is stable and reliable are not presented. We believe that the currently available displacement-based formulations of fluids and fluid-structure interactions are not yet satisfactory and some misunderstandings about the nature of spurious non-zero frequency rotational modes must still be clarified.

In nonlinear analyses, three issues have to be considered:

- In problems involving large free surface and large fluid-structure interfacial motions, automatic adaptive procedures are necessary [17] [18].
- In convection dominated conditions, the Galerkin method no longer provides the best approximation for discretized spaces [19] [20].
- There are only a handful of elements (such as the 9/3 and $9/4-c$ elements) satisfying the inf-sup condition (or Babuška-Brezzi condition), which is a requirement for a reliable finite element procedure in the analysis of incompressible (or almost incompressible) materials (including fluids) [21] [22] [23] [24] [25].

It has been found that the available upwinding schemes work well for lower order elements [26] [27]. In fact, the SUPG method was initially proposed for 4-node isoparametric elements [28]. Much research has been performed to find a suitable upwinding technique for higher order elements; however, the outcome has not been satisfying [29]. Some researchers believe that the use of a suitable Petrov-Galerkin formulation can *circumvent* the inf-sup condition [20] [19]. In practical problems involving fluid flows and fluid-structure interactions, there will be certain convection dominated regions mixing with the low Reynolds number or Peclet number flow regions. Therefore, it is highly desirable to have a procedure for incorporating upwinding schemes into the elements that satisfy the inf-sup condition. We believe that there is much research to be done to find a way to accommodate the requirements of both the upwinding schemes and the inf-sup condition.

1.2 Thesis Objective

More than two decades ago, the displacement-based formulation for fluids drew many researchers' attention simply because, at the time, the displacement-based finite element codes for structures were fully developed and people thought that they could extend the applications of these codes to the problems involving fluid flows and fluid-structure interactions with little effort [1]. Unfortunately, the effort did not turn out successful, even for the linear problems, due to the reported existence of non-zero frequency spurious modes and to the difficulties in handling the large motions of fluids. It has long been believed that spurious non-zero frequency rotational modes are caused by the irrotationality constraint [9] [30] [16], and many methods have been proposed to eliminate these modes. In this thesis, we will correct this misunderstanding by showing that the true origins of the spurious non-zero frequencies are in the use of the pure displacement-based formulation (including the penalty formulations) and in the mishandling of the fluid-structure interfacial conditions. We will propose $\mathbf{u}/p$ based formulations with proper elements (i.e. mixed elements that satisfy the inf-sup condition). In addition, we address some subtle points on the boundary conditions around fluid-structure interfaces and free surfaces. The solutions of some selected generic test problems demonstrate that if $\mathbf{u}/p$ based formulations are used with proper elements and boundary conditions, we will no longer encounter the spurious non-zero frequency pressure modes and rotational modes. Indeed, we show mathematically that rotational modes will have zero frequency if we use common inviscid acoustic fluid models.

To extend the primitive variable formulations to nonlinear analyses, we reach a conclusion that a $\mathbf{v}/p$ formulation is a proper approach. For the convection dominated problems, we develop a mixed upwinding formulation by adopting a CVFEM upwinding scheme [31] into 9-node elements which satisfy the inf-sup condition. We also compare the SUPG formulation for 4-node elements with the proposed upwinding formulation for 9-node elements; and point out the advantages and disadvantages

of both upwinding approaches. To avoid excessive mesh distortions, the ALE formulation is incorporated into the proposed upwinding scheme.

In summary, we will develop a unified finite element procedure for linear and nonlinear analyses of incompressible (or almost incompressible) fluids and fluid-structure interaction problems.

1.3 Thesis Outline

In Chapter 2, we start from fundamental momentum, mass and energy conservation equations and discuss commonly used mathematical models for fluids. The difficulties and confusion about the pure displacement formulation will be discussed in Chapter 3. Also in Chapter 3, we propose $\mathbf{u}$/p and $\mathbf{v}$/p formulations for both linear and nonlinear analyses. In Chapter 4, based on the mathematical model of the isentropic, irrotational and inviscid fluid model, we present a $\mathbf{u}$-p-$\mathbf{\Lambda}$ formulation, i.e., a mathematically more comprehensive form of the often used penalty formulation, and a $\mathbf{v}$-p-$\mathbf{\Lambda}$ formulation as the extension to nonlinear problems. We also compare the $\mathbf{u}$/p and $\mathbf{u}$-p-$\mathbf{\Lambda}$ formulations at the end of Chapter 4 and point out the inner relationship between different formulations and mathematical models. Some important issues of the fluid-structure interaction problems are discussed in Chapter 5. In Chapter 6, selected test examples are analyzed to confirm the ideas in this thesis and demonstrate the capabilities of the proposed formulations. In Chapter 7, mode superposition methods in primitive variable and potential-based formulations are discussed. Recommended future research on the subject of this thesis will be addressed in the concluding chapter.

Chapter 2

Mathematical Models

2.1 Governing Equations

In continuous media, including fluids and solids, the governing equations for the mechanical behaviors can be derived from the mass, momentum and energy conservation laws [32]. To express these conservation laws mathematically, we have to use certain kinematical descriptions of the physical quantities we are interested in. In the finite element analysis, we always attach the unknowns to mesh points and the time rate of change of any quantity a (or the mesh referential derivative with respect to time) can be expressed as,

$$a^* = \frac{\partial a}{\partial t} + \mathbf{v}^m \cdot \nabla a \tag{2.1}$$

where $\mathbf{v}^m$ is the mesh velocity which could be linked to the material velocity or assigned arbitrarily, provided that the boundary of meshes moves with the material boundary and the elements keep regular shapes. If the mesh velocity $\mathbf{v}^m$ is the same as the material velocity $\mathbf{v}$, we have the pure Lagrangian formulation and $a^* = \dot{a} = \frac{da}{dt}$; while $\mathbf{v}^m = \mathbf{0}$ gives the pure Eulerian formulation and $a^* = \frac{\partial a}{\partial t}$. From Eq. (2.1), it is obvious that in nonlinear analysis with arbitrary Lagrangian-Eulerian (ALE) descrip-

tions, it is more convenient to use the velocities as the primitive variables than the displacements in describing the fluid motion. In solid mechanics, Lagrangian formulations (total Lagrangian formulation and updated Lagrangian formulation [33]) are commonly used for both linear and nonlinear analysis. In fluid mechanics, if the control domain is fixed, the Eulerian formulation can be naturally adopted; however ALE formulations show the capability and potential for analysis involving large boundary motions such as free surfaces and fluid-structure interfaces.

We write the mass conservation equation as,

$$\rho \nabla \cdot \mathbf{v} + \dot{\rho} = 0 \tag{2.2}$$

where ρ is the mass density.

For the linear problems of solid mechanics, from Eq. (2.2), we can derive

$$p = -\kappa u_{i,i} \tag{2.3}$$

where p is the pressure (actually the pressure due to the volumetric strain), κ is the bulk modulus and $\mathbf{u}$ is the displacement vector. However, if we use the general ALE description within which $\mathbf{v}^m$ is neither $\mathbf{v}$ nor $\mathbf{0}$, the mass conservation equation can be rewritten as,

$$\rho \nabla \cdot \mathbf{v} + \rho^* + (\mathbf{v} - \mathbf{v}^m) \cdot \nabla \rho = 0 \tag{2.4}$$

The energy conservation equation (the so-called first law of thermodynamics) is generally expressed as,

$$dQ + dW = dE + dT \tag{2.5}$$

where dQ, dW, dE and dT are the heat added to the system, work done by the surroundings to the system, internal energy increase of the system and the kinetic

energy increase of the system respectively.

The momentum conservation equation is commonly written as,

$$\rho \dot{v}_i = \tau_{ij,j} + f_i^B \tag{2.6}$$

where $\boldsymbol{\tau}$ and $\boldsymbol{f}^B$ are the stress tensor and body force vector.

For linear elastic solids, the strain $\boldsymbol{\epsilon}$ and the deviatoric strain $\boldsymbol{\epsilon}'$ are defined as,

$$\epsilon_{ij} = \frac{1}{2}(u_{i,j} + u_{j,i}) \tag{2.7}$$

$$\epsilon'_{ij} = \epsilon_{ij} - \frac{1}{3}\epsilon_{kk}\delta_{ij} \tag{2.8}$$

and the constitutive relations can be written as,

$$\tau_{ij} = \kappa \epsilon_{kk}\delta_{ij} + 2G\epsilon'_{ij} \tag{2.9}$$

where G is the shear modulus.

For fluids, we commonly use,

$$\tau_{ij} = (-p + \lambda e_{kk})\delta_{ij} + \mu(v_{i,j} + v_{j,i}) \tag{2.10}$$

the so-called Newtonian fluid model, where μ stands for the viscous shear coefficient or dynamic viscosity. From Stokes hypothesis ($\lambda = -\frac{2}{3}\mu$), Eq. (2.10) has the same form as Eq. (2.9), but velocity strains are used instead of the strains due to displacements. Note here p is mainly the dynamic pressure, which is different from the pressure $p = -\kappa\epsilon_{kk}$ for solids.

In this thesis, we use the elastic material models for solids, including the hyperelastic material model [34]. As for the nonlinear analysis of fluids, we use the Newtonian fluid model; for acoustic fluids, we have two approaches; one is to introduce an artificial shear modulus G (zero or $O(\frac{1}{\beta})$) and the other is to assume the inviscid fluid

model (indeed, *inviscid* might not be a proper term for acoustic fluids undergoing small displacements and the physical meaning of this model is actually zero shear modulus).

All three conservation equations shall hold on any point within the domain of the continuous media we are interested in.

Much research has been done in the area of solid mechanics [35], in fact, the finite element method was first introduced in the context of structural and solid mechanics. In this thesis, we focus our attention on fluid models, fluid-structure interfaces and free surfaces.

There are two major fluid mechanics categories; one deals with compressible fluids, such as aerodynamics, the other deals with incompressible fluids, such as hydrodynamics. For the physical problems, where the changes of density ρ, temperature θ, pressure p and velocity vector $\mathbf{v}$ are equally significant, compressible fluid models are applied and all the three conservation equations and one state equation relating ρ, p and θ are used. In this thesis, we consider only the fluid models which are incompressible (or almost incompressible) such as the models used in the analysis of acoustoelastic/slosh problems and interaction problems involving the Navier-Stokes flows; the interaction between the mechanical and thermal processes is neglected, i.e., only the mechanical equations are needed to describe the fluid and solid response. Of course, in nature, a different practical engineering focus may lead us to a different mathematical model which simplifies the physical problems.

From the momentum equation, ignoring the inertia force, we can easily get the control equations for hydrostatic problems,

$$\nabla(p + \rho g x_2) = \mathbf{0} \tag{2.11}$$

where we can see that the pressure p is solely related with the boundary condition, the position $\mathbf{x}$, the mass density ρ and the gravity g. For linear problems, the solution of Eq. (2.11) can be added to the dynamic solutions excluding the hydrostatic pressure.

2.2 Acoustic Fluid Models

For isentropic acoustic fluids, we have,

$$\frac{dp}{d\rho} = c^2. \tag{2.12}$$

where c is the compressible wave velocity (or sound speed).

Substituting Eq. (2.12) into Eq. (2.2), we get

$$\nabla \cdot \mathbf{v} + \frac{\dot{p}}{\beta} = 0 \tag{2.13}$$

where the bulk modulus $\beta = \rho c^2$.

In linear analyses, for any quantity a, the material time derivative $\frac{da}{dt}$ (or $\frac{Da}{Dt}$) and the mesh referential derivative a^* are the same as the spatial time derivative $\frac{\partial}{\partial t}$ and the equilibrium position stays the same as the original configuration. Therefore, we can use displacements instead of velocities as primitive variables in the momentum and continuity equations. If we assume zero shear modulus for acoustic fluids, we have,

$$\rho\ddot{\mathbf{u}} + \nabla p - \boldsymbol{f}^B = \mathbf{0} \tag{2.14}$$

$$\nabla \cdot \mathbf{u} + \frac{p}{\beta} = 0 \tag{2.15}$$

Comparing Eq. (2.15) with Eq. (2.3), we find that $\kappa = \beta$ and the fluid pressure definition is exactly the same as for solids.

Since $\nabla \times \nabla\phi = \mathbf{0}$ for any smooth scalar valued function ϕ, if the non-conservative forces are ignored, Eq. (2.14) implies

$$\frac{\partial}{\partial t}(\nabla \times \mathbf{v}) = \mathbf{0} \tag{2.16}$$

and hence the motion is always circulation preserving, i.e. it is a motion in which the vorticity does not change with time.

If the fluid starts from rest, we have the irrotationality constraint,

$$\nabla \times \mathbf{u} = \mathbf{0} \tag{2.17}$$

In actuality, if we define a displacement potential ϕ, with $\mathbf{u} = \nabla\phi$ [12], or a velocity potential ϕ, with $\mathbf{v} = \nabla\phi$ [14], Eq. (2.17) and Eq. (2.16) are automatically satisfied. Unfortunately, there are a few disadvantages of the potential formulations:
1) Non-symmetric matrices are obtained [36]. The procedure to make the matrices symmetric enlarges the bandwidth of the matrices and involve more computation effort [37] [13].
2) Special elements are needed along the fluid-structure interfaces.
3) The stiffness and mass matrices for fluids are not the physical ones as for structures, therefore, it is difficult to apply dynamic loading and use the standard spectrum method (refer to Chapter 7).

Another mathematical model for acoustic fluids is to introduce a shear modulus G (zero or $O(\frac{1}{\beta})$), and the momentum equation (2.6) can be rewritten as,

$$\rho\ddot{u}_i + p_{,i} = G(u_{i,jj} + \frac{1}{3}u_{j,ji}) + f_i^B \tag{2.18}$$

Substituting Eq. (2.15) into the above equation, we have,

$$\rho\ddot{u}_i + (1 + \frac{G}{3\beta})p_{,i} = Gu_{i,jj} + f_i^B \tag{2.19}$$

In fact, the time scale corresponding to shearing is much larger than that of the compressible wave, and we can expect that the rotational modes have the minimum amount of energy and shear waves can be negligible compared with compressible waves. This implies that, in the transient analysis, the so-called rotational modes do not distract the major interest. In the frequency analysis, we show that if we use

u/p formulations with elements which satisfy the inf-sup condition and impose the boundary conditions (especially the fluid-structure interfacial conditions) properly, there exist no non-zero frequency spurious modes.

2.3 Incompressible Fluid Models

For the fluid models used in this thesis, the bulk modulus β is the material property which is assumed to be constant. If we are interested in compressible waves interacting with structures, the mathematical model for the fluid (or air) is called acoustic model as discussed in the last section. However, for the problems within which the fluid compressibility is not of the prime interest, we can actually use the incompressible fluid models. The parameter to characterize these two types of interests is $K = \frac{L\omega}{c}$, where L and ω are the characteristic length and frequency of our mathematical model. If $K \ll 1$, we can use the incompressible fluid model.

The continuity equation for the incompressible fluids is

$$\nabla \cdot \mathbf{v} = 0 \tag{2.20}$$

One mathematical model for incompressible fluids is the inviscid model, which gives the extra constraint

$$\nabla \times \mathbf{v} = \mathbf{0} \tag{2.21}$$

if the fluid starts from rest.

As for the inviscid fluid models, there are two finite element procedures, one is called the primitive variable formulation and the other is called the potential formulation which uses the velocity potential ϕ, where $\mathbf{v} = \nabla\phi$, or the displacement potential ϕ, where $\mathbf{u} = \nabla\phi$. It is important to keep in mind that both approaches solve the Laplacian equation,

$$\nabla^2\phi = 0 \tag{2.22}$$

As we know, for ocean and aeronautical engineering, to calculate the lifting forces on the structures interacting with the fluid (or air), some vorticities have to be added to represent the effects of viscosity. The area of such approaches is not within the scope of this thesis.

Another mathematical model is more general. Rather than assuming the inviscid model and imposing the irrotationality constraint (2.21), we use the Navier-Stokes equations

$$\rho\dot{v}_i = -p_{,i} + \mu v_{i,jj} + f_i^B \tag{2.23}$$

with the constraint of Eq. (2.20).

We know immediately that to derive Eq. (2.23) we use Eq. (2.20) once to simplify the viscous shear force terms. The bridge between the incompressible and acoustic fluid models is the so-called artificial compressibility β for the hydrodynamists who use Eq. (2.13) instead of Eq. (2.20) [36] [38]. In fact, here β is not artificial at all; β is the physical bulk modulus of fluids.

Chapter 3

u/p and v/p Formulations

Historically, two interrelated constraints, i.e., the incompressibility and irrotationality constraints created some confusion for acoustic fluid models and formulations. In this chapter, we start from the basic pure displacement-based formulation and address the often encountered difficulties. As a proper approach, **u**/p and **v**/p formulations are proposed for linear and nonlinear problems.

3.1 Understanding of Irrotationality

For the isentropic and inviscid fluid models, in terms of the displacements only, we have by substituting Eq. (2.15) into Eq. (2.14),

$$\beta \nabla(\nabla \cdot \mathbf{u}) + \boldsymbol{f}^B = \mathbf{0} \tag{3.1}$$

where $\boldsymbol{f}^B = -\rho \ddot{\mathbf{u}}$, if the other body forces are ignored.

The variational form of Eq. (3.1) can be written as,

$$\int_{V_f} \{\beta(\nabla \cdot \mathbf{u})(\nabla \cdot \delta\mathbf{u}) - \boldsymbol{f}^B \cdot \delta\mathbf{u}\} dV + \int_{S_f} \bar{p}\, \delta u_n^S \, dS = 0 \tag{3.2}$$

where u_n^S is the displacement normal to S_f.

This is the often used pure displacement-based formulation. It was widely reported that this formulation produces spurious non-zero frequency modes [15] [9] [11] [39]. From the rigid cavity test problem in [9], Hamdi, et al concluded that the observed spurious non-zero frequency modes are the rotational modes. Historically, many researchers also believed that the non-zero frequency rotational modes were due to the constraint of Eq. (2.17). As pointed out in [2] [9], the irrotationality constraint is "lost" in the finite element formulation; therefore, the following penalty formulation was proposed [9],

$$\int_{V_f} \{\beta(\nabla \cdot \mathbf{u})(\nabla \cdot \delta\mathbf{u}) + \alpha(\nabla \times \mathbf{u})(\nabla \times \delta\mathbf{u}) - \boldsymbol{f}^B \cdot \delta\mathbf{u}\} dV + \int_{S_f} \bar{p}\, \delta u_n^S \, dS = 0 \quad (3.3)$$

where α is the large penalty parameter.

Interestingly, for some problems, the so-called spurious non-zero frequency rotational modes disappeared with the above formulation. Considering the fact that penalty formulations are too "stiff", researchers often use reduced integration methods for the terms,

$$\int_{V_f} \{\beta(\nabla \cdot \mathbf{u})(\nabla \cdot \delta\mathbf{u}) + \alpha(\nabla \times \mathbf{u})(\nabla \times \delta\mathbf{u})\} dV \quad (3.4)$$

It is well known now that this penalty formulation with the reduced integration technique does not have a sound mathematical background and is often found unreliable.

By introducing a penalty term on the irrotationality constraint and applying the reduced integration method to the pure displacement-based formulation, the spurious non-zero frequency modes can be eliminated in some cases; however, while this actually somehow "confirmed" many researchers' misunderstanding about the causes of the reported spurious modes, we believe that it was coincidental. Since acoustic media

are nearly incompressible with a high bulk modulus, it should be obvious that the pure displacement-based formulation and its penalty formulation introduce non-zero frequency spurious modes (such as the familiar checkerboard pressure mode). A proper procedure is to replace the pure displacement-based formulation by u/p formulations and apply mixed elements that satisfy the inf-sup condition. In actuality, if the acoustic fluid models allow the existence of a small amount of shear modulus, we will no longer have the constraint of Eq. (2.17) and shall also expect the rotational modes to be in the lowest end of the frequency spectrum. For acoustic fluid models with no shear modulus (or inviscid acoustic fluid models), the rotational modes will have zero frequency. In conclusion, irrotationality constraint and incompressibility constraint have different physical significance.

In the frequency analysis without the effects of gravitational forces and other body forces, Eq. (3.1) can be written as,

$$\beta\nabla(\nabla\cdot\widetilde{\mathbf{U}})+\rho\omega^2\widetilde{\mathbf{U}}=\mathbf{0} \tag{3.5}$$

where $\widetilde{\mathbf{U}}$ represents the eigenfunction. It then follows that

$$\omega^2(\nabla\times\widetilde{\mathbf{U}})=\mathbf{0} \tag{3.6}$$

since $\beta\nabla\times(\nabla(\nabla\cdot\widetilde{\mathbf{U}}))=\mathbf{0}$.

It is apparent that in a frequency analysis, for the solutions corresponding to the rotational motions ($\nabla\times\widetilde{\mathbf{U}}\neq\mathbf{0}$), the frequencies are zero; while for the solutions corresponding to the irrotational motions ($\nabla\times\widetilde{\mathbf{U}}=\mathbf{0}$), the frequencies can be non-zero. One may view the first type of solutions as the way the system responds to the rotational initial conditions.

3.2 u/p Formulation

3.2.1 Control Equations

The variational approaches for potential-based formulations are discussed in [40], here for our displacement-based mixed formulation, we define a variational indicator,

$$\begin{aligned}\Pi &= \int_{V_f} \{\frac{p^2}{2\beta} - \mathbf{u}\cdot\boldsymbol{f}^B - \lambda_p(\frac{p}{\beta} + \nabla\cdot\mathbf{u})\}dV \\ &\quad + \int_{V_f} \frac{G}{2}(\nabla\cdot\mathbf{u})^2 dV + \int_{S_f} \bar{p}\, u_n^s\, dS\end{aligned}$$

where the variables are p, $\mathbf{u}$, and the Lagrange multiplier λ_p. We note that the first two terms correspond to the usual strain energy (given in terms of the pressure) and the potential of the externally applied body forces. The third term implies the mass conservation equation. The fourth term is the potential corresponding to the artificial shear modulus G, which we assign a constant of the order $\frac{1}{\beta}$ for the fluids we are interested in. The last term is the potential due to any applied boundary pressure on the surface S_f. To include the surface gravity waves, we simply add a surface gravitational potential term $\int_{S_f} \frac{1}{2}\rho g u_s^2 dS$.

Invoking the stationarity of Π, we identify the Lagrange multiplier λ_p to be the pressure p and obtain the governing equations,

$$\nabla p - \boldsymbol{f}^B - G\nabla^2\mathbf{u} = \mathbf{0} \tag{3.7}$$

$$\nabla\cdot\mathbf{u} + \frac{p}{\beta} = 0 \tag{3.8}$$

and the boundary conditions

$$\begin{aligned} \mathbf{u}\cdot\mathbf{n} &= \bar{u}_n \quad \text{on } S_u \\ p &= \bar{p} \quad \text{on } S_f \end{aligned} \tag{3.9}$$

The pressure $\bar{p}$ is commonly assigned to be zero on the free surface, provided the surface gravity waves are ignored.

3.2.2 Finite Element Discretizations

Applying the standard Galerkin discretization procedure, and hence for a typical finite element, we have

$$\begin{aligned} \mathbf{u} &= \mathbf{H}\widehat{\mathbf{U}} \\ p &= \mathbf{H}_p\hat{\mathbf{P}} \\ \nabla\cdot\mathbf{u} &= (\nabla\cdot\mathbf{H})\widehat{\mathbf{U}} &&= \mathbf{B}\widehat{\mathbf{U}} \\ \nabla\times\mathbf{u} &= (\nabla\times\mathbf{H})\widehat{\mathbf{U}} &&= \mathbf{D}\widehat{\mathbf{U}} \end{aligned}$$

where $\mathbf{H}$ and $\mathbf{H}_p$ are the interpolation matrices, and $\widehat{\mathbf{U}}$ and $\hat{\mathbf{P}}$ are the vectors of solution variables.

The matrix equations of the u/p formulation are

$$\begin{bmatrix} \mathbf{M} & \mathbf{0} \\ \mathbf{0} & \mathbf{0} \end{bmatrix} \begin{Bmatrix} \ddot{\widehat{\mathbf{U}}} \\ \ddot{\hat{\mathbf{P}}} \end{Bmatrix} + \begin{bmatrix} \mathbf{K} & \mathbf{L} \\ \mathbf{L}^T & \mathbf{A} \end{bmatrix} \begin{Bmatrix} \widehat{\mathbf{U}} \\ \hat{\mathbf{P}} \end{Bmatrix} = \begin{Bmatrix} \mathbf{R} \\ \mathbf{0} \end{Bmatrix} \tag{3.10}$$

where

$$\begin{aligned} \mathbf{M} &= \int_{V_f} \rho\mathbf{H}^T\mathbf{H}dV \qquad & \mathbf{L} &= -\int_{V_f} \mathbf{B}^T\mathbf{H}_p dV \\ \mathbf{K} &= \int_{V_f} G\mathbf{B}^T\mathbf{B}dV \qquad & \mathbf{A} &= -\int_{V_f} \frac{1}{\beta}\mathbf{H}_p^T\mathbf{H}_p dV \\ \mathbf{R} &= -\int_{S_f} \mathbf{H}_n^{ST}\bar{p}\, dS \end{aligned}$$

Define the following finite element spaces [35] [41],

$$\begin{aligned} V_h &= \{\mathbf{v}_h \mid \frac{\partial(v_h)i}{\partial x_j} \in L^2(Vol), \quad \mathbf{v}_h = \mathbf{0} \quad on \quad S_u\} \\ D_h &= \{q_h \mid q_h = \nabla \cdot \mathbf{v}_h \quad \text{for some} \quad \mathbf{v}_h \in V_h\} \\ K_h(q_h) &= \{\mathbf{v}_h \mid \mathbf{v}_h \in V_h, \quad \nabla \cdot \mathbf{v}_h = q_h\} \end{aligned} \tag{3.11}$$

with the subscript h denoting the element "size" of the mesh considered.

Since β is large and the pressure is the finite value confined by the boundary force conditions, the quantity $\|\nabla \cdot \mathbf{u}_h\|$ will be small, indeed, the larger β, the smaller is $\|\nabla \cdot \mathbf{u}_h\|$. It is then difficult to obtain an accurate pressure prediction $p_h = -\beta \nabla \cdot \mathbf{u}_h$. In the 1970's, some mathematicians [21] [22] discovered that if a sequence of finite element spaces with mixed elements satisfy the inf-sup condition,

$$\inf_{q_h \in D_h} \sup_{\mathbf{v}_h \in V_h} \frac{\int_\Omega q_h \; div(\mathbf{v}_h) \; d\Omega}{\|q_h\| \; \|\mathbf{v}_h\|} \geq \beta_h > \beta_o > 0 \tag{3.12}$$

we can have the following convergence requirement,

$$\|\mathbf{u} - \mathbf{u}_h\| \leq C d(\mathbf{u}, V_h) \tag{3.13}$$

where C is the constant independent of h and material properties. In fact, if Eq. (3.12) is satisfied, the element is optimal for the displacement (or velocity) and pressure interpolations employed; that means, the discretizations using the element are stable and have the "best" error bounds that we can expect for the interpolations used.

Since $\mathbf{M}$ and $\mathbf{K}$ are the positive definite matrices and we have,

$$\begin{aligned} \mathbf{Q}^T \mathbf{K} \mathbf{Q} &= \mathbf{P} \\ \mathbf{Q}^T \mathbf{M} \mathbf{Q} &= \mathbf{I} \end{aligned} \tag{3.14}$$

where $\mathbf{Q}$ is the transformation matrix and $\mathbf{P}$ is the diagonal matrix listing the corre-

sponding eigenvalues.

In transient analysis, at each time step, the following equation holds,

$$\mathbf{K}' = \mathbf{K} + \mathcal{C}\mathbf{M} \tag{3.15}$$

where the constant $\mathcal{C}$ is the positive number related to the direct integration scheme used (for instance, $\mathcal{C} = \frac{4}{\Delta t^2}$ for the trapezoidal rule). Therefore, from Eqs. (3.14), we have $\mathbf{K}'$ as a positive definite matrix and the ellipticity condition [25] [35] is satisfied for every time step in the dynamic analysis. In the limit case, $G = 0$ and $\mathbf{K} = \mathbf{0}$, the positive definite mass matrix $\mathbf{M}$ still guarantees the satisfaction of the ellipticity condition.

The key to the success of this mixed finite element formulation is to choose the appropriate interpolations for the displacements and pressure. Without restricting the essence of our exposition, let us consider two-dimensional solutions. The finite element formulation for three-dimensional solutions is then directly obtained [35].

Considering the incompressible (or almost incompressible) analysis of solids and viscous fluids, it is well-established that finite elements which satisfy the inf-sup condition are effective and reliable. Appropriate interpolations are summarized in references [35], [25] and [42]. The u/p elements give continuous displacements and discontinuous pressures whereas the $u/p-c$ elements yield continuous displacements and pressures across the element boundaries.

For the fluid element formulation considered here, we use the same displacement/pressure interpolations that satisfy the inf-sup condition in the analysis of solids (and viscid fluids). Two proposed elements (9/3 and $9/4-c$ elements) are schematically depicted in Fig. 3-1. For the 9/3 element, we interpolate the pressure linearly as

$$p = p_1 + p_2 r + p_3 s \tag{3.16}$$

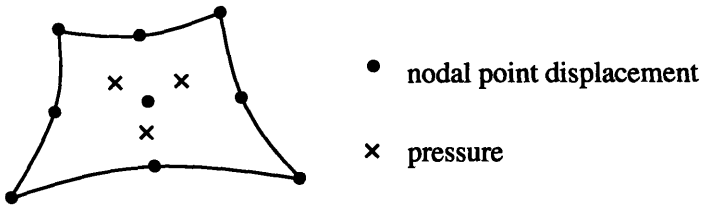

9/3 element

continuous displacement and discontinuous pressure

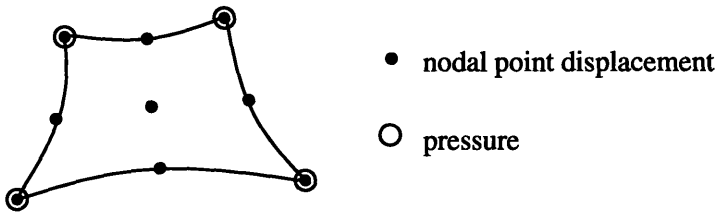

9/4-c element

continuous displacement and continuous pressure

Figure 3-1: Two elements for the u/p formulation. Full numerical integration is used (i.e. 3×3 Gauss integration).

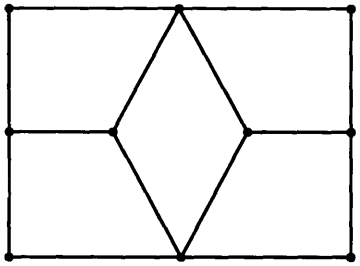

Type I macroelement with 4/1 elements

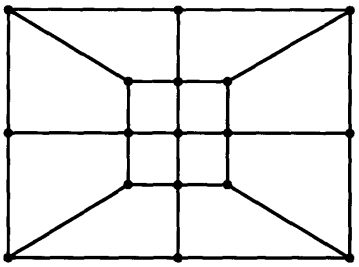

Type II macroelement with 4/1 elements

Figure 3-2: Two macroelements for the u/p formulation. Full numerical integration is used (i.e. 2×2 Gauss integration).

and for the $9/4 - c$ element we use the bilinear interpolations

$$p = p_1 + p_2 r + p_3 s + p_4 rs \tag{3.17}$$

Of course, there are a few other elements available. It is interesting to know that so far there is no available simple 4-node element ($Q1/P0$ or $Q1/Q1$ element) satisfying the inf-sup condition with general meshes [43]; however, researchers found [25] [44] that some special macroelements constructed with 4/1 elements pass the inf-sup condition. Fig. 3-2 shows the two types of macroelements used in this thesis.

Using the proposed u/p formulation, we no longer need to impose the constraint of Eq. (2.17) and can literally choose all the elements satisfying the inf-sup condition. Another benefit is that this u/p formulation can be easily extended to nonlinear analyses.

3.2.3 Number of Zero Modes

To predict mathematically the number of zero modes, we first consider a fluid domain with

$$\mathbf{u} \cdot \mathbf{n} = 0 \quad \text{on } S \tag{3.18}$$

The analogy of this analysis to structures and fluid-structure systems is straight forward. Eq. (3.18) shall be satisfied on the discretized boundaries; and the proper choice of boundary tangential directions is discussed in Chapter 5,

Considering that the shear modulus G is $O(\frac{1}{\beta})$, we take $\mathbf{K} = \mathbf{0}$ as the limit case. Since $\mathbf{M}$ and $\mathbf{A}$ are positive definite matrices, we need only to consider the stiffness matrix $\mathbf{K}^* = \mathbf{L}\mathbf{A}^{-1}\mathbf{L}^T$ to understand the zero modes.

For the matrices we consider here, we can write any $n \times m$ matrix $\mathbf{L}$ in a form [45]

$$\mathbf{L} = \mathbf{PEQ} \tag{3.19}$$

where $\mathbf{P}$ and $\mathbf{Q}$ are the invertible matrices with dimensions $n \times n$ and $m \times m$, while $\mathbf{E}$ is the matrix of dimension $n \times m$ in the form,

$$\begin{bmatrix} \mathbf{I}_r & \mathbf{0} \\ \mathbf{0} & \mathbf{0} \end{bmatrix}$$

where $\mathbf{I}_r$ is a $r \times r$ dimension unit matrix and r is the rank of $\mathbf{L}$. From the consistency of our finite element discretizations, and due to the existence of a constant pressure distribution, we have $1 \leq r \leq m - 1$ (refer to Appendix A). Using Eq. (3.19), we get

$$\mathbf{K}^* = \mathbf{PEQA}^{-1}\mathbf{Q}^T\mathbf{E}^T\mathbf{P}^T = \mathbf{PA}'\mathbf{P}^T \tag{3.20}$$

where $\mathbf{A}'$ has the form

$$\begin{bmatrix} \mathbf{K}_r & \mathbf{0} \\ \mathbf{0} & \mathbf{0} \end{bmatrix}$$

and $\mathbf{K}_r$ is a $r \times r$ dimension invertible matrix.

It is then obvious that the number of zero modes is $k = n - r$, i.e.

$$k \geq n - m + 1 \tag{3.21}$$

Notice in the above discussion, we consider n as the number of displacement degrees of freedom and m is the number of pressure degrees of freedom. With the presence of free surfaces, we have the number of zero modes,

$$k \geq n - m \tag{3.22}$$

Since the free surface is the material surface, we will have one implicit constraint imposed from the mass conservation. That implies for a free surface with i degrees of displacement freedom, the actual independent degrees of freedom is $i - 1$. If we consider the gravitational effects (i.e. including the sloshing modes), the number of zero modes will be,

$$k \geq n - m - i + 1 \tag{3.23}$$

3.2.4 Free Surface Condition

In this thesis, we ignore the surface tension and assign $\bar{p} = 0$ on the free surfaces. To apply the proposed u/p formulation to the analysis involving free surfaces, we introduce a free surface gravity wave potential W_f, denoted as,

$$W_f = \int_{S_f} \frac{1}{2} u_s^2 \rho g dS_f \tag{3.24}$$

where u_s is the free surface elevation referring to its static equilibrium position S_f. A similar approach has already been discussed in [30]. We often discretize u_s with the isoparametric elements of the same order on the free surface as in the fluid domain. For instance, in two dimensional analysis, if we use 9-node elements for the fluid

domain, on the free surface, we can use 3-node elements. Therefore we have $u_s = \mathbf{H}_s\widehat{\mathbf{U}}_s = \sum_{i=1}^{3} h_i \widehat{U}_s^i$ where $h_1 = (s^2 - s)/2$, $h_2 = (s^2 + s)/2$, $h_3 = 1 - s^2$.

From the variation of W_f, i.e. $\delta W_f = \int_{S_f} \delta u_s \rho g u_s dS_f$, we derive the additional stiffness term for the nodal displacements u_s on the free surface,

$$\mathbf{K}_{ss} = \int_{S_f} \rho g \mathbf{H}_s^T \mathbf{H}_s dS \tag{3.25}$$

3.3 v/p Formulation

The natural extension of the proposed **u**/p formulation to nonlinear analyses is a **v**/p formulation. Since the nonlinearities are introduced from the large free surface motions and the large relative motions between structures and fluids, we apply the ALE kinematic description [46] in our **v**/p formulation and use the velocity **v** as the primitive variable instead of the displacement **u**.

For the viscous fluid model undergoing large motions, the governing equations (momentum and continuity equations) are given as,

$$\rho\dot{\mathbf{v}} + \nabla p - \boldsymbol{f}^B = \mu\nabla^2\mathbf{v} \tag{3.26}$$

$$\nabla \cdot \mathbf{v} + \frac{\dot{p}}{\beta} = 0 \tag{3.27}$$

where μ is the dynamic viscosity of fluids, and the boundary conditions are,

$$\begin{aligned} \mathbf{v} \cdot \mathbf{n} &= \bar{v}_n \quad \text{on } S_u \\ p &= \bar{p} \quad \text{on } S_f \end{aligned} \tag{3.28}$$

In Eq. (3.26), $\dot{\mathbf{v}}$ stands for $\mathbf{v}^* + (\mathbf{v} - \mathbf{v}^m) \cdot \nabla\mathbf{v}$. Note that in the analysis of incompressible fluid (sloshing problems), i.e. where the dynamic pressure part is dominating, $\dot{p}$ can be approximated as p^*. However, to produce more accurate pres-

sure results in the analysis of almost incompressible fluid (acoustoelastic problems), we have to use $\dot{p} = p^* + (\mathbf{v} - \mathbf{v}^m) \cdot \nabla p$.

3.3.1 Variational Forms

The variational forms of Eqs. (3.26) and (3.27) are,

$$\begin{aligned}
\delta W_v &= \int_{V_f} \rho \delta \mathbf{v} \cdot \{\mathbf{v}^* + (\mathbf{v} - \mathbf{v}^m) \cdot \nabla \mathbf{v}\} dV - \int_{V_f} p \nabla \cdot \delta \mathbf{v} dV \\
&\quad - \int_{V_f} \delta \mathbf{v} \cdot \boldsymbol{f}^B dV - \int_{V_f} \mu \delta \mathbf{v} \cdot \nabla^2 \mathbf{v} dV + \int_{S_f} \delta v_n \bar{p} \, dS \\
\delta W_p &= -\int_{V_f} \delta p \{\nabla \cdot \mathbf{v} + \frac{1}{\beta}[p^* + (\mathbf{v} - \mathbf{v}^m) \cdot \nabla p]\} dV
\end{aligned} \tag{3.29}$$

where V_f is the fluid domain and $\boldsymbol{f}^B$ is the body force excluding the inertia force. Note that $\delta \mathbf{v}$ is the arbitrary admissible velocity, i.e. $\delta \mathbf{v} \cdot \mathbf{n} = 0$ on S_u, and $\bar{p}$ is commonly assigned to be zero on the free surfaces.

We know that the bulk modulus β is a large constant (numerically sufficiently large) for incompressible (or almost incompressible) fluids. This implies that a full explicit temporal scheme will not be suitable for this formulation because of the excessive time step limitation for the stability requirement. However, many approaches such as mixed explicit and implicit, predictor corrector, multistage and multistep schemes are available. Here, for simplicity, we use the trapezoidal temporal scheme with the conventional Newton-Raphson iteration method for the nonlinear equations. We will use the standard Galerkin formulation in this chapter, however, the difficulties introduced by the convective terms and their remedy will be addressed in Chapter 5.

Denote $\delta \mathbf{W}$ and $\delta \mathbf{R}$ as the left and right sides of equilibrium equations in variational forms, just like the internal and external virtual work. Note that if the bound-

ary motion is large enough, we have to include the surface tractions and body forces in $\delta\mathbf{W}$ and take into account their contributions to the tangent stiffness matrices. For the applied nodal forces, if they are fixed with mesh points, they should be included in $\delta\mathbf{R}$.

In the incremental analysis, at any time t, the equilibrium equations must be satisfied [35],

$$\delta^t\mathbf{W} = \delta^t\mathbf{R} \tag{3.30}$$

where $\delta\mathbf{W} = (\delta W_v, \delta W_p)^T$.

From the Taylor expansion, we have the following,

$$\delta^t\mathbf{W}^*\Delta t \simeq \delta^{t+\Delta t}\mathbf{R} - \delta^t\mathbf{W} \tag{3.31}$$

from which, we can derive the incremental stiffness matrix.

In the ALE formulation, all the variables are described on finite element mesh points. Therefore, the increment of a is defined as $\Delta a = a^*\Delta t$. Since we denote $\mathbf{y}$, $\mathbf{x}$ and $\mathbf{z}$ as the spatial, material and mesh point coordinates [46], the derivative of any quantity a with respect to the spatial coordinate y_i is denoted as $a_{,i} = \dfrac{\partial a}{\partial y_i}$ and its time rate of change following the mesh point is $-\dfrac{\partial a}{\partial y_k}\dfrac{\partial v_k^m}{\partial y_i}$, where $\mathbf{v}^m$ is the mesh velocity (or denoted as $\mathbf{u}^{m*}$). Therefore, we have,

$$\begin{aligned}
\delta W_v^* \;=\; & \int_{V_f} \rho\delta v_i\{v_i^{**} + (v_k^* - v_k^{m^*})\frac{\partial v_i}{\partial y_k} + (v_k - v_k^m)\frac{\partial v_i^*}{\partial y_k} - (v_k - v_k^m)\frac{\partial v_i}{\partial y_j}\frac{\partial v_j^m}{\partial y_k}\}dV \\
& - \int_{V_f} (p^*\frac{\partial \delta v_k}{\partial y_k} - p\frac{\partial \delta v_k}{\partial y_j}\frac{\partial v_j^m}{\partial y_k} + p\frac{\partial \delta v_n}{\partial y_n}\frac{\partial v_k^m}{\partial y_k} - \mu\frac{\partial \delta v_k}{\partial y_n}\frac{\partial v_k^*}{\partial y_n})dV \\
& - \int_{V_f} \mu(\frac{\partial \delta v_k}{\partial y_i}\frac{\partial v_i^m}{\partial y_n}\frac{\partial v_k}{\partial y_n} + \frac{\partial \delta v_k}{\partial y_n}\frac{\partial v_k}{\partial y_i}\frac{\partial v_i^m}{\partial y_n} - \frac{\partial \delta v_k}{\partial y_n}\frac{\partial v_k}{\partial y_n}\frac{\partial v_n^m}{\partial y_n})dV
\end{aligned}$$

$$+\int_{V_f} \delta v_i \{\rho[v_i^* + (v_k - v_k^m)\frac{\partial v_i}{\partial y_k}] - f_i^B\}\frac{\partial v_n^m}{\partial y_n} dV \tag{3.32}$$

$$\begin{aligned}\delta W_p^* = & -\int_{V_f} \delta p\{\frac{\partial v_k^*}{\partial y_k} - \frac{\partial v_k}{\partial y_n}\frac{\partial v_n^m}{\partial y_k} + \frac{1}{\beta}[p^{**} + (v_k^* - v_k^{m^*})\frac{\partial p}{\partial y_k}]\}dV \\ & +\int_{V_f} \frac{\delta p}{\beta}\{(v_k - v_k^m)\frac{\partial p}{\partial y_n}\frac{\partial v_n^m}{\partial y_k} - (v_k - v_k^m)\frac{\partial p^*}{\partial y_k}\}dV \\ & -\int_{V_f} \delta p\{\frac{\partial v_k}{\partial y_k} + \frac{1}{\beta}[p^* + (v_k - v_k^m)\frac{\partial p}{\partial y_k}]\}\frac{\partial v_n^m}{\partial y_n} dV \end{aligned} \tag{3.33}$$

3.3.2 Finite Element Discretization

Since we have,

$$\Delta^t \mathbf{W} = \frac{\partial^t \mathbf{W}}{\partial \mathbf{\Theta}}\Delta\mathbf{\Theta} + \frac{\partial^t \mathbf{W}}{\partial \mathbf{\Theta}^*}\Delta\mathbf{\Theta}^* \tag{3.34}$$

where $\mathbf{\Theta}^T = [\widehat{\mathbf{V}} \quad \widehat{\mathbf{P}} \quad \widehat{\mathbf{U}}^m]$, applying the standard Galerkin finite element procedure, we get,

$$\mathbf{C}\Delta\mathbf{\Theta}^* + \mathbf{K}\Delta\mathbf{\Theta} = \Delta\mathbf{R} \tag{3.35}$$

where

$$\mathbf{C} = \begin{bmatrix} \mathbf{C}_{vv} & \mathbf{0} & \mathbf{C}_{vv}^m \\ \mathbf{0} & \mathbf{C}_{pp} & \mathbf{C}_{pv}^m \end{bmatrix}, \quad \mathbf{K} = \begin{bmatrix} \mathbf{K}_{vv} & \mathbf{K}_{vp} & \mathbf{K}_{vv}^m \\ \mathbf{K}_{pv} & \mathbf{K}_{pp} & \mathbf{K}_{pv}^m \end{bmatrix}$$

$$\Delta\mathbf{R} = \begin{Bmatrix} \mathbf{R}_v \\ \mathbf{0} \end{Bmatrix} - \begin{Bmatrix} \mathbf{F}_v \\ \mathbf{F}_p \end{Bmatrix}$$

$$\delta\mathbf{V}^T\mathbf{F}_v = \delta W_v \quad , \delta\mathbf{P}^T\mathbf{F}_p = \delta W_p$$

and

$$\delta\mathbf{V}^T\mathbf{C}_{vv}\Delta\widehat{\mathbf{V}}^* = \int_{V_f}\rho\delta v_i\Delta v_i^* dV \qquad \delta\mathbf{V}^T\mathbf{K}_{vp}\Delta\widehat{\mathbf{P}} = -\int_{V_f}\frac{\partial\delta v_k}{\partial y_k}\Delta p dV$$

$$\delta\mathbf{P}^T\mathbf{K}_{pp}\Delta\widehat{\mathbf{P}} = -\int_{V_f}(v_k - v_k^m)\frac{\delta p}{\beta}\frac{\partial\Delta p}{\partial y_k}dV \qquad \delta\mathbf{P}^T\mathbf{C}_{pp}\Delta\widehat{\mathbf{P}} = -\int_{V_f}\delta p\frac{\Delta p^*}{\beta}dV$$

$$\delta\mathbf{V}^T\mathbf{C}_{vv}^m\Delta\widehat{\mathbf{V}}^m = -\int_{V_f}\rho\delta v_i\frac{\partial v_i}{\partial y_k}\Delta v_k^m dV \qquad \delta\mathbf{P}^T\mathbf{C}_{pv}^m\Delta\widehat{\mathbf{V}}^m = \int_{V_f}\delta p\frac{\partial p}{\partial y_k}\frac{\Delta v_k^m}{\beta}dV$$

$$\begin{aligned}
\delta\mathbf{V}^T\mathbf{K}_{vv}^m\Delta\widehat{\mathbf{U}}^m &= \int_{V_f}\{p\frac{\partial\delta v_k}{\partial y_j}\frac{\partial\Delta u_j^m}{\partial y_k} - (v_k - v_k^m)\frac{\partial v_i}{\partial y_j}\frac{\partial\Delta u_j^m}{\partial y_k} - p\frac{\partial\delta v_n}{\partial y_n}\frac{\partial\Delta u_k^m}{\partial y_k}\}dV \\
&\quad -\int_{V_f}\mu(\frac{\partial\delta v_k}{\partial y_i}\frac{\partial\Delta u_i^m}{\partial y_n}\frac{\partial v_k}{\partial y_n} + \frac{\partial\delta v_k}{\partial y_n}\frac{\partial v_k}{\partial y_i}\frac{\partial\Delta u_i^m}{\partial y_n} - \frac{\partial\delta v_k}{\partial y_n}\frac{\partial v_k}{\partial y_n}\frac{\partial\Delta u_i^m}{\partial y_i})dV \\
&\quad +\int_{V_f}\delta v_i\{\rho[v_i^* + (v_k - v_k^m)\frac{\partial v_i}{\partial y_k}] - f_i^B\}\frac{\partial\Delta u_n^m}{\partial y_n}dV \\
\delta\mathbf{P}^T\mathbf{K}_{pv}^m\Delta\widehat{\mathbf{U}}^m &= \int_{V_f}\{\delta p\frac{\partial v_k}{\partial y_n}\frac{\partial\Delta u_n^m}{\partial y_k} + \frac{\delta p}{\beta}(v_k - v_k^m)\frac{\partial p}{\partial y_n}\frac{\partial\Delta u_n^m}{\partial y_k}\}dV \\
&\quad -\int_{V_f}\delta p\{\frac{\partial v_k}{\partial y_k} + \frac{1}{\beta}[p^* + (v_k - v_k^m)\frac{\partial p}{\partial y_k}]\}\frac{\partial\Delta u_n^m}{\partial y_n}dV \\
\delta\mathbf{V}^T\mathbf{K}_{vv}\Delta\widehat{\mathbf{V}} &= \int_{V_f}\{\rho\delta v_i\frac{\partial v_i}{\partial y_k}\Delta v_k + (v_k - v_k^m)\frac{\partial\Delta v_i}{\partial y_k} + \mu\frac{\partial\delta v_k}{\partial y_n}\frac{\partial\Delta v_k}{\partial y_n}\}dV \\
\delta\mathbf{P}^T\mathbf{K}_{pv}\Delta\widehat{\mathbf{V}} &= -\int_{V_f}\delta p(\frac{\partial\Delta v_k}{\partial y_k} + \frac{\Delta v_k}{\beta}\frac{\partial p}{\partial y_k})dV
\end{aligned}$$

The trapezoidal temporal discretization is as the following [47],

$$\begin{aligned}
{}^{t+\Delta t}\mathbf{b} &= {}^t\mathbf{b} + \frac{\Delta t}{2}({}^t\dot{\mathbf{b}} + {}^{t+\Delta t}\dot{\mathbf{b}}) \\
{}^{t+\Delta t}\dot{\mathbf{b}} &= {}^t\dot{\mathbf{b}} + \frac{\Delta t}{2}({}^t\ddot{\mathbf{b}} + {}^{t+\Delta t}\ddot{\mathbf{b}})
\end{aligned} \tag{3.36}$$

and consequently,

$${}^{t+\Delta t}\mathbf{b} = {}^t\mathbf{b} + {}^t\dot{\mathbf{b}}\Delta t + \frac{\Delta t^2}{4}({}^t\ddot{\mathbf{b}} + {}^{t+\Delta t}\ddot{\mathbf{b}}) \tag{3.37}$$

where $\mathbf{b}$ can stand for $\widehat{\mathbf{U}}^m$, $\widehat{\mathbf{V}}$ or $\hat{\mathbf{P}}$.

Since $\widehat{\mathbf{V}}$ and $\hat{\mathbf{P}}$ are independent variables, and $\widehat{\mathbf{U}}^m$ is the mesh displacement which can be assigned independently, or related with the material displacement $\widehat{\mathbf{U}}$ (refer to Chapter 5), we assign a linear relation between the motion of meshes and the boundary material points as follows,

$$\begin{aligned} \Delta\widehat{\mathbf{U}}^{m^*} &= \mathcal{L}\Delta\widehat{\mathbf{V}} \\ \Delta\widehat{\mathbf{U}}^{m} &= \mathcal{L}\Delta\widehat{\mathbf{U}} \end{aligned} \tag{3.38}$$

where the relation $\mathcal{L}$ is selected such that the mesh regularity is preserved during the time evolutions. If we use mixed elements with discontinuous pressure, such as the 9/3 element, we can statically condense out $\hat{\mathbf{P}}$ unknowns on the element level, by using,

$$\Delta\hat{\mathbf{P}} = -(\frac{2\mathbf{C}_{pp}}{\Delta t} + \mathbf{K}_{pp})^{-1}((\mathbf{K}_{pv} + \mathbf{C}^m_{pv}\mathcal{L} + \mathbf{K}^m_{pv}\mathcal{L}\frac{\Delta t}{2})\Delta\widehat{\mathbf{V}} + \mathbf{F}_p) \tag{3.39}$$

Chapter 4

u-p-Λ and v-p-Λ Formulations

4.1 Introduction

From the discussion in Chapter 3, we know that if we use the $\mathbf{u}$/p formulation with proper elements (such as the 9/3 and $9/4-c$ elements) we will not have spurious non-zero frequency modes. With the artificial shear modulus G (0 or $O(\frac{1}{\beta})$), we expect some zero frequency (or numerically sufficiently small) rotational modes. In the last chapter, we discuss the mathematical prediction of the number of zero modes, and we know that if many such zero frequency modes exist, they can significantly reduce the effectiveness of the solution algorithm. To impose the constraint of Eq. (2.17), historically, penalty formulations, along with reduced integration techniques, are widely used [2]. Consequently many researchers have encountered the so-called non-zero frequency spurious rotational modes and various remedy procedures have been proposed [9] [30] [16]. One common interesting idea from the penalty formulations is that a large shear modulus is introduced to shift the modes due to shearing to the high end of the frequency spectrum. In this chapter, a $\mathbf{u}$-p-$\mathbf{\Lambda}$ formulation is presented and it is believed that this formulation is the proper approach to impose the constraint of Eq. (2.17). For the nonlinear analysis, we will start from the isentropic, inviscid and irrotational fluid model and impose the constraint of Eq. (2.21).

4.2 u-p-Λ Formulation

4.2.1 Variational Formulations

In order to impose the constraint of Eq. (2.17), we introduce,

$$\nabla \times \mathbf{u} = \frac{\mathbf{\Lambda}}{\alpha} \tag{4.1}$$

where $\mathbf{\Lambda}$ is a "vorticity moment". The magnitude of $\mathbf{\Lambda}$ shall be small while α is a constant of large value.

Based on our experience with the u/p formulation in Chapter 3, we propose the following variational indicator for the finite element formulation of the fluid model considered here

$$\begin{aligned} \Pi \;=\; & \int_{V_f} \{ \frac{p^2}{2\beta} - \mathbf{u} \cdot \boldsymbol{f}^B - \lambda_p (\frac{p}{\beta} + \nabla \cdot \mathbf{u}) \\ & + \frac{\mathbf{\Lambda} \cdot \mathbf{\Lambda}}{2\alpha} - \lambda_\Lambda \cdot (\frac{\mathbf{\Lambda}}{\alpha} - \nabla \times \mathbf{u}) \} dV \\ & + \int_{S_f} \bar{p}\, u_n^s \, dS \end{aligned} \tag{4.2}$$

where the variables are p, $\mathbf{u}$, $\mathbf{\Lambda}$, and the Lagrange multipliers λ_p and λ_Λ. The constant β is the bulk modulus and the constant α has large value. We note that the first two terms correspond to the usual strain energy (given in terms of the pressure) and the potential of the externally applied body forces. The third term implies the constraint of Eq. (3.8), the fourth term is included to be able to statically condense out the degrees of freedom of the vorticity moment, and the fifth term represents the constraint from Eq. (4.1). For the fourth and fifth terms we require that the constant α is large, and we use $\alpha = 1000\beta$. However, from our numerical tests, we find that α can be any numerically reasonable value larger than β, say $10\beta \leq \alpha \leq 10^4\beta$. The last term is the potential due to any applied boundary pressure on the surface S_f.

Invoking the stationarity of Π, we identify the Lagrange multipliers λ_p and λ_Λ to be the pressure p and vorticity moment $\mathbf{\Lambda}$, respectively, and we obtain the field

equations

$$\nabla p - \boldsymbol{f}^B + \nabla \times \boldsymbol{\Lambda} = \mathbf{0} \tag{4.3}$$

$$\nabla \cdot \mathbf{u} + \frac{p}{\beta} = 0 \tag{4.4}$$

$$\nabla \times \mathbf{u} - \frac{\boldsymbol{\Lambda}}{\alpha} = \mathbf{0} \tag{4.5}$$

and the boundary conditions

$$\begin{aligned} \mathbf{u} \cdot \mathbf{n} &= \bar{u}_n \quad \text{on } S_u \\ p &= \bar{p} \quad \text{on } S_f \\ \boldsymbol{\Lambda} &= \mathbf{0} \quad \text{on } S \end{aligned} \tag{4.6}$$

4.2.2 Finite Element Discretization

We use the standard Galerkin finite element discretization [35] and hence for a typical element, we have

$$\begin{aligned} \mathbf{u} &= \mathbf{H}\widehat{\mathbf{U}} \\ p &= \mathbf{H}_p\widehat{\mathbf{P}} \\ \boldsymbol{\Lambda} &= \mathbf{H}_\Lambda\widehat{\boldsymbol{\Lambda}} \\ \nabla \cdot \mathbf{u} &= (\nabla \cdot \mathbf{H})\widehat{\mathbf{U}} = \mathbf{B}\widehat{\mathbf{U}} \\ \nabla \times \mathbf{u} &= (\nabla \times \mathbf{H})\widehat{\mathbf{U}} = \mathbf{D}\widehat{\mathbf{U}} \end{aligned}$$

where $\mathbf{H}$, $\mathbf{H}_p$ and $\mathbf{H}_\Lambda$ are the interpolation matrices, and $\widehat{\mathbf{U}}$, $\widehat{\mathbf{P}}$ and $\widehat{\boldsymbol{\Lambda}}$ are the vectors of solution variables.

The matrix equations of our formulation are

$$\begin{bmatrix} \mathbf{M} & \mathbf{0} & \mathbf{0} \\ \mathbf{0} & \mathbf{0} & \mathbf{0} \\ \mathbf{0} & \mathbf{0} & \mathbf{0} \end{bmatrix} \begin{Bmatrix} \ddot{\widehat{\mathbf{U}}} \\ \ddot{\widehat{\mathbf{P}}} \\ \ddot{\widehat{\mathbf{\Lambda}}} \end{Bmatrix} + \begin{bmatrix} \mathbf{0} & \mathbf{L} & \mathbf{Q} \\ \mathbf{L}^T & \mathbf{A} & \mathbf{0} \\ \mathbf{Q}^T & \mathbf{0} & \mathbf{G} \end{bmatrix} \begin{Bmatrix} \widehat{\mathbf{U}} \\ \widehat{\mathbf{P}} \\ \widehat{\mathbf{\Lambda}} \end{Bmatrix} = \begin{Bmatrix} \mathbf{R} \\ \mathbf{0} \\ \mathbf{0} \end{Bmatrix} \tag{4.7}$$

where

$$\mathbf{M} = \int_{V_f} \rho \mathbf{H}^T \mathbf{H} dV \qquad \mathbf{L} = -\int_{V_f} \mathbf{B}^T \mathbf{H}_p dV$$

$$\mathbf{Q} = \int_{V_f} \mathbf{D}^T \mathbf{H}_\Lambda dV \qquad \mathbf{A} = -\int_{V_f} \frac{1}{\beta} \mathbf{H}_p^T \mathbf{H}_p dV$$

$$\mathbf{G} = -\int_{V_f} \frac{1}{\alpha} \mathbf{H}_\Lambda^T \mathbf{H}_\Lambda dV \qquad \mathbf{R} = -\int_{S_f} \mathbf{H}_n^{S^T} \bar{p} dS$$

The key to the success of the finite element discretization is to choose the appropriate interpolations for the displacements, pressure and vorticity moment. Extending the idea from Chapter 3, for the inviscid fluid element formulation considered here, we use the displacement/pressure interpolations that satisfy the inf-sup condition in the analysis of solids (and viscid fluids) and use the same interpolation for the vorticity moment as for the pressure. Thus, two proposed elements are the $9-3-3$ and $9-4c-4c$ elements schematically depicted in Fig. 4-1.

Hence, for the $9-3-3$ element, we interpolate the pressure and vorticity moment linearly as

$$p = p_1 + p_2 r + p_3 s \tag{4.8}$$

$$\mathbf{\Lambda} = \mathbf{\Lambda}_1 + \mathbf{\Lambda}_2 r + \mathbf{\Lambda}_3 s \tag{4.9}$$

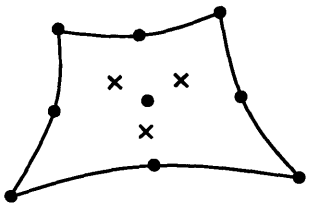

• nodal point displacement

× pressure and vorticity moment

9-3-3 element

continuous displacement, discontinuous pressure
and vorticity moment

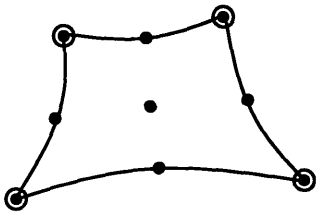

• nodal point displacement

○ pressure and vorticity moment

9-4c-4c element

continuous displacement, pressure and vorticity moment

Figure 4-1: Two elements for the $\mathbf{u} - p - \mathbf{\Lambda}$ formulation. Full numerical integration is used (i.e. 3×3 Gauss integration).

and for the $9-4c-4c$ element we use the bilinear interpolations

$$p = p_1 + p_2 r + p_3 s + p_4 rs \tag{4.10}$$

$$\Lambda = \Lambda_1 + \Lambda_2 r + \Lambda_3 s + \Lambda_4 rs \tag{4.11}$$

Of course, additional elements could be proposed using this approach. In each case, the vorticity moment would be interpolated with functions that, when used for the pressure interpolation, give a stable element for (almost) incompressible conditions. For instance, a reasonable element is also the $9-3-1$ element, which does not impose the zero vorticity as strongly as the $9-3-3$ element. On the other hand, the $4-1-1$ element with regular meshes is not recommended; however, some macroelements constructed with $4-1-1$ elements can be applicable to certain analysis cases (refer to Chapter 2 and 6). For all elements full numerical integration is used [35].

While we do not have a mathematical analysis to prove that the proposed elements are indeed stable, based on our experience we can expect a good element behavior. Namely, the constraints in Eq. (4.4) and (4.5) are very similar in nature and are not coupled in the formulation (see the variational indicator in Eq. (4.2)). Hence, we can reasonably assume that the two constraints should be imposed with the same interpolations in the element discretization.

The treatment to include the surface waves is exactly the same as used for the **u**/p formulation in Chapter 3. The mathematical prediction of the number of zero frequency modes is also the same as in Chapter 3, however, the number of vorticity moment unknowns shall be included in m.

4.3 v-p-Λ Formulation

4.3.1 Field Equations

Based on the **u**-p-**Λ** formulation for linear problems, we propose a **v**-p-**Λ** formulation for nonlinear analyses with the ALE kinematic description.

Note that in the **u**-p-**Λ** formulation, we introduced **Λ** (so-called vorticity moment for displacements) and a large parameter α to impose the irrotationality constraint (2.17). Similar to the approach in linear analyses, in nonlinear analyses, to impose the irrotationality constraint, we introduce **Λ** as the vorticity moment for velocities and replace the constraint (2.21) with,

$$\nabla \times \mathbf{v} - \frac{\mathbf{\Lambda}}{\alpha} = \mathbf{0} \tag{4.12}$$

Consequently, the field equations are modified as follows,

$$\rho[\mathbf{v}^* + (\mathbf{v} - \mathbf{v}^m) \cdot \nabla \mathbf{v}] + \nabla p - \boldsymbol{f}^B + \nabla \times \mathbf{\Lambda} = \mathbf{0} \tag{4.13}$$

$$\nabla \cdot \mathbf{v} + \frac{\dot{p}}{\beta} = 0 \tag{4.14}$$

$$\nabla \times \mathbf{v} - \frac{\mathbf{\Lambda}}{\alpha} = \mathbf{0} \tag{4.15}$$

with the boundary conditions

$$\begin{aligned} \mathbf{v} \cdot \mathbf{n} &= \bar{v}_n \quad \text{on } S_u \\ p &= \bar{p} \quad \text{on } S_f \\ \mathbf{\Lambda} &= \mathbf{0} \quad \text{on } S \end{aligned} \tag{4.16}$$

4.3.2 Variational Forms

With the boundary conditions in Eq. (4.16), we have the variational forms of Eqs. (4.13), (4.14) and (4.15):

$$
\begin{aligned}
\delta W_v &= \int_{V_f} \rho \delta \mathbf{v} \cdot \{\mathbf{v}^* + (\mathbf{v} - \mathbf{v}^m) \cdot \nabla \mathbf{v}\} dV - \int_{V_f} p \nabla \cdot \delta \mathbf{v} dV \\
&\quad - \int_{V_f} \delta \mathbf{v} \cdot \boldsymbol{f}^B dV + \int_{V_f} \boldsymbol{\Lambda} \cdot (\nabla \times \delta \mathbf{v}) dV + \int_{S_f} \delta v_n \bar{p} \, dS \\
\delta W_p &= - \int_{V_f} \delta p \{\nabla \cdot \mathbf{v} + \frac{1}{\beta}[p^* + (\mathbf{v} - \mathbf{v}^m) \cdot \nabla p]\} dV \\
\delta W_\Lambda &= \int_{V_f} \delta \boldsymbol{\Lambda} \cdot (\nabla \times \mathbf{v} - \frac{\boldsymbol{\Lambda}}{\alpha}) dV
\end{aligned} \tag{4.17}
$$

where V_f is the fluid domain and $\boldsymbol{f}^B$ is the body forces excluding the inertia force. Note that $\delta \mathbf{v}$ is the arbitrary admissible velocity, i.e. $\delta \mathbf{v} \cdot \mathbf{n} = 0 \quad \text{on } S_u$, and on the free surfaces, $\bar{p}$ is commonly assigned to be zero.

As in Chapter 3, we have in the incremental analysis, at any time t, the equilibrium equations,

$$
\delta^t \mathbf{W} = \delta^t \mathbf{R} \tag{4.18}
$$

where $\delta \mathbf{W} = (\delta W_v, \delta W_p, \delta W_\Lambda)^T$.

The time change rates of δW_v, δW_p and δW_Λ are given as,

$$
\begin{aligned}
\delta W_v^* &= \int_{V_f} \rho \delta v_i \{v_i^{**} + (v_k^* - v_k^{m^*}) \frac{\partial v_i}{\partial y_k} + (v_k - v_k^m) \frac{\partial v_i^*}{\partial y_k} - (v_k - v_k^m) \frac{\partial v_i}{\partial y_j} \frac{\partial v_j^m}{\partial y_k}\} dV \\
&\quad - \int_{V_f} (p^* \frac{\partial \delta v_k}{\partial y_k} - p \frac{\partial \delta v_k}{\partial y_j} \frac{\partial v_j^m}{\partial y_k} - \Lambda_k^* \epsilon_{kij} \frac{\partial \delta v_j}{\partial y_i} + \Lambda_k \epsilon_{kij} \frac{\partial \delta v_j}{\partial y_n} \frac{\partial v_n^m}{\partial y_i}) dV \\
&\quad + \int_{V_f} \delta v_i \{\rho [v_i^* + (v_k - v_k^m) \frac{\partial v_i}{\partial y_k}] - f_i^B\} \frac{\partial v_n^m}{\partial y_n} dV \\
&\quad - \int_{V_f} (p \frac{\partial \delta v_n}{\partial y_n} - \Lambda_k \epsilon_{kij} \frac{\partial \delta v_j}{\partial y_i}) \frac{\partial v_n^m}{\partial y_n} dV
\end{aligned} \tag{4.19}
$$

$$\begin{aligned}
\delta W_p^* &= -\int_{V_f} \delta p\{\frac{\partial v_k^*}{\partial y_k} - \frac{\partial v_k}{\partial y_n}\frac{\partial v_n^m}{\partial y_k} + \frac{1}{\beta}[p^{**} + (v_k^* - v_k^{m^*})\frac{\partial p}{\partial y_k}]\}dV \\
&\quad + \int_{V_f} \frac{\delta p}{\beta}\{(v_k - v_k^m)\frac{\partial p}{\partial y_n}\frac{\partial v_n^m}{\partial y_k} - (v_k - v_k^m)\frac{\partial p^*}{\partial y_k}\}dV \\
&\quad - \int_{V_f} \delta p\{\frac{\partial v_k}{\partial y_k} + \frac{1}{\beta}[p^* + (v_k - v_k^m)\frac{\partial p}{\partial y_k}]\}\frac{\partial v_n^m}{\partial y_n}dV \qquad (4.20) \\
\delta W_\Lambda^* &= \int_{V_f} \delta\Lambda_k\{\epsilon_{kij}\frac{\partial v_j^*}{\partial y_i} - \epsilon_{kij}\frac{\partial v_j}{\partial y_n}\frac{\partial v_n^m}{\partial y_i} - \frac{\Lambda_k^*}{\alpha} + (\epsilon_{kij}\frac{\partial v_j}{\partial y_i} - \frac{\Lambda_k}{\alpha})\frac{\partial v_n^m}{\partial y_n}\}dV \qquad (4.21)
\end{aligned}$$

4.3.3 Finite Element Discretization

Applying the finite element procedure as in Chapter 3, we have,

$$\mathbf{C}\Delta\mathbf{\Theta}^* + \mathbf{K}\Delta\mathbf{\Theta} = \Delta\mathbf{R} \qquad (4.22)$$

where $\mathbf{\Theta}^T = [\widehat{\mathbf{V}}\ \ \hat{\mathbf{P}}\ \ \hat{\mathbf{\Lambda}}\ \ \widehat{\mathbf{U}}^m]$,

$$\mathbf{C} = \begin{bmatrix} \mathbf{C}_{vv} & \mathbf{0} & \mathbf{0} & \mathbf{C}_{vv}^m \\ \mathbf{0} & \mathbf{C}_{pp} & \mathbf{0} & \mathbf{C}_{pv}^m \\ \mathbf{0} & \mathbf{0} & \mathbf{0} & \mathbf{0} \end{bmatrix}, \quad \mathbf{K} = \begin{bmatrix} \mathbf{K}_{vv} & \mathbf{K}_{vp} & \mathbf{K}_{v\Lambda} & \mathbf{K}_{vv}^m \\ \mathbf{K}_{pv} & \mathbf{K}_{pp} & \mathbf{0} & \mathbf{K}_{pv}^m \\ \mathbf{K}_{\Lambda v} & \mathbf{0} & \mathbf{K}_{\Lambda\Lambda} & \mathbf{K}_{\Lambda v}^m \end{bmatrix}$$

$$\Delta\mathbf{R} = \begin{Bmatrix} \mathbf{R}_v \\ \mathbf{0} \\ \mathbf{0} \end{Bmatrix} - \begin{Bmatrix} \mathbf{F}_v \\ \mathbf{F}_p \\ \mathbf{F}_\Lambda \end{Bmatrix}$$

$$\delta\mathbf{V}^T\mathbf{F}_v = \delta W_v \ , \ \delta\mathbf{P}^T\mathbf{F}_p = \delta W_p \ , \ \delta\mathbf{\Lambda}^T\mathbf{F}_\Lambda = \delta W_\Lambda$$

and

$$\delta\mathbf{V}^T\mathbf{C}_{vv}\Delta\widehat{\mathbf{V}}^* = \int_{V_f}\rho\delta v_i\Delta v_i^* dV \qquad \delta\mathbf{V}^T\mathbf{K}_{vp}\Delta\widehat{\mathbf{P}} = -\int_{V_f}\frac{\partial\delta v_k}{\partial y_k}\Delta p dV$$

$$\delta\mathbf{P}^T\mathbf{K}_{pp}\Delta\widehat{\mathbf{P}} = -\int_{V_f}(v_k - v_k^m)\frac{\delta p}{\beta}\frac{\partial\Delta p}{\partial y_k}dV \qquad \delta\mathbf{P}^T\mathbf{C}_{pp}\Delta\widehat{\mathbf{P}} = -\int_{V_f}\delta p\frac{\Delta p^*}{\beta}dV$$

$$\delta\mathbf{\Lambda}^T\mathbf{K}_{\Lambda\Lambda}\Delta\widehat{\mathbf{\Lambda}} = -\int_{V_f}\frac{1}{\alpha}\delta\Lambda_k\Delta\Lambda_k dV \qquad \delta\mathbf{V}^T\mathbf{K}_{v\Lambda}\Delta\widehat{\mathbf{\Lambda}} = \int_{V_f}\epsilon_{kij}\frac{\partial\delta v_j}{\partial y_i}\Delta\Lambda_k dV$$

$$\delta\mathbf{V}^T\mathbf{C}_{vv}^m\Delta\widehat{\mathbf{V}}^m = -\int_{V_f}\rho\delta v_i\frac{\partial v_i}{\partial y_k}\Delta v_k^m dV \qquad \delta\mathbf{P}^T\mathbf{C}_{pv}^m\Delta\widehat{\mathbf{V}}^m = \int_{V_f}\delta p\frac{\partial p}{\partial y_k}\frac{\Delta v_k^m}{\beta}dV$$

$$\begin{aligned}
\delta\mathbf{V}^T\mathbf{K}_{vv}^m\Delta\widehat{\mathbf{U}}^m &= \int_{V_f}\{p\frac{\partial\delta v_k}{\partial y_j}\frac{\partial\Delta u_j^m}{\partial y_k} - \Lambda_k\epsilon_{kij}\frac{\partial\delta v_j}{\partial y_n}\frac{\partial\Delta u_n^m}{\partial y_i} - (v_k - v_k^m)\frac{\partial v_i}{\partial y_j}\frac{\partial\Delta u_j^m}{\partial y_k}\}dV \\
&\quad + \int_{V_f}\delta v_i\{\rho[v_i^* + (v_k - v_k^m)\frac{\partial v_i}{\partial y_k}] - f_i^B\}\frac{\partial\Delta u_n^m}{\partial y_n}dV \\
&\quad - \int_{V_f}(\delta p\frac{\partial\delta v_k}{\partial y_k} - \Lambda_k\epsilon_{kij}\frac{\partial\delta v_j}{\partial y_i})\frac{\partial\Delta u_n^m}{\partial y_n}dV \\
\delta\mathbf{P}^T\mathbf{K}_{pv}^m\Delta\widehat{\mathbf{U}}^m &= \int_{V_f}\{\delta p\frac{\partial v_k}{\partial y_n}\frac{\partial\Delta u_n^m}{\partial y_k} + \frac{\delta p}{\beta}(v_k - v_k^m)\frac{\partial p}{\partial y_n}\frac{\partial\Delta u_n^m}{\partial y_k}dV \\
&\quad - \int_{V_f}\delta p\{\frac{\partial v_k}{\partial y_k} + \frac{1}{\beta}[p^* + (v_k - v_k^m)\frac{\partial p}{\partial y_k}]\}\frac{\partial\Delta u_k^m}{\partial y_k}dV \\
\delta\mathbf{\Lambda}^T\mathbf{K}_{\Lambda v}^m\Delta\widehat{\mathbf{U}}^m &= \int_{V_f}\delta\Lambda_k\{(\epsilon_{kij}\frac{\partial v_j}{\partial y_i} - \frac{\Lambda_k}{\alpha})\frac{\partial\Delta u_n^m}{\partial y_n} - \epsilon_{kij}\frac{\partial v_j}{\partial y_n}\frac{\partial\Delta u_n^m}{\partial y_i}\}dV \\
\delta\mathbf{V}^T\mathbf{K}_{vv}\Delta\widehat{\mathbf{V}} &= \int_{V_f}\{\rho\delta v_i\frac{\partial v_i}{\partial y_k}\Delta v_k + (v_k - v_k^m)\frac{\partial\Delta v_i}{\partial y_k}\}dV \\
\delta\mathbf{P}^T\mathbf{K}_{pv}\Delta\widehat{\mathbf{V}} &= -\int_{V_f}\delta p(\frac{\partial\Delta v_k}{\partial y_k} + \frac{\Delta v_k}{\beta}\frac{\partial p}{\partial y_k})dV
\end{aligned}$$

Defining the relation between $\widehat{\mathbf{U}}$ and $\widehat{\mathbf{U}}^m$ as $\mathcal{L}$, again if we use the discontinuous type of 9-node elements, such as the $9-3-3$ element, we can statically condense out $\widehat{\mathbf{\Lambda}}$ and $\widehat{\mathbf{P}}$ unknowns in the element level, by using,

$$\Delta\widehat{\mathbf{P}} = -(\frac{2\mathbf{C}_{pp}}{\Delta t} + \mathbf{K}_{pp})^{-1}((\mathbf{K}_{pv} + \mathbf{C}_{pv}^m\mathcal{L} + \mathbf{K}_{pv}^m\mathcal{L}\frac{\Delta t}{2})\Delta\widehat{\mathbf{V}} + \mathbf{F}_p) \tag{4.23}$$

$$\Delta\widehat{\mathbf{\Lambda}} = -\mathbf{K}_{\Lambda\Lambda}^{-1}((\mathbf{K}_{\Lambda v} + \mathbf{K}_{\Lambda v}^{m}\mathcal{L}\frac{\Delta t}{2})\Delta\widehat{\mathbf{V}} + \mathbf{F}_{\Lambda}) \tag{4.24}$$

4.4 Discussions

The reason for proposing the **u**-p-$\mathbf{\Lambda}$ formulation in linear analyses is simply to reduce the number of zero frequency modes by imposing the constraint of Eq. (2.17). After defining the "vorticity moment" $\mathbf{\Lambda}$, it is clear that the frequencies of $\mathbf{\Lambda}$ modes depend on α in the same way as the frequencies of p modes depend on β. Since α is a numerically large variable ($10\beta \leq \alpha \leq 10^4\beta$), we in effect shift the frequencies of the rotational modes to the very high range and we shall expect the frequencies of rotational modes to be in the higher range of the frequency spectrum than the pressure modes.

If we substitute Eq. (4.5) into Eq. (4.3), we have the following set of equations,

$$\nabla p - \boldsymbol{f}^{B} + \alpha\nabla\times(\nabla\times\mathbf{u}) = \mathbf{0} \tag{4.25}$$

$$\nabla\cdot\mathbf{u} + \frac{p}{\beta} = 0 \tag{4.26}$$

Since we have,

$$\nabla(\nabla\cdot\mathbf{u}) \equiv \nabla^2\mathbf{u} + \nabla\times(\nabla\times\mathbf{u}) \tag{4.27}$$

by substituting Eq. (4.26), we can rewrite Eq. (4.25) as,

$$(1-\frac{\alpha}{\beta})\nabla p - \boldsymbol{f}^{B} = \alpha\nabla^2\mathbf{u} \tag{4.28}$$

Therefore, we can see immediately that the term $\alpha\nabla^2\mathbf{u}$ is the stiffness term for **u**. In the **u**-p-$\mathbf{\Lambda}$ formulation, the large value of α means high stiffness for **u**, and the modes introduced by this term shall be in the highest range of the frequency

spectrum. If we extend the same philosophy to the nonlinear problems, similarly we will get,

$$\nabla p - \frac{\alpha}{\beta}\nabla \dot{p} - \boldsymbol{f}^B = \alpha \nabla^2 \mathbf{v} \tag{4.29}$$

$$\nabla \cdot \mathbf{v} + \frac{\dot{p}}{\beta} = 0 \tag{4.30}$$

where $\boldsymbol{f}^B$ is the body force including the inertia force.

However, the term $\alpha\nabla^2\mathbf{v}$ acts as the viscosity term instead of the stiffness term! If we apply the large value for α used in the **u**-p-$\mathbf{\Lambda}$ formulation to the **v**-p-$\mathbf{\Lambda}$ formulation, we actually bring into the formulation a very large amount of viscosity.

Now if we change our philosophy to shifting the frequencies of rotational modes to the very lowest end of the spectrum, i.e. numerically sufficiently small (around $10^{-5} - 10^{-3}$) instead of the highest end of the spectrum, we will have the equivalent formulation as the **u**/p formulation, and the number of zero frequency modes is discussed in Chapter 3. To achieve this, we simply introduce a small variable α ($\frac{1}{10^4\beta} \leq \alpha \leq \frac{1}{10\beta}$). Since $\frac{1}{\beta}$ is the small value of $O(\epsilon)$, α is $O(\epsilon)$ and $\frac{\alpha}{\beta}$ is $O(\epsilon^2)$. Ignoring $O(\epsilon^2)$ terms, we have for the linear problems,

$$\nabla p - \boldsymbol{f}^B = \alpha \nabla^2 \mathbf{u} \tag{4.31}$$

$$\nabla \cdot \mathbf{u} + \frac{p}{\beta} = 0 \tag{4.32}$$

where α is identified as G and the inertia force $-\rho\ddot{\mathbf{u}}$ is included in $\boldsymbol{f}^B$.

For one element (size 2×2) with $\beta = 2.1 \times 10^9 \quad Pa$, $\rho = 998.2 \quad kg/m^3$ and $\alpha = 2.1 \times 10^{12} \quad Pa$, the element eigenvalues (the first three non-zero frequencies are listed in Tab. 4-1) and element eigenvectors (shown in Figs. 4-2 and 4-3) are calculated with **u**/p and **u**-p-$\mathbf{\Lambda}$ formulations. It is clearly indicated that the highest three frequencies

Element	No. of zero modes Theory	Result	First (rad/sec)	Second (rad/sec)	Third (rad/sec)
9/3	15	15	3552.85	6153.71	6153.71
$9-3-3$	12	12	3552.85	6067.56	6067.56

Table 4-1: Frequency analysis of typical mixed elements.

calculated with the **u**-p-$\mathbf{\Lambda}$ formulation are introduced by the assigned $\alpha = 1000\beta$.

For nonlinear problems, we get,

$$\nabla p - \boldsymbol{f}^B = \alpha \nabla^2 \mathbf{v} \tag{4.33}$$

$$\nabla \cdot \mathbf{v} + \frac{\dot{p}}{\beta} = 0 \tag{4.34}$$

where α is identified as μ and the inertia force $-\rho \dfrac{D\mathbf{v}}{Dt}$ is included in $\boldsymbol{f}^B$.

Eqs. (4.33) and (4.34) are the familiar Navier-Stokes equations including the artificial compressibility β.

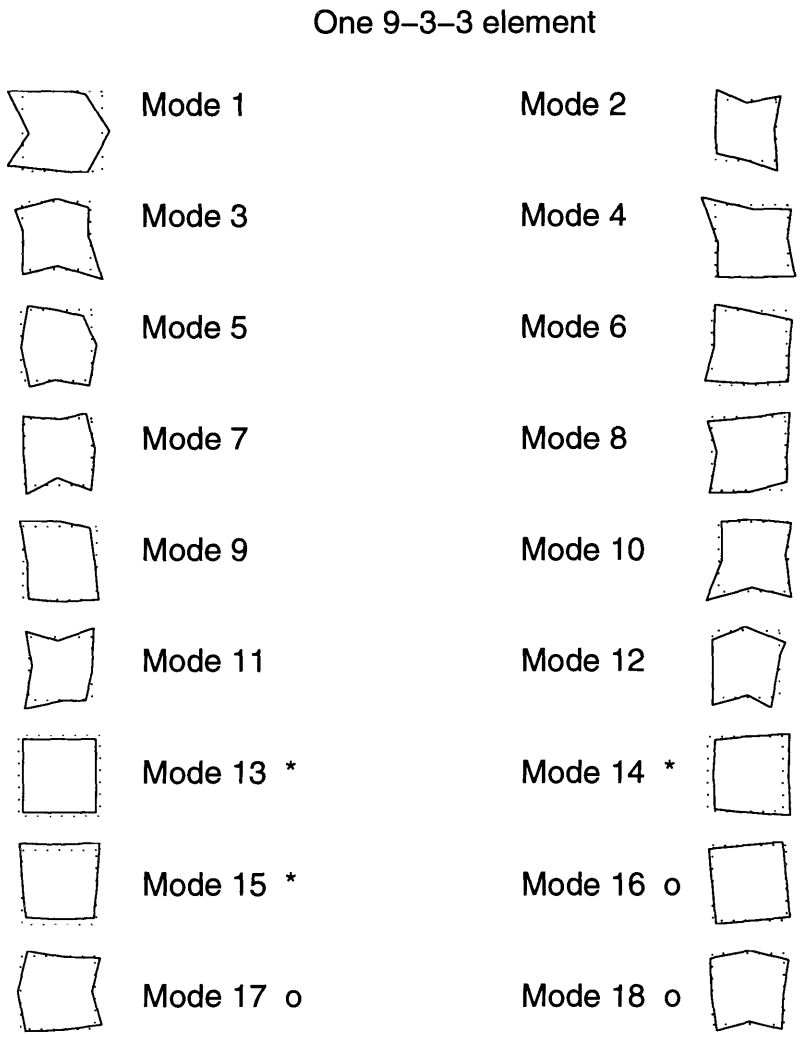

Figure 4-2: Mode shapes of one 9-3-3 element; * frequencies are physical ones and ^{o} frequencies are due to the large parameter α.

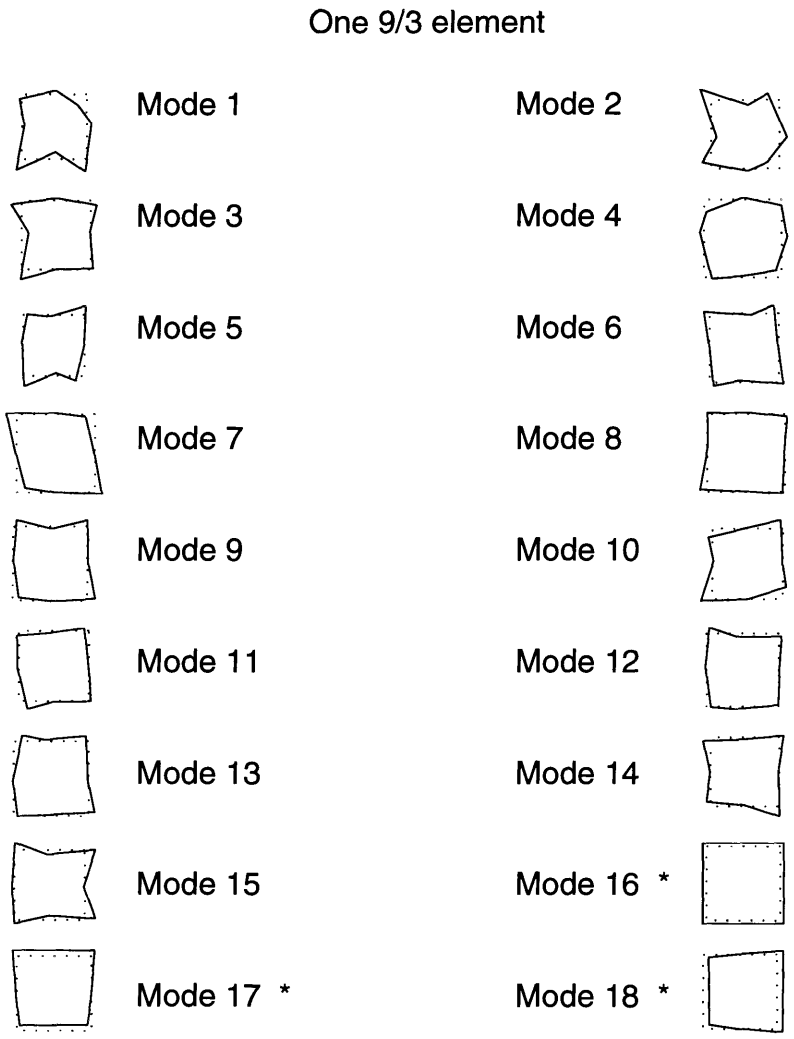

Figure 4-3: Mode shapes of one 9/3 element; * frequencies are physical ones.

Chapter 5

Fluid-structure Interactions

5.1 Introduction

With primitive variable formulations for fluids, the coupling between fluids and structures are rather natural. If noslipping boundary conditions are used, the coupling procedure between the fluids and structures is directly obtained by the element assemblage process [35]. If slipping boundary conditions are used, we can assign different nodal numbers for the same spatial position on the fluid-structure interfaces shown in Fig. 5-1. The constraints between fluid side nodes and structure side nodes can be imposed in the same way as for structure matrices. Commonly we use the skew coordinate systems to assign the continuous normal displacements (or velocities) and discontinuous tangential motions around the fluid-structure interfaces.

In addition, if slipping boundaries are used, the mass conservation (or the impermeability condition) has to be imposed along with the momentum conservation.

There are three issues or rather three difficulties in the nonlinear finite element procedures for both fluids and solids, especially for fluids and fluid-structure interaction problems. The first is to maintain mesh regularity during the time evolution; the second is to get rid of the spatial oscillations in convection dominated problems with the standard Galerkin formulations [48] [49] [50] and the third is to select suitable

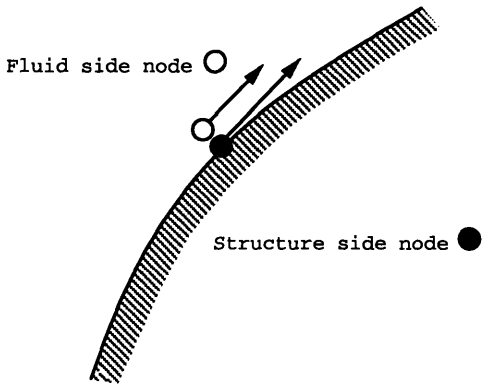

Figure 5-1: Fluid-structure interface nodes.

mixed elements which satisfy the inf-sup condition in the analysis of incompressible (or almost incompressible) materials.

Unlike the area of almost incompressible media, within which many conclusive results have been drawn in the 1980's, many upwinding schemes have been proposed, but none of them is completely satisfactory [51] [52] [28] [29]. Many researchers are still wondering whether or not such an elegant conclusion as the inf-sup condition can be reached.

The SUPG formulation was originally proposed in the context of finite element methods; while the skewed positive influence coefficient upwinding procedure was initially developed for the control volume finite element method [31]. Both upwinding formulations were introduced for 4-node elements [52]. Considering the fact that the SUPG formulation retains the oscillations (refer to Chapter 6) and 4-node elements do not satisfy the inf-sup condition, in this thesis, we extend the control volume finite element upwinding procedure to 9-node elements in a mixed approach with both the standard Galerkin formulation and the control volume finite element method. The very reason for this extension to high order elements is that we want to use elements which satisfy the inf-sup condition. Considering the fact that no available simple 4-node element satisfies the inf-sup condition with general meshes [43], we naturally

select 9/3 and 9/4 – c elements which satisfy the inf-sup condition. In fact, the 9/3 element is proved mathematically to be the optimal second order element.

To avoid the mesh entanglements, researchers have two options; one is to use adaptive procedures and the other is to use arbitrary Lagrangian-Eulerian (ALE) descriptions. A survey of adaptive procedures is available in [53]. In this thesis, we use the ALE formulation which is summarized in [46].

5.2 ALE Descriptions

The essence of ALE formulations is that the spatial position for the description of the state variables is neither fixed in space, nor attached with material particles. Therefore, we can arbitrarily select proper mesh motions so as to avoid excessive mesh distortions and follow the moving boundaries. Fundamentally, there are two ways of relating the mesh and material particle motions. The first type is used for the closed domain problems or the problems where the material boundaries are known. In this ALE description, the mesh velocities (or displacements) along the boundary are commonly assigned to be the same as the material particle, i.e. $\mathbf{v}^m = \mathbf{v}$ or set to follow the boundaries. The second type is for the problems with unknown material boundaries, such as the large amplitude free surfaces and fluid-structure interfaces. In this case, the mesh configurations can not be assigned arbitrarily, due to the fact that the mesh domain has to be the same as the material domain. Consequently, we have to introduce additional unknowns of mesh displacements on the material surfaces. For example, on the 2D free surface, where $v_1^m = 0$ and $v_2 = v_2^m$, the kinematical relation,

$$u_s^* = v_2 - v_1 \frac{\partial u_s}{\partial y_1} \tag{5.1}$$

provides the link between the mesh displacements over the fluid domain and u_s.

Since in the whole formulation, the mesh velocities can be set independently, as

long as the mesh domain covers the material domain and mesh regularity is maintained, the final results shall be the same. Obviously, choices for the mesh velocities are not unique.

5.3 Upwinding Techniques

Many formulations can be used, though not completely satisfactory, to get rid of the spatial oscillations of the standard Galerkin formulation for convection dominated problems [29]. In this thesis, we develop a mixed formulation of the standard Galerkin and control volume finite element methods with 9/3 and $9/4-c$ elements and extend the scheme to the Navier-Stokes equations.

We treat one 9-node element as four 4-node elements in dealing with the convective terms only. Fig. 5-2 shows the typical 4-node element for the upwinding control volume finite element method. The commonly used testing problem is the heat transfer problem governed by,

$$\mathbf{v} \cdot \nabla\theta - \alpha\nabla^2\theta = 0 \tag{5.2}$$

The variational form of the above equation is,

$$\int_V \delta\theta(\mathbf{v} \cdot \nabla\theta - \alpha\nabla^2\theta)dV = 0 \tag{5.3}$$

In the standard Galerkin formulation, $\delta\theta$ has the same interpolation function as for θ. For the SUPG formulation, $\delta\theta$ can be assigned as the combination of the same interpolation function for θ and an elementwise continuous interpolant which is often the derivative of the interpolant for θ to suit its purpose of carrying the sign of the "wind" direction [52]. In the artificial viscosity approach, some constants (depending on isotropic and anisotropic viscosity models) are introduced to the diffusion terms and the standard Galerkin formulation is used. Other approaches such as the Galerkin

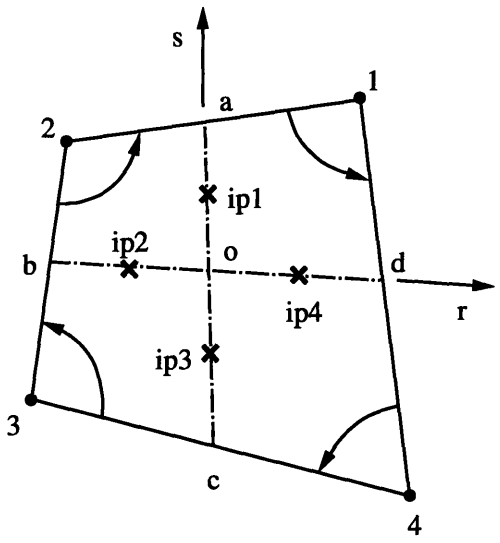

Figure 5-2: Typical 4-node element in the CVFEM upwinding scheme.

least squares method can also be applied. Interestingly, in the one dimensional cases, many of the above methods will give the same set of discretized equations which provide the exact solutions on the nodal points (so-called super convergence).

The idea of the control volume finite element method (CVFEM) is different from the Galerkin method (shown in Fig. 5-3). The approximation is directed to each node, upon which the conservation equations hold for the integral over the control volume,

$$\int_V (\mathbf{v} \cdot \nabla\theta - \alpha\nabla^2\theta) dV = 0 \tag{5.4}$$

In fact, we can actually get Eq. (5.4) by setting $\delta\theta = 1$ on the control volume around individual nodes in the variational form of Eq. (5.3). If the velocity satisfies,

$$\nabla \cdot \mathbf{v} = 0 \tag{5.5}$$

which is true for the heat transfer problems with incompressible fluids, we can later

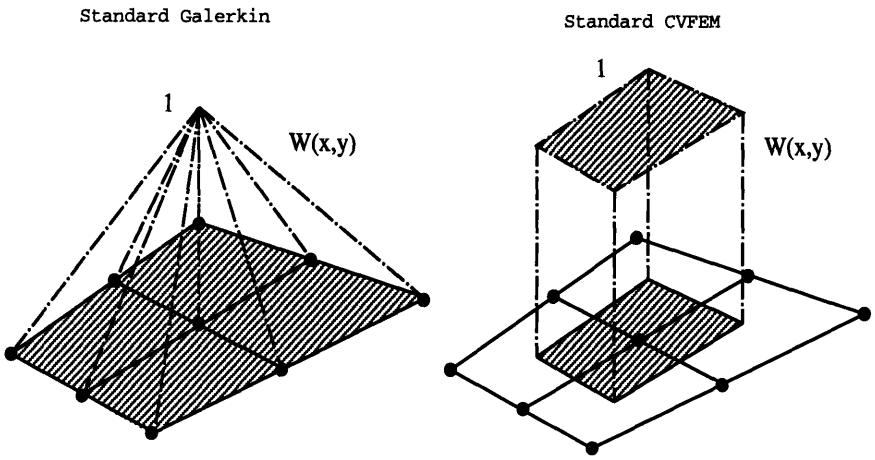

Figure 5-3: Typical interpolant functions.

on get,

$$\int_S (\mathbf{v} \cdot \mathbf{n}\theta - \alpha \nabla\theta \cdot \mathbf{n}) dS = 0 \tag{5.6}$$

We know immediately that on the element boundary the contributions from the elements sharing the same boundaries will cancel each other except for the domain boundary. Therefore, the important parts left are the evaluation of Eq. (5.6) on the inner sides illustrated in Fig. 5-2. Since $\mathbf{v}$ is known and the only unknown θ is interpolated with 4-node elements, the integration of Eq. (5.6) can be evaluated by one Gaussian Quadrature point. In the standard CVFEM, θ is evaluated solely from the isoparametric interpolation functions. In the Schneider and Raw upwinding scheme, to achieve an optimal diagonal dominating discretized equation (i.e. requiring that the diagonal entity is positive and *all* the off-diagonal entities are negative), the values of θ at the interpolation points, $ip1(r = 0, s = 0.5)$,$ip2(r = -0.5, s = 0)$,$ip3(r = 0, s = -0.5)$ and $ip4(r = 0.5, s = 0)$ are evaluated according to the mass flux in and out of the control volumes. Take the control volume on node 1 as an example, the contributions from the convective terms in Eq. (5.6) to the discretized equation for node 1 is,

$$\mathbf{v}\cdot\mathbf{n}|_{ao}\theta_{ip1}+\mathbf{v}\cdot\mathbf{n}|_{od}\theta_{ip4} \tag{5.7}$$

For the standard CVFEM, we have,

$$\theta_{ip1}=\sum_{i=1}^{4}h_i|_{ip1}\theta_i \tag{5.8}$$

where

$$\begin{aligned} h_1 &= \frac{(1+r)(1+s)}{4} & h_2 &= \frac{(1-r)(1+s)}{4} \\ h_3 &= \frac{(1-r)(1-s)}{4} & h_4 &= \frac{(1+r)(1-s)}{4} \end{aligned}$$

Notice, here we use the counterclockwise convention to define the normal directions on the inner surfaces of the control volume and the mass flux is,

$$\dot{m}=\mathbf{v}\cdot\mathbf{n} \tag{5.9}$$

where the positive sign of $\dot{m}$ indicates the flux out of the control volume.

In the Schneider and Raw upwinding scheme, if $\dot{m}_{ao}<0$, which indicates that the flow direction is from left to right, we define,

$$\theta_{ip1}=(1-f)\theta_2+f\theta_{ip2} \tag{5.10}$$

where the ratio of the mass fluxes $f=-\dfrac{\dot{m}_{bo}}{\dot{m}_{oa}}$ and $0\le f\le 1$.

If $\dot{m}_{ao}>0$, which indicates that the flow comes from right to left, we then have,

$$\theta_{ip1}=(1-f)\theta_1+f\theta_{ip4} \tag{5.11}$$

where $f=-\dfrac{\dot{m}_{od}}{\dot{m}_{ao}}$ and $0\le f\le 1$.

To extend this approach to solve nonlinear fluid-structure interaction problems

with ALE formulations, we simply use the mass flux of

$$\dot{m} = (\mathbf{v} - \mathbf{v}^m) \cdot \mathbf{n} \tag{5.12}$$

Since the convective terms are nonlinear, we use the successive iteration procedure in the ALE formulation of the Navier-Stokes equations. In order to achieve faster convergence rate of iterative procedures, we could use the true tangent stiffness matrix or include a line search option. In the successive iteration procedure, $\mathbf{v} - \mathbf{v}^m$ in Eq. (5.12) is taken from the last iteration step.

5.4 Boundary Conditions

The above mathematical models appear to be rather natural when considering the free surfaces and the interactions between different media, but we have to look more deeply into the boundary conditions. Different mathematical models will have different boundary conditions and some subtle points arise in imposing the boundary conditions. From the numerical examples in Chapter 6, we find the existence of non-zero spurious frequencies when wrong boundary conditions are imposed.

In the interaction problems, if there is no slipping between different continuous media, the particles on both sides will share the same displacements and shall also satisfy the force balance. For the interface between fluids and structures shown in Fig. 5-4, if no additional assumptions are made for the fluids, the particles on both sides of the mesh points S_1 and S_2 shall have the same displacements and velocities, while the force balance holds. For the normal displacements, we have,

$$u_n^f|_{S_1,S_2} = u_n^s|_{S_1,S_2} \tag{5.13}$$

$$u_t^f|_{S_1,S_2} = u_t^s|_{S_1,S_2} \tag{5.14}$$

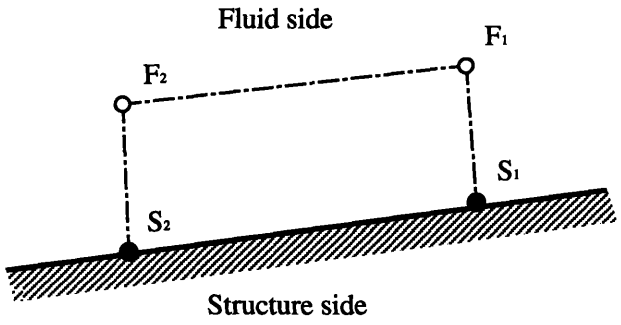

Figure 5-4: Fluid-structure interface.

As the fluid viscosity decreases, the layer $F_1F_2S_2S_1$ will get thinner and the normal direction gradient of the tangential velocity around the fluid-structure interface will become greater, therefore, in the limit (inviscid fluid models), we have,

$$u_n|_{F_1,F_2} = u_n^s|_{S_1,S_2} \tag{5.15}$$

$$u_t|_{F_1,F_2} \neq u_t^s|_{S_1,S_2} \tag{5.16}$$

To satisfy the mass conservation over the layer $F_1F_2S_2S_1$, we have the following discussion on the slipping boundary condition for inviscid fluid models.

Let us consider typical boundary lines composed of two adjacent 3 or 4-node elements, see Fig. 5-5, and two 9-node elements, see Fig. 5-6. Based on our assumption, the displacement component tangential to the solid is not restrained (while the displacement component normal to the solid is restrained to be equal to the displacement of the solid). The choice of directions of nodal tangential displacements (from which also follow the normal displacements) is critical.

Considering the solution of actual fluid flows and fluid flows with structural in-

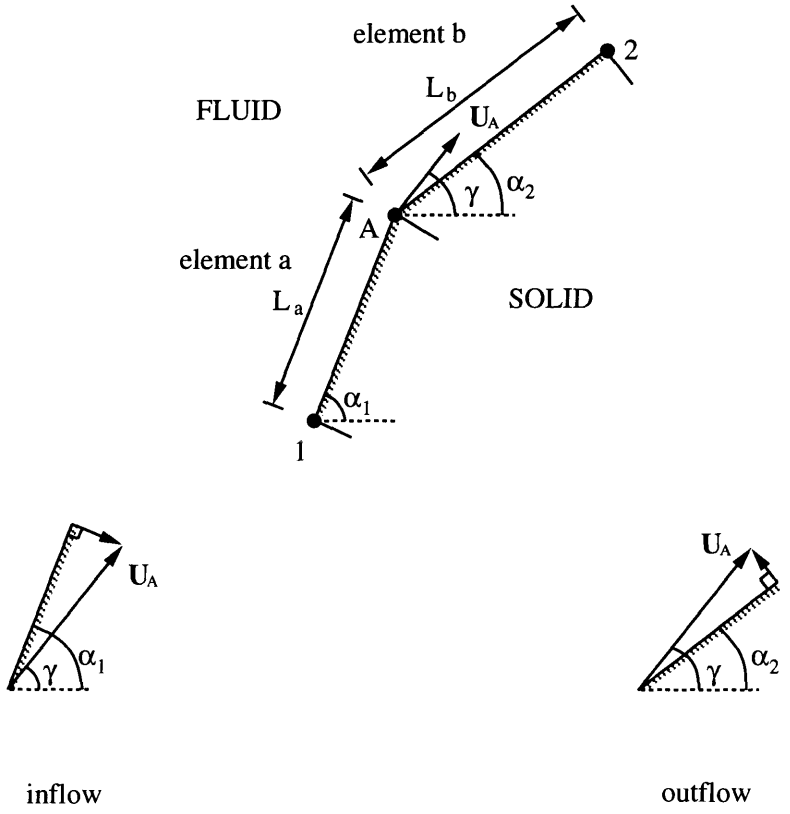

Figure 5-5: Tangential direction at node A for 3 or 4-node elements.

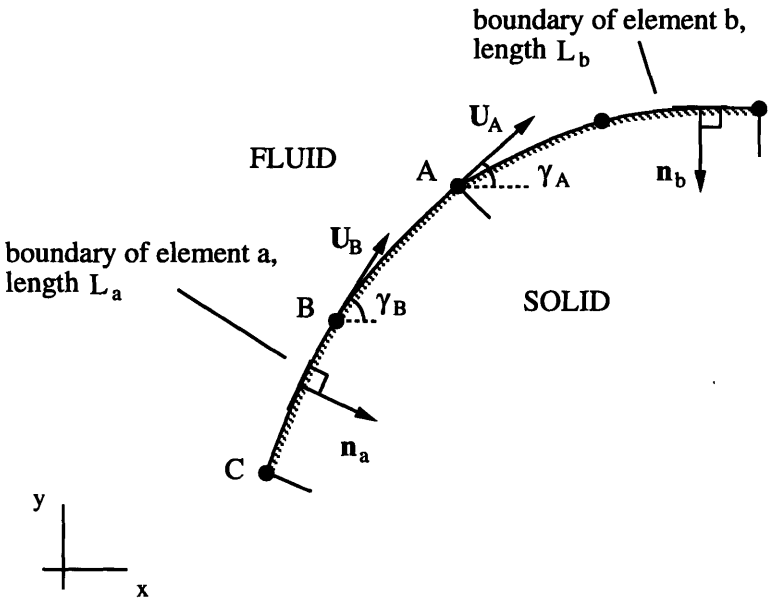

Figure 5-6: Tangential directions at nodes A and B for 9-node elements.

teractions (in which the fluid is modeled using the Navier-Stokes equations including wall turbulence effects or the Euler equations), we are accustomed to choosing these directions such that in the finite element discretization there is no transport of fluid across the fluid-structure interfaces. It is important that we employ the same concept also in the definition of the tangential directions at boundary nodes of the fluid considered here, including the acoustic fluid which does not flow but only undergoes (infinitesimally) small displacements.

While we do not recommend using the $Q1/P0$ or $Q1/Q1$ element of the mixed formulation, lower-order elements (3-node triangular two-dimensional and 4-node tetrahedral three-dimensional elements) are effectively employed in fluid flow analysis and could be used in our formulations [35] [54] [55]. Hence, consider first the boundary representation in Fig. 5-5. This case was already discussed by Donea [56].

In the following discussion, we use displacements to discuss the mass conservation and the same concepts hold for the velocities.

For the displacement $\mathbf{U}_A$, we have the spurious fluxes ΔV_a and ΔV_b across the element lengths L_a and L_b. Mass conservation requires that $\Delta V_a + \Delta V_b = 0$ and hence we must choose γ given by

$$\tan\gamma = \frac{L_a \sin\alpha_1 + L_b \sin\alpha_2}{L_a \cos\alpha_1 + L_b \cos\alpha_2} \tag{5.17}$$

We note that γ is actually given by the direction of the line from node 1 to node 2. In general, the direction of $\mathbf{U}_A$ is not given by the mean of the angles α_1 and α_2, but only in the specific case when $L_a = L_b$

$$\gamma = \frac{1}{2}(\alpha_1 + \alpha_2) \tag{5.18}$$

We employ the same concept to establish the appropriate tangential directions at the typical nodes A and B of our 9-node elements in Fig. 5-6. For node A, we need to have

$$\int_{L_a} \mathbf{u}_a^A \cdot \mathbf{n}_a dl + \int_{L_b} \mathbf{u}_b^A \cdot \mathbf{n}_b dl = 0 \tag{5.19}$$

where

$$\begin{aligned} \mathbf{n}_a dl &= (-\frac{\partial y_a}{\partial s} ds,\ \frac{\partial x_a}{\partial s} ds) \\ \mathbf{n}_b dl &= (-\frac{\partial y_b}{\partial s} ds,\ \frac{\partial x_b}{\partial s} ds) \end{aligned} \tag{5.20}$$

In the above equations, x_a, y_a, x_b and y_b are the interpolated coordinates on the boundaries of elements a and b, while $\mathbf{u}_a^A$ and $\mathbf{u}_b^A$ are the interpolated displacements corresponding to the displacement $\mathbf{U}_A$ at node A,

$$\begin{aligned} \mathbf{u}_a^A &= \frac{s^2 + s}{2} \mathbf{U}_A \\ \mathbf{u}_b^A &= \frac{s^2 - s}{2} \mathbf{U}_A \end{aligned} \tag{5.21}$$

For element a, mass conservation requires

$$\int_{L_a} \mathbf{u}_a^B \cdot \mathbf{n}_a dl = 0 \tag{5.22}$$

where $\mathbf{u}_a^B$ is the interpolated displacement on the boundary of element a based on the nodal displacement $\mathbf{U}_B$

$$\mathbf{u}_a^B = (1 - s^2)\mathbf{U}_B \tag{5.23}$$

The relation (5.22) shows that the appropriate tangential direction γ_B at node B is given by

$$\tan \gamma_B = \frac{\partial y}{\partial s} / \frac{\partial x}{\partial s} \tag{5.24}$$

Our numerical experiments have shown that it is important to allocate the appropriate tangential directions at all boundary nodes. Otherwise, spurious non-zero energy modes are obtained in the finite element solution.

In the nonlinear analysis, within each time increment, we still have to satisfy the mass conservation on the discretized slipping boundary. However, after each incremental step, the material configuration will be updated as well as the mesh configuration. Therefore, the conditions of Eqs. (5.19) and (5.22) should be satisfied at every time step. That means we have to modify the flow tangential directions on the fluid-structure interfaces at every time step and it is somewhat involved (especially for high order elements) to impose the perfect inviscid mathematical model for practical problems. Nevertheless, the physical world always allows us to use the viscous fluid models, and in practice, different meshing techniques could be used along the fluid boundaries and fluid-structure interfaces.

5.5 Free Surface Condition

On the free surface (for simplicity we focus on 2D problems, however, the analysis is directly applicable to 3D), if we assign, $v_1^m = 0$ and $v_2^m = v_2$, we will have,

$$u_s^* = v_2 - v_1 \frac{\partial u_s}{\partial y_1} \tag{5.25}$$

To discretize the above equation, we can either use the standard Galerkin formulation with some upwinding techniques for the term $-v_1 \frac{\partial u_s}{\partial y_1}$, or we can use upwinding finite difference schemes. The typical SUPG method is,

$$\int_{S_f} (\delta u_s + \delta w_s)(u_s^* - v_2 + v_1 \frac{\partial u_s}{\partial y_1}) dS = 0 \tag{5.26}$$

where δu_s is the standard virtual displacement with the same interpolation function as for u_s; and δw_s is the elementwise continuous interpolant carrying the sign of v_1 (often assigned as $\frac{\partial \delta u_s}{\partial y_1}$).

In this thesis, we will use the following upwinding finite difference scheme for Eq. (5.25),

$$\hat{U}_s^{i^*} + \hat{V}_1^i \frac{2\hat{U}_s^{i+1} + 3\hat{U}_s^i - 6\hat{U}_s^{i-1} + \hat{U}_s^{i-2}}{2\hat{Y}_1^{i+1} + 3\hat{Y}_1^i - 6\hat{Y}_1^{i-1} + \hat{Y}_1^{i-2}} - \hat{V}_2^i = 0 \tag{5.27}$$

where the nodes are numbered sequentially from upstream to downstream [57].

Chapter 6

Numerical Examples

The proposed $\mathbf{u}/\mathrm{p}$, $\mathbf{u}$-p-$\mathbf{\Lambda}$, $\mathbf{v}/\mathrm{p}$ and $\mathbf{v}$-p-$\mathbf{\Lambda}$ formulations have been implemented experimentally. The following cases are chosen to demonstrate the capability of the formulations and to confirm the key arguments.

6.1 Linear Vibration Problems

To demonstrate the capability of the proposed $\mathbf{u}/\mathrm{p}$ and $\mathbf{u}$-p-$\mathbf{\Lambda}$ formulations for linear analyses, we solved eight generic test problems involving fluids and fluid-structure interactions. We set the tall water column and rigid cavity problems exactly the same as used in [11] [9] [2] in order to compare the results with those from either the pure displacement-based formulation or the displacement formulation with a penalty term on the irrotationality constraint. We aim to clarify the long lasting misunderstanding about the causes of the non-zero spurious modes with the chosen examples. We consider these analysis cases to be good tests because, while they pertain to simple problems, the degree of complexity is sufficient in exhibiting deficiencies in formulations.

Until the proposed $\mathbf{u}/\mathrm{p}$ and $\mathbf{u}$-p-$\mathbf{\Lambda}$ formulations in this thesis, we were not able to obtain accurate solutions to all these problems with a displacement-based formulation

(or a formulation derived therefrom).

In all test problems, we want to evaluate the lowest frequencies of the complete systems. We also give the number of the zero frequencies k present in the analyses using the $\mathbf{u}$/p and $\mathbf{u}$-p-$\mathbf{\Lambda}$ formulations. The mathematical predictions of zero frequency modes are obtained from the formulas discussed in Chapter 3. Of course, we do not calculate the mode shapes corresponding to the zero frequencies, but simply shift to the non-zero frequencies sought [35].

The results are found to be in good agreement with those calculated with the $\mathbf{u} - \phi$ formulation, or the analytical solutions and the numbers of zero frequencies match with the mathematical predictions. The pressure bands or distributions are quite smooth indicating accurate solutions.

6.1.1 Tall Water Column Problem

Fig. 6-1 shows the tall water column considered in [2]. The acoustic speed $c = \sqrt{\beta/\rho}$. The governing equations for the fluid field are,

$$\nabla^2 p = \frac{1}{c^2}\frac{\partial^2 p}{\partial t^2} \tag{6.1}$$

$$\frac{\partial^2 \mathbf{u}}{\partial t^2} = -\frac{1}{\rho}\nabla p \tag{6.2}$$

with the initial condition

$$\mathbf{u} = \mathbf{0} \quad \text{at} \quad t = 0$$

and the boundary conditions

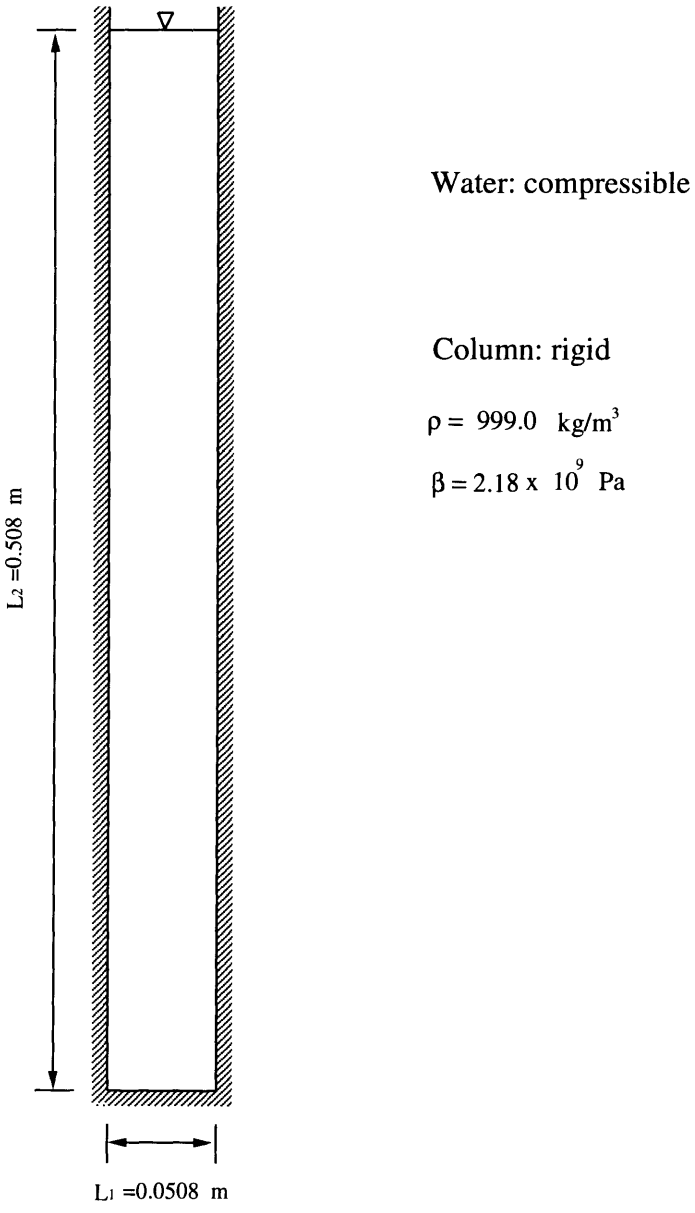

Figure 6-1: Tall water column problem.

$$
\begin{aligned}
u_1 = 0 \quad &\text{at} \quad x_1 = 0, L_1 \\
u_2 = 0 \quad &\text{at} \quad x_2 = 0 \\
p = 0 \quad &\text{at} \quad x_2 = L_2
\end{aligned}
$$

The analytical solutions of the above equations are given,

$$
\begin{aligned}
u_1 &= A\lambda_1 \sin(\lambda ct)\cos(\lambda_2 x_2)\sin(\lambda_1 x_1) \\
u_2 &= A\lambda_2 \sin(\lambda ct)\sin(\lambda_2 x_2)\cos(\lambda_1 x_1) \\
p &= -\rho\lambda^2 c^2 A \sin(\lambda ct)\cos(\lambda_2 x_2)\cos(\lambda_1 x_1)
\end{aligned}
\tag{6.3}
$$

with

$$
\begin{aligned}
\lambda_1 &= \frac{n\pi}{L_1} \qquad n = 0, 1, 2, \quad ... \\
\lambda_2 &= \frac{m\pi}{2L_2} \qquad m = 1, 3, 5, \quad ... \\
\lambda^2 &= \lambda_1^2 + \lambda_2^2 \\
\omega &= c\lambda
\end{aligned}
\tag{6.4}
$$

Notice that the free surface condition is $p = 0$ with no gravity effects and if no further mathematical assumptions are made on the displacements of the free surface, we shall expect surface elevations for some modes (indicated from the analytical solutions in Eqs. (6.3)).

In this thesis, we use the same mesh as was used in [2] [11], however, we apply $9/4-c$ and $9/3$ elements for the **u**/p formulation and $9-4c-4c$ and $9-3-3$ elements for the **u**-p-$\mathbf{\Lambda}$ formulation. The lowest four displacement modes are shown in Fig. 6-2, and Fig. 6-3 gives the corresponding pressure distributions. There is no spurious non-zero frequency mode observed, therefore, it is clear that those reported non-zero frequency spurious modes were induced by the pure displacement-based formulation (including its penalty formulation), which should not be used for incompressible (or almost incompressible) materials. Interestingly, the difference of the **u**/p and **u**-p-

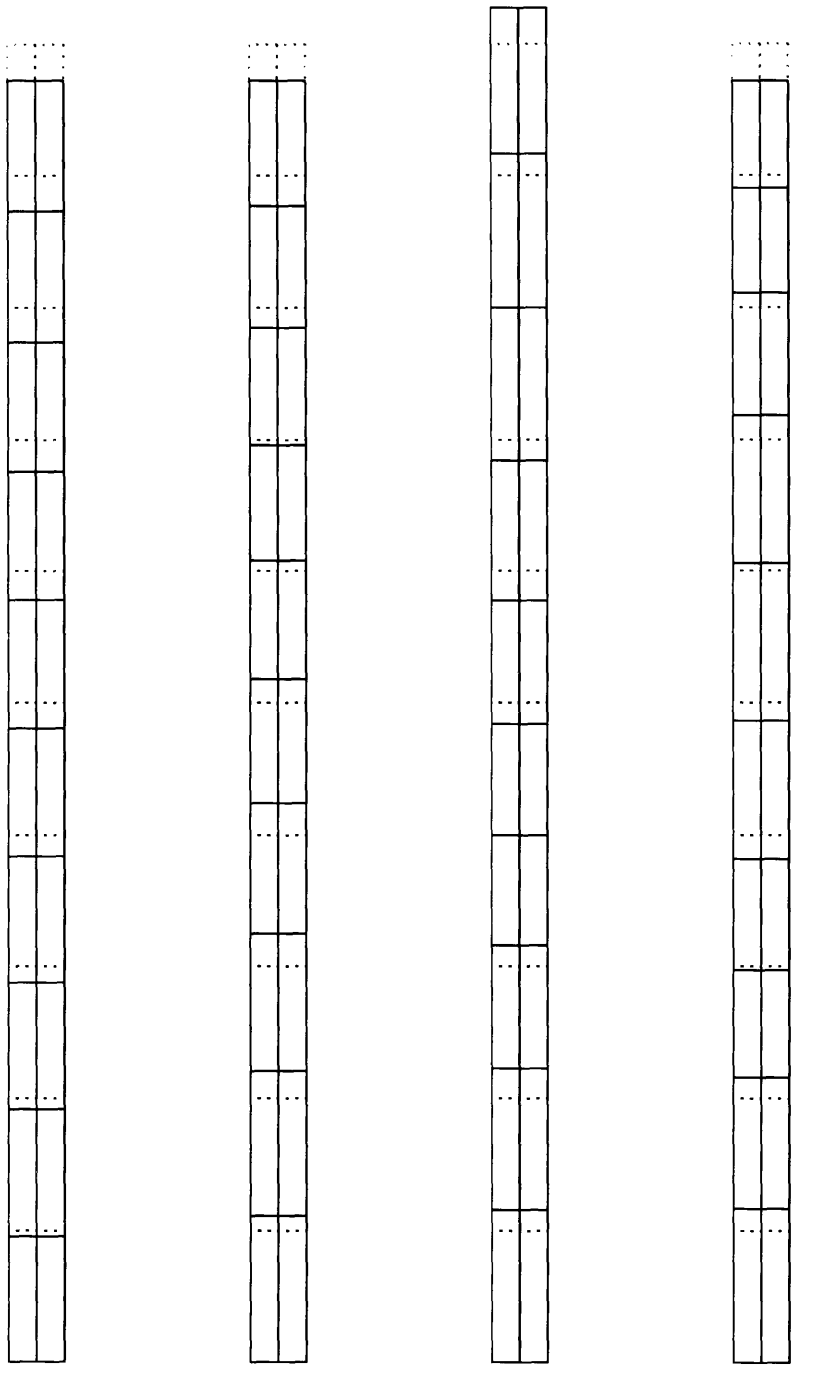

Figure 6-2: First four modes of the tall water column problem.

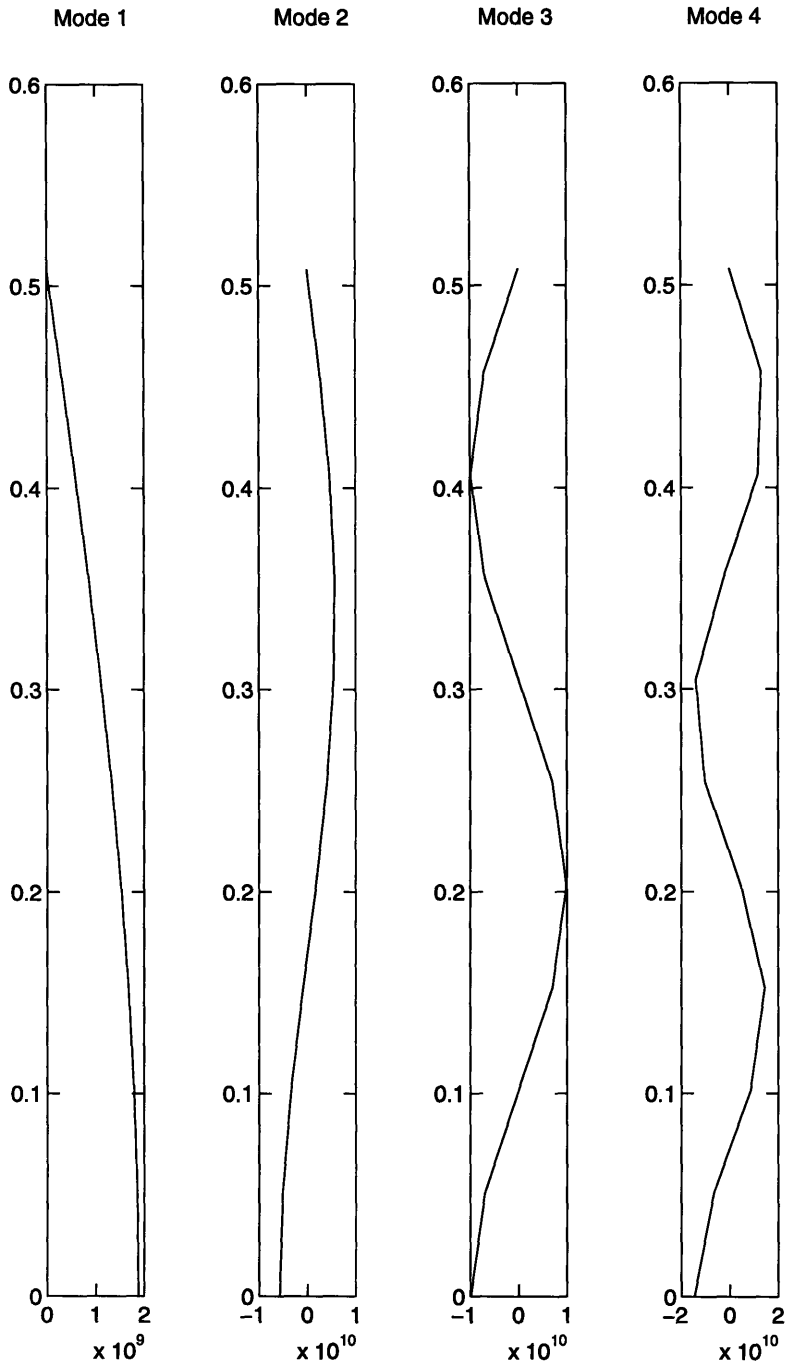

Figure 6-3: Pressure distributions corresponding to the first four modes of the tall water column problem.

Mode #	Frequencies (rad/sec)	n,m
1	4567.74	$n = 0, \quad m = 1$
2	13703.2	$n = 0, \quad m = 3$
3	22838.7	$n = 0, \quad m = 5$
4	31974.2	$n = 0, \quad m = 7$

Table 6-1: Analytic solution of acoustic frequencies of the tall water column problem.

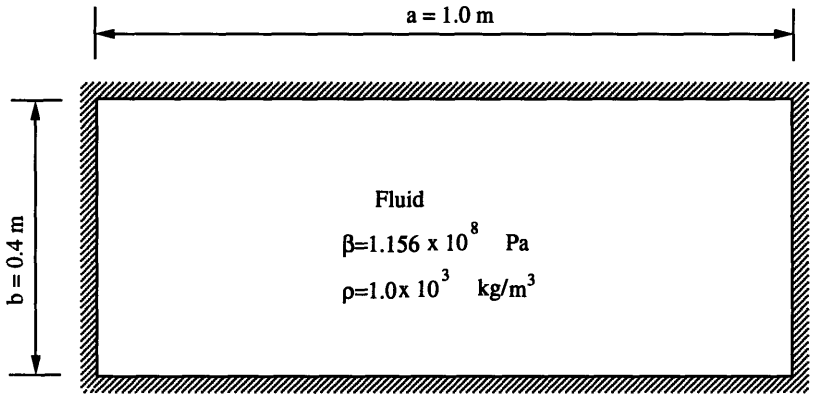

Figure 6-4: Rigid cavity problem.

$\mathbf{\Lambda}$ formulations is mainly the number of zero frequency modes as discussed in Chapter 3 and 4. The number of zero frequency modes from the **u**/p formulation is greater than the number of zero frequency modes from the **u**-p-$\mathbf{\Lambda}$ formulation, and the difference between the two is the number of $\mathbf{\Lambda}$ unknowns. The analytical solution of the frequencies are listed in Tab. 6-1.

Tab. 6-2 gives the frequency solutions using both the **u**/p and **u**-p-$\mathbf{\Lambda}$ formulations with different mixed finite elements.

6.1.2 Rigid Cavity Problem

In the reference [9], Hamdi, et al tested the rigid cavity problem shown in Fig 6-4.

The analytical frequency solution is,

	Mixed Finite Element Choice							
	$9/4-c$	$9-4c-4c$	$9/3$	$9-3-3$	$4/1$	$4-1-1$	Type I $4/1$ (Macro)	Type I $4-1-1$ (Macro)
Zero modes (Theory)	130	97	103	43	83	3	103	3
Zero modes (Result)	130	97	103	43	83	3	103	3
First four acoustic modes (rad/sec)	4567.77	4567.77	4567.74	4567.74	4568.92	4568.91	4584.36	4568.49
	13709.8	13709.8	13703.7	13703.7	13734.9	13734.9	13769.6	13723.6
	22915.4	22915.4	22844.6	22844.6	22985.7	22985.7	23007.7	22933.4
	32332.9	32332.9	32004.8	32004.8	32378.3	32378.3	32342.2	32236.3

Table 6-2: Frequency analysis of the tall water column problem.

	Mixed Finite Element Choice							
	$9/4-c$	$9-4c-4c$	$9/3$	$9-3-3$	$4/1$	$4-1-1$	Type I $4/1$ (Macro)	Type I $4-1-1$ (Macro)
Zero modes (Theory)	75	55	59	23	47	-1	59	-1
Zero modes (Result)	75	55	59	23	47	0	59	0
First four acoustic modes (Hz)	170.6	170.6	170.0	170.0	171.1	171.1	172.6	170.4
	353.5	353.5	341.3	341.3	348.8	348.8	347.8	342.7
	429.5	429.5	425.3	425.3	429.9	429.9	429.5	428.1
	462.2	462.1	468.1	468.3	459.3	459.3	464.0	461.8

Table 6-3: Frequency analysis of the rigid cavity problem.

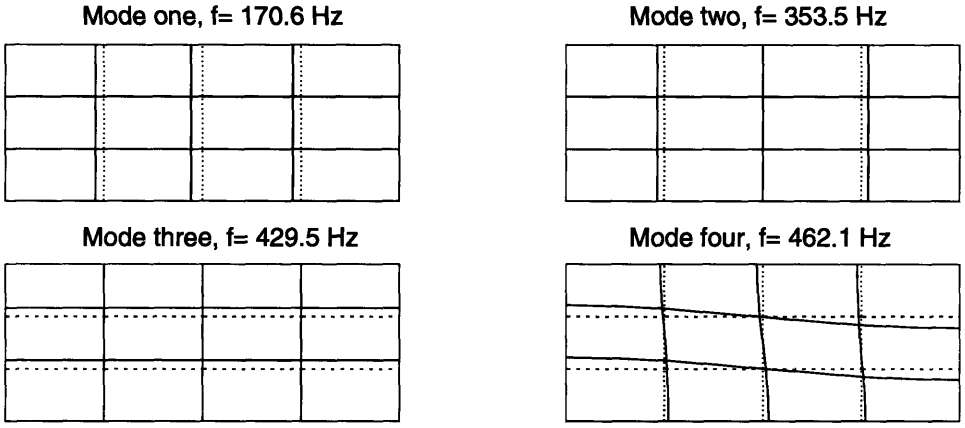

Figure 6-5: First four modes of the rigid cavity problem.

Mode #	Frequencies (Hz)	n,m
1	170.0	$n = 1, \quad m = 0$
2	340.0	$n = 2, \quad m = 0$
3	425.0	$n = 0, \quad m = 1$
4	457.7	$n = 1, \quad m = 1$

Table 6-4: Analytic solution of acoustic frequencies of the rigid cavity problem.

$$\omega = c\pi\sqrt{(\frac{n}{a})^2 + (\frac{m}{b})^2} \tag{6.5}$$

where n, m are integers and c is the acoustic speed.

Figs. 6-5 and 6-6 show the mode shapes and the pressure bands of the first four non-zero frequencies. Tab. 6-3 lists the frequencies calculated with both the **u**/p and **u**-p-$\mathbf{\Lambda}$ formulations with different types of mixed elements. The first four analytical frequencies calculated from Eq. (6.5) are listed in Tab. 6-4.

It was reported in [9] that the displacement-based formulation introduced non-zero frequency spurious modes (which were identified as rotational modes) and these spurious modes could be eliminated by applying a penalty term of the irrotationality

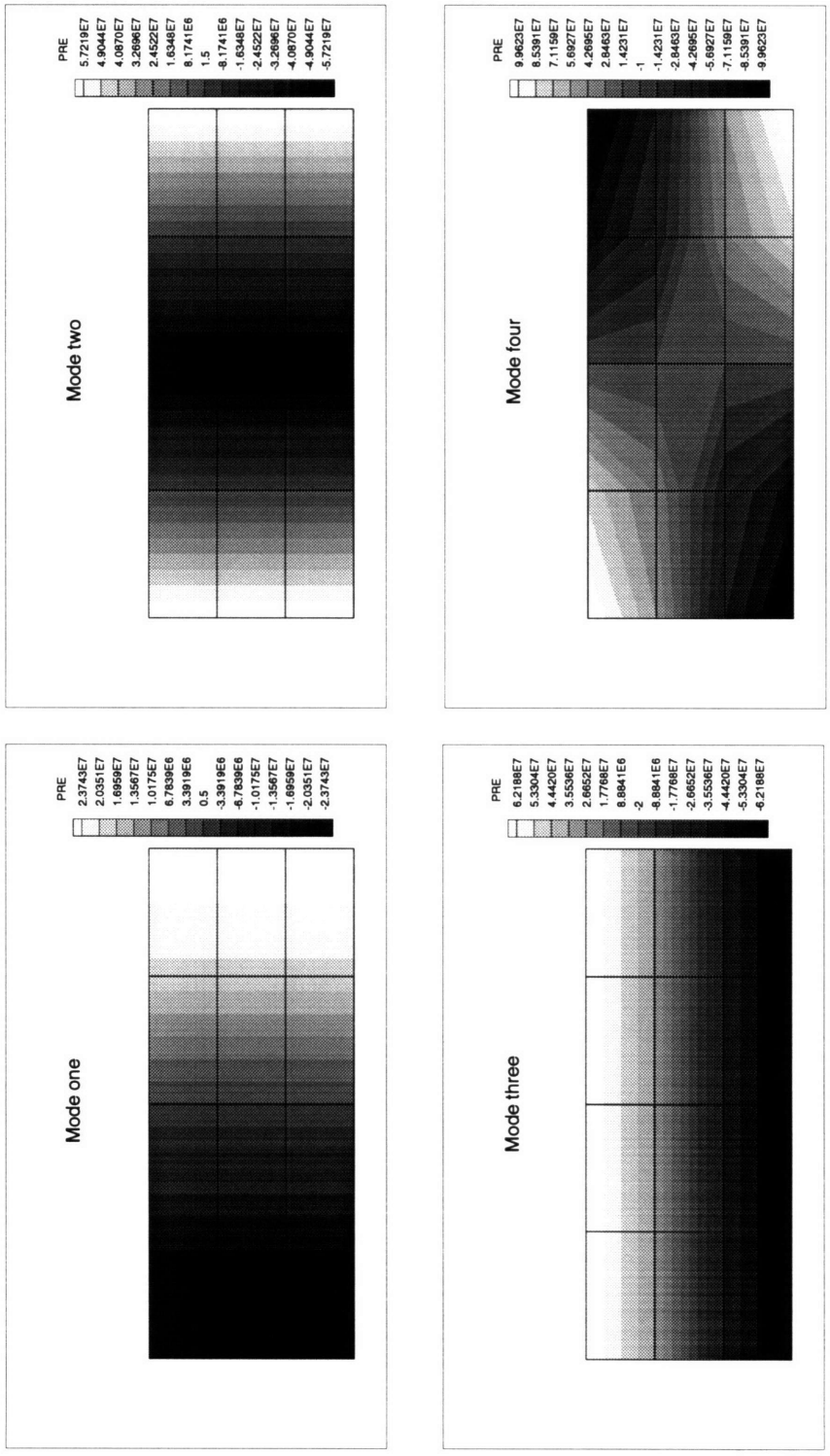

Figure 6-6: Pressure bands of the first four modes of the rigid cavity problem.

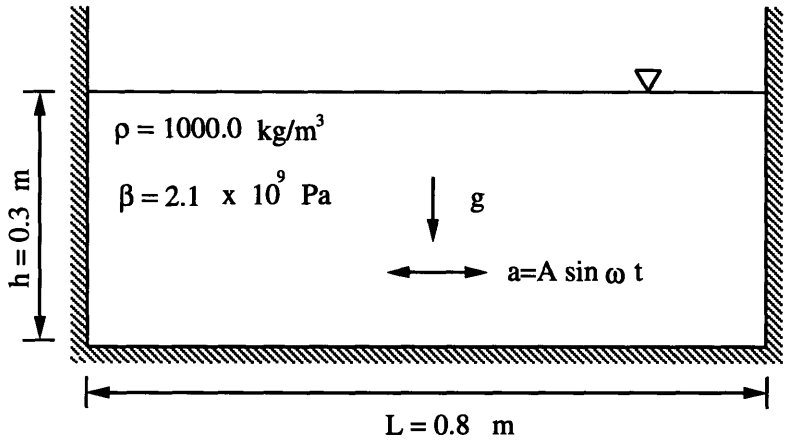

Figure 6-7: Sloshing water tank problem.

constraint of Eq. (2.17). From the calculated results, we conclude that if we use the u/p or u-p-Λ formulation with elements satisfying the inf-sup condition, we will not encounter the spurious non-zero frequency rotational modes. In actuality, the spurious rotational modes are related to the familiar spurious pressure modes (through Eq. (4.27)).

6.1.3 Sloshing Problem

To demonstrate the capability of predicting the sloshing modes, we analyze a rigid rectangular tank shown in Fig. 6-7. The analytical solution of the sloshing frequencies is given as,

$$\omega = \sqrt{gktanh(kh)} \tag{6.6}$$

where $kL = n\pi, \quad n = 1, 2, 3, ...$

The acoustic frequency can be calculated from Eqs. (6.4). The computed fre-

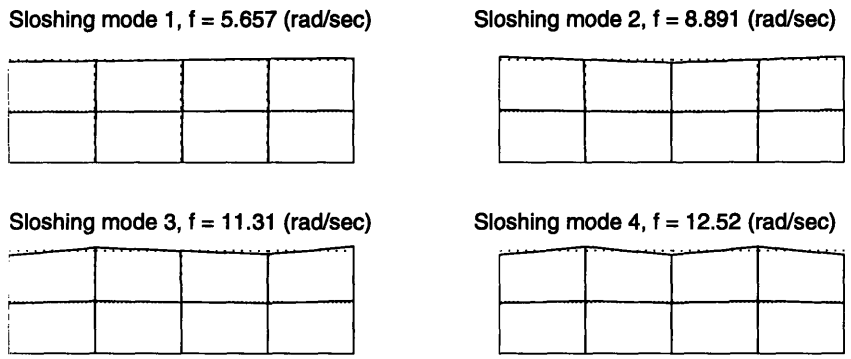

Figure 6-8: First four sloshing modes of the sloshing water tank problem.

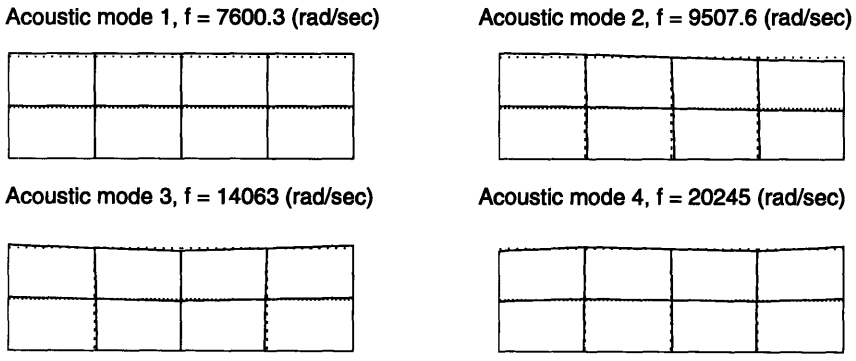

Figure 6-9: First four acoustic modes of the sloshing water tank problem.

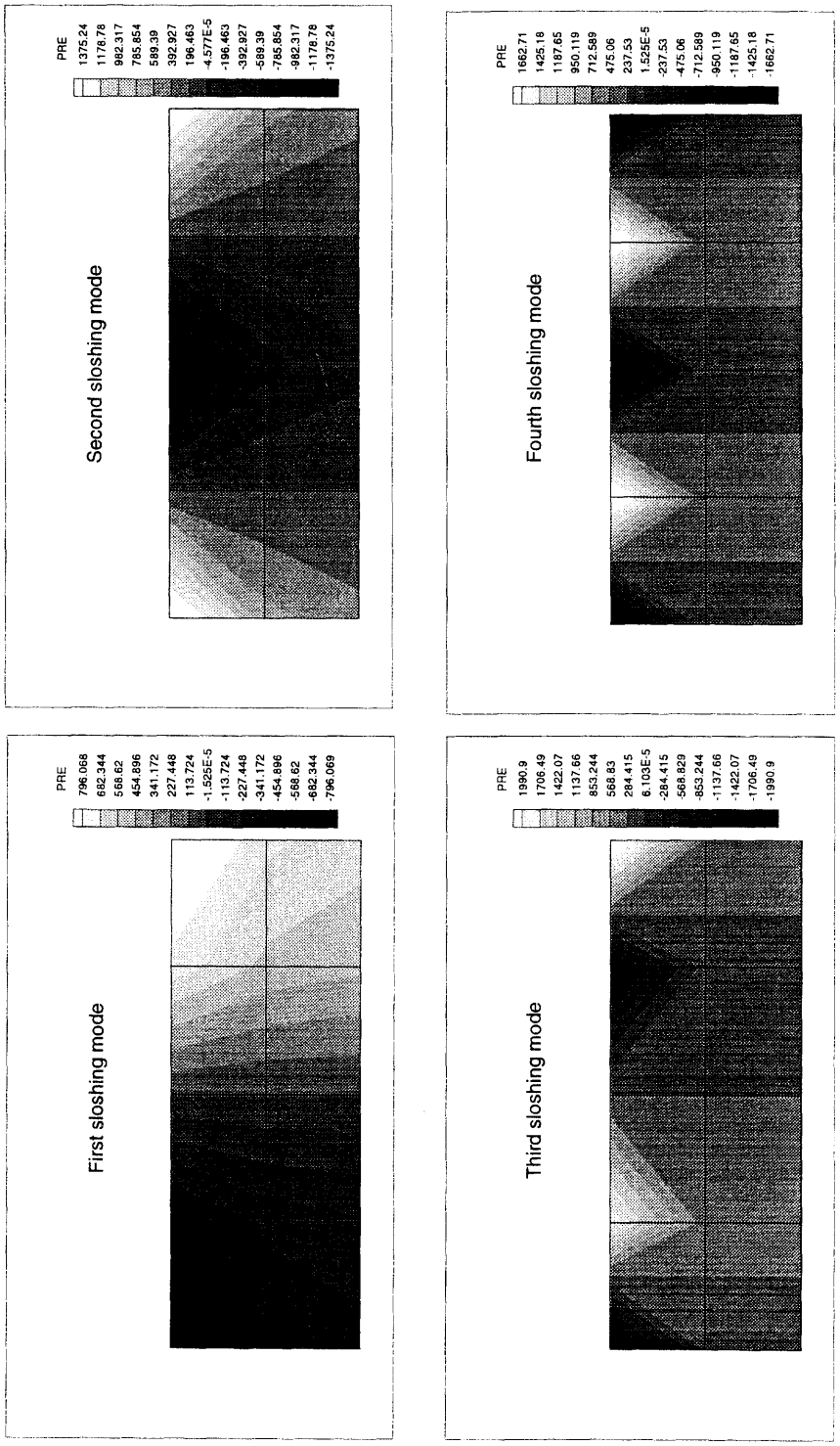

Figure 6-10: Pressure bands of sloshing modes of the sloshing water tank problem.

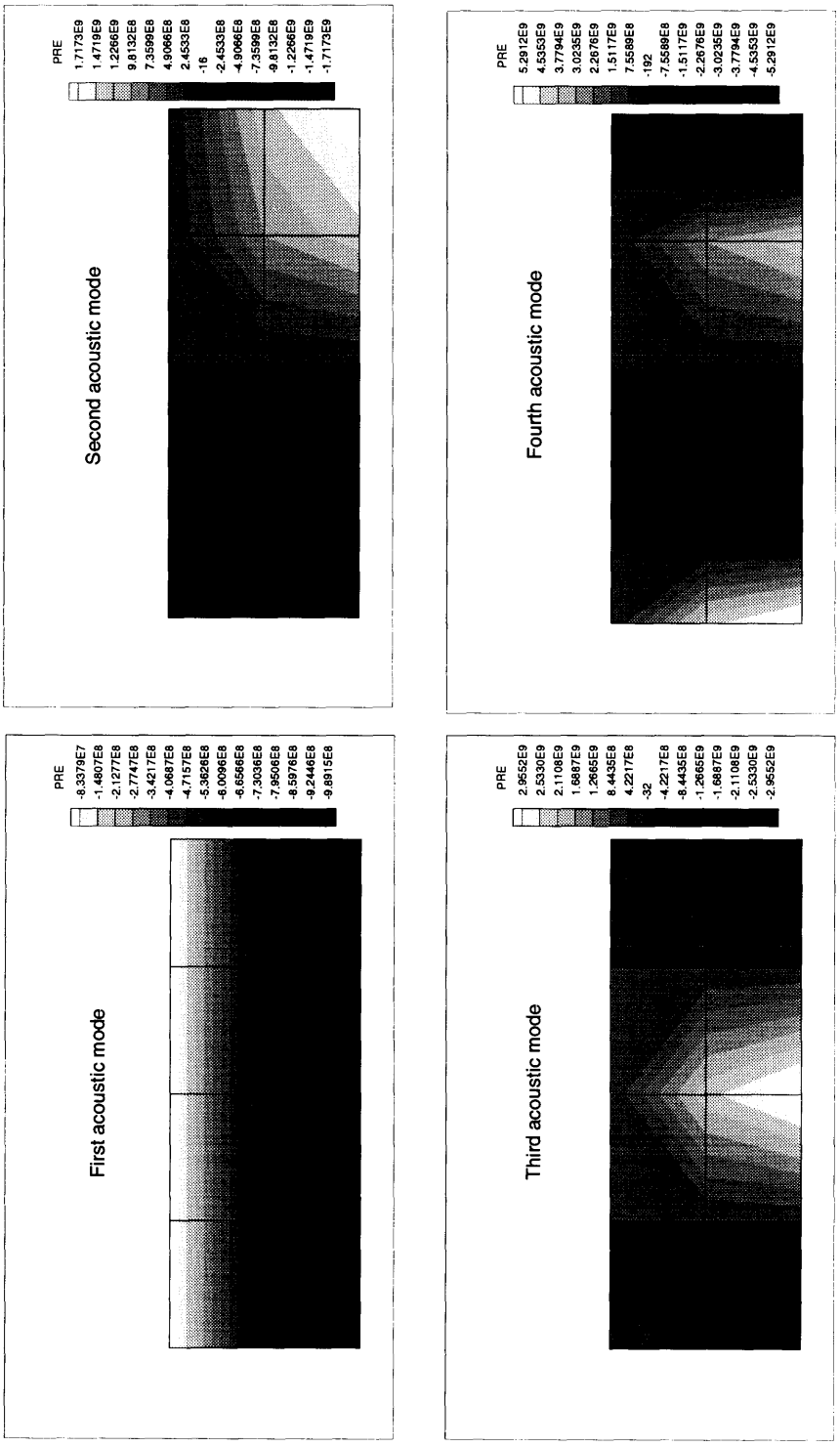

Figure 6-11: Pressure bands of acoustic modes of the sloshing water tank problem.

	Mixed Finite Element Choice							
	$9/4-c$	$9-4c-4c$	$9/3$	$9-3-3$	$4/1$	$4-1-1$	Type I $4/1$ (Macro)	Type I $4-1-1$ (Macro)
Zero modes (Theory)	48	33	39	15	31	-1	47	-1
Zero modes (Result)	48	33	39	15	31	0	47	0
First four sloshing modes (rad/sec)	5.657	5.656	5.713	5.712	5.684	5.683	5.711	5.639
	8.891	8.882	9.308	9.295	8.838	8.8170	8.833	8.680
	11.31	11.25	12.02	12.00	11.09	10.99	11.01	8.935
	12.52	12.45	17.08	16.65	13.17	12.85	13.20	10.69
First four acoustic modes (rad/sec)	7600.3	7600.4	7589.6	7589.6	7636.5	7636.5	7643.8	7619.1
	9507.6	9506.5	9834.0	9817.6	9486.6	9483.7	9602.2	9541.4
	14063	14058	14861	14775	13783	13775	13993	13853
	20245	20234	20732	20607	19327	19317	19390	19127

Table 6-5: Frequency analysis of the sloshing water tank problem.

Mode #	Sloshing frequencies (rad/sec)	Acoustic frequencies (rad/sec)	n,m
1	5.641	7,587.67	$n = 0, \quad m = 1$
2	8.695	9,484.58	$n = 1, \quad m = 1$
3	10.74	13,678.86	$n = 2, \quad m = 1$
4	12.41	18,682.46	$n = 3, \quad m = 1$

Table 6-6: Analytic solution of acoustic frequencies of the sloshing water tank problem.

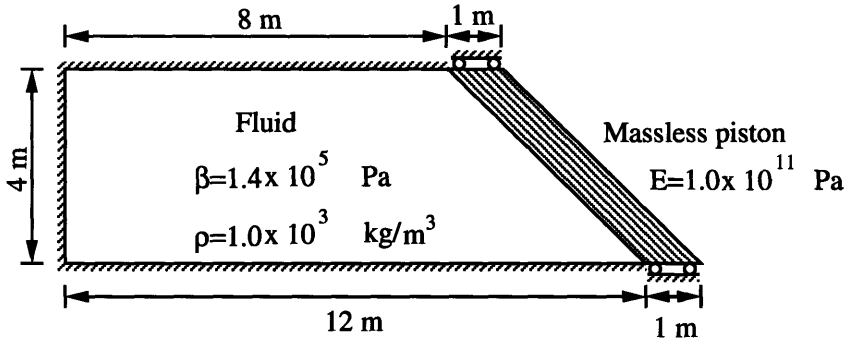

Figure 6-12: Tilted piston-container system.

quencies are listed in Tab. 6-5; while the analytical frequency solutions for both the sloshing and acoustic modes are listed in Tab. 6-6.

The first four sloshing and acoustic modes and their pressure bands are shown in Figs. 6-8, 6-9, 6-10 and 6-11 respectively.

6.1.4 Fluid-structure Interaction Problems

Fig. 6-12 describes the tilted piston-container problem. The massless elastic piston moves horizontally. Fig. 6-13 describes the problem of a rigid cylinder vibrating in an acoustic cavity. The cylinder is suspended from a spring and vibrates vertically in the fluid. Fig. 6-14 shows a rigid ellipse on a spring in the same acoustic cavity.

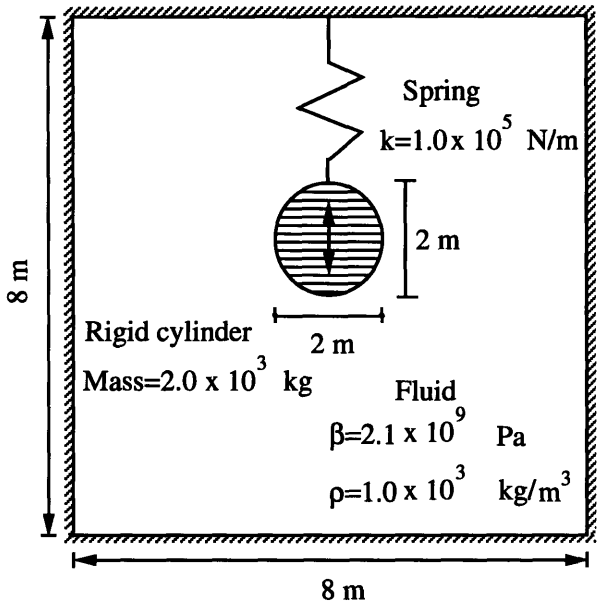

Figure 6-13: A rigid cylinder vibrating in an acoustic cavity.

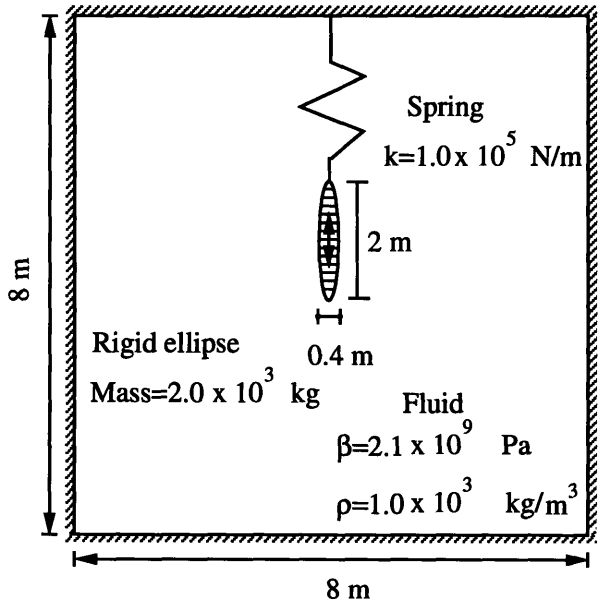

Figure 6-14: A rigid ellipse vibrating in an acoustic cavity.

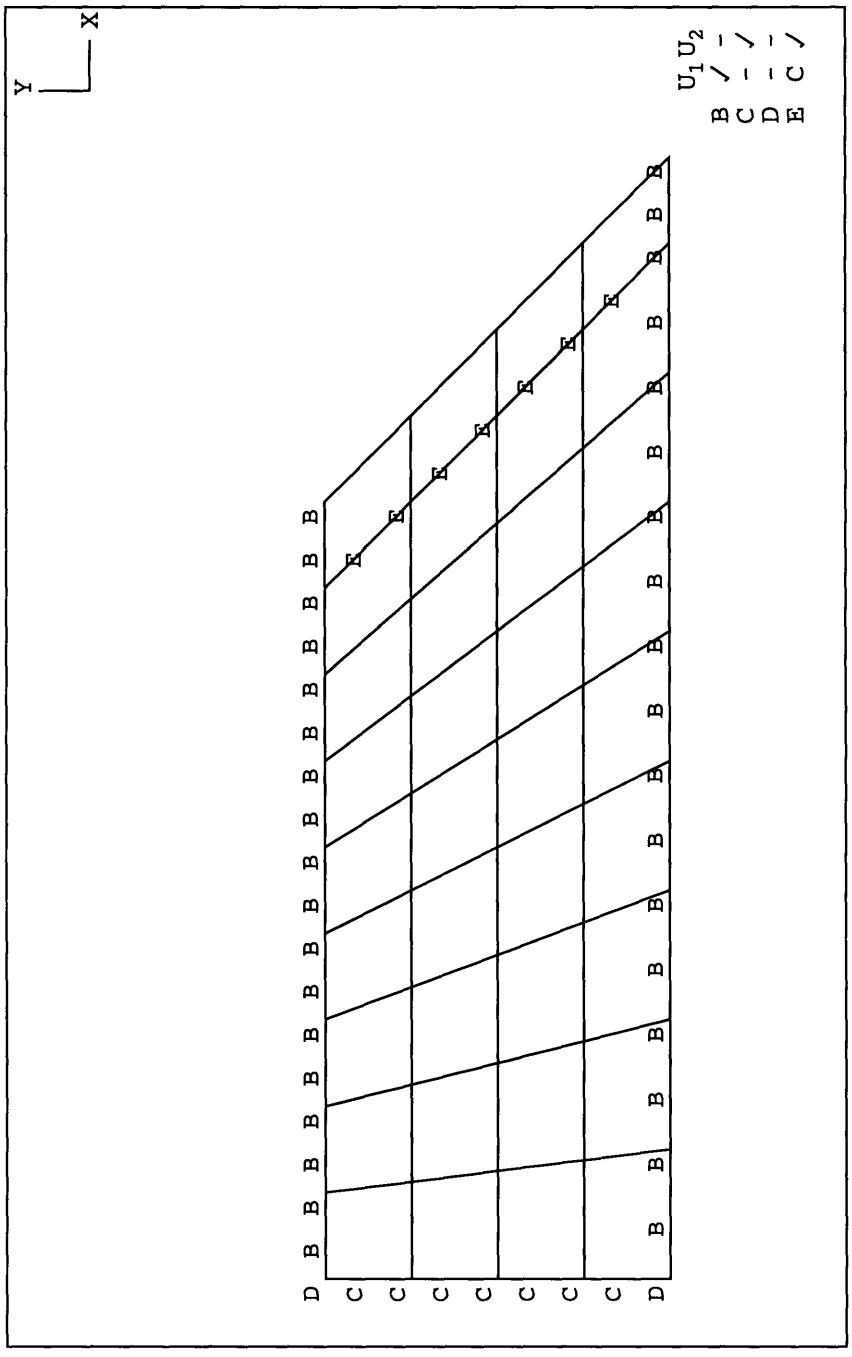

Figure 6-15: Typical mesh for the tilted piston-container system.

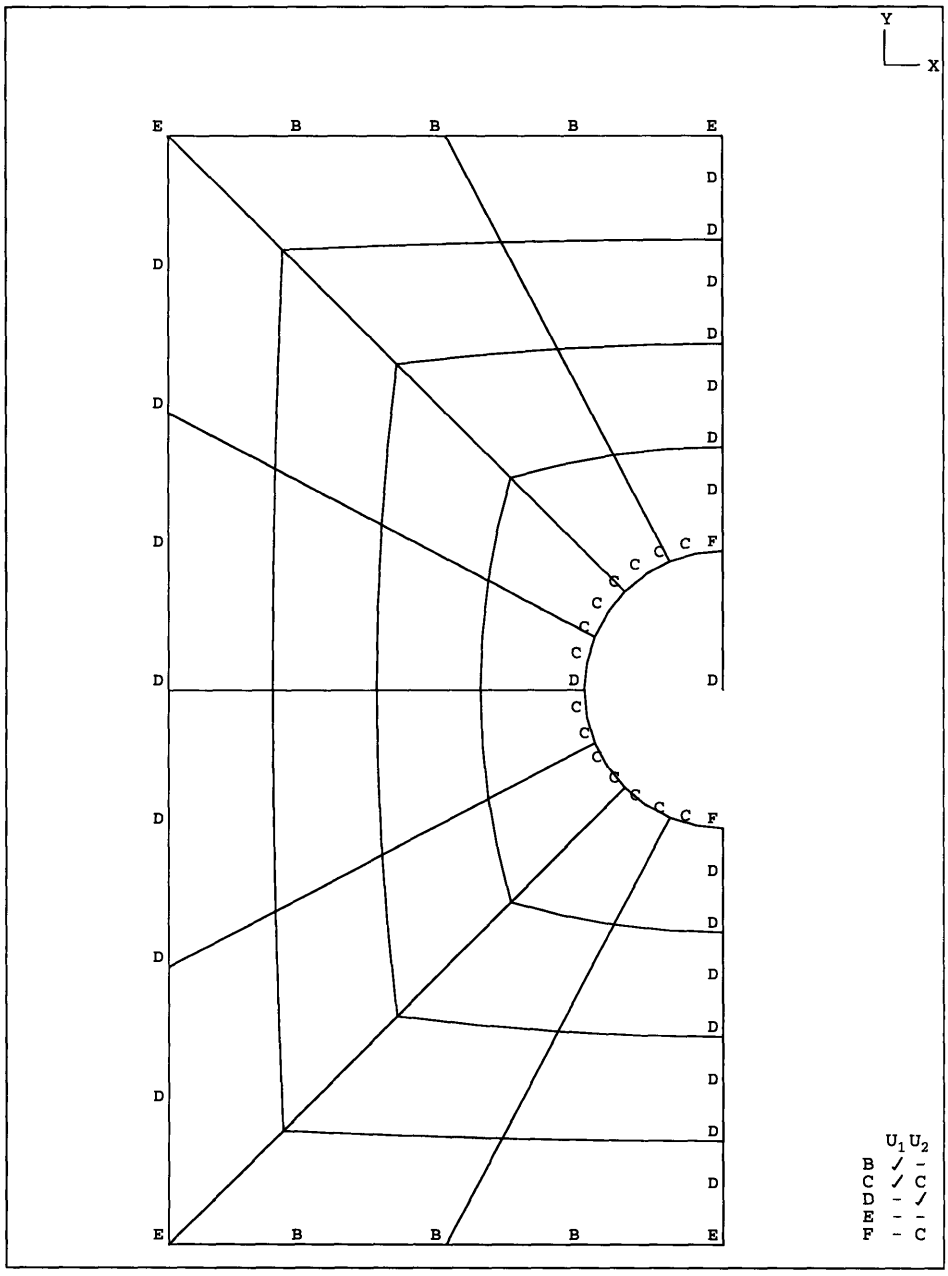

Figure 6-16: Typical mesh for the rigid cylinder problem.

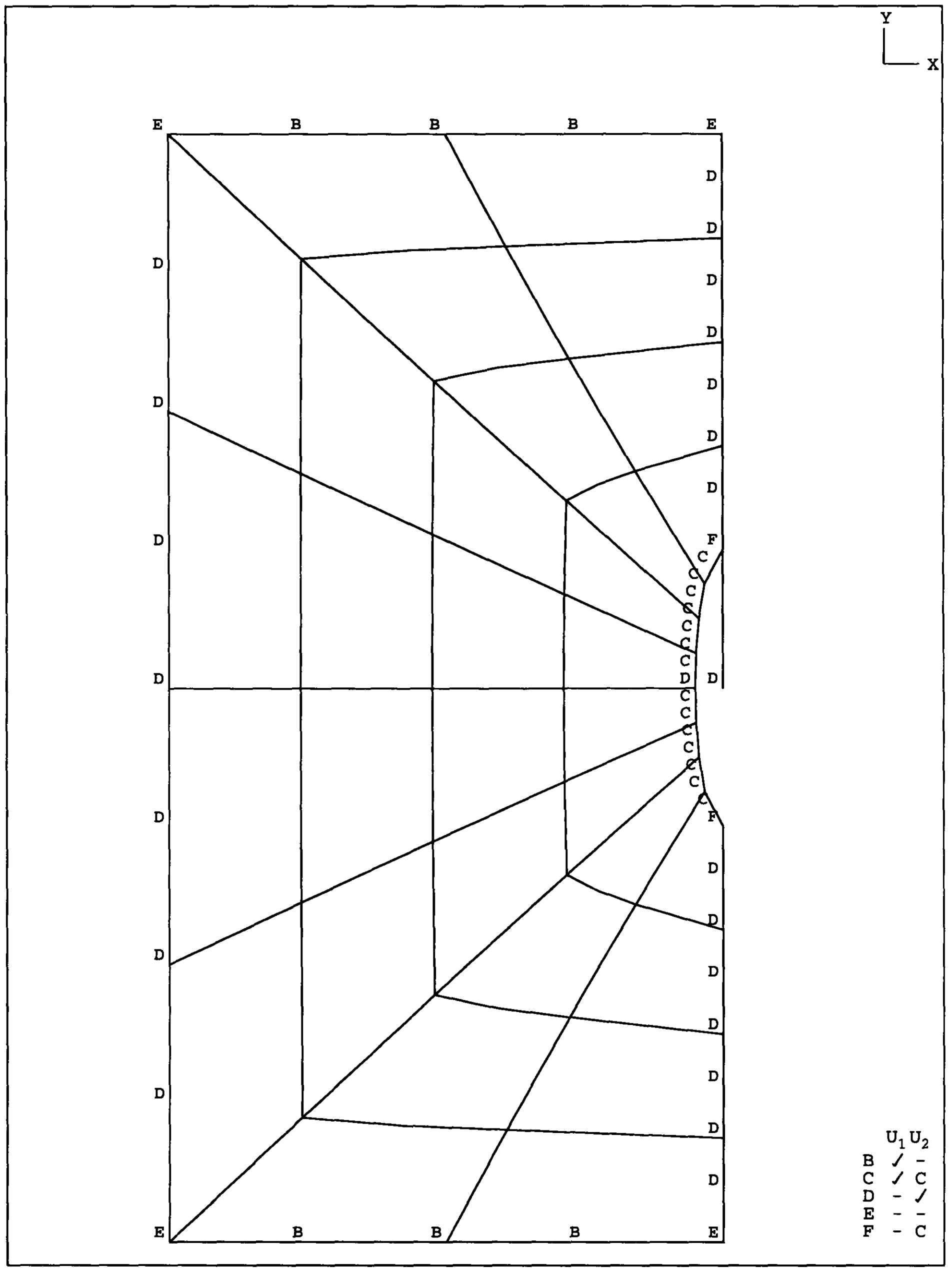

Figure 6-17: Typical mesh for the rigid ellipse problem.

Test case	Mesh, no. of elements	Number of zero frequencies		Frequencies (rad/sec)			
		Theory	Result	First	Second	Third	Fourth
Tilted	4	≥ 19	19	1.898	6.063	9.275	10.45
piston-	16	≥ 79	79	1.867	5.702	9.239	9.808
container	32	≥ 159	159	1.862	5.605	9.192	9.397
Rigid	2	≥ 7	7	3.899	718.2	1178	1326
cylinder	8	≥ 37	37	4.259	611.5	1193	1330
problem	32	≥ 157	157	4.285	589.6	1138	1254
Rigid	2	≥ 7	7	6.192	697.8	1216	1269
ellipse	8	≥ 37	37	6.755	591.7	1229	1235
problem	32	≥ 157	157	6.848	572.6	1157	1178

Table 6-7: Analysis of test problems using the **u**/p formulation with 9/3 elements.

Test case	Mesh, no. of elements	Number of zero frequencies		Frequencies (rad/sec)			
		Theory	Result	First	Second	Third	Fourth
Tilted	4	≥ 7	7	1.895	6.054	9.256	10.32
piston-	16	≥ 31	31	1.867	5.696	9.236	9.792
container	32	≥ 63	63	1.862	5.603	9.189	9.391
Rigid	2	≥ 1	1	3.846	628.2	928.6	1341
cylinder	8	≥ 13	13	4.228	609.5	1191	1326
problem	32	≥ 61	61	4.281	589.4	1138	1252
Rigid	2	≥ 1	1	5.511	629.9	932.6	1246
ellipse	8	≥ 13	13	6.612	589.1	1220	1232
problem	32	≥ 61	61	6.827	572.1	1155	1176

Table 6-8: Analysis of test problems using the **u**-p-$\mathbf{\Lambda}$ formulation with 9-3-3 elements.

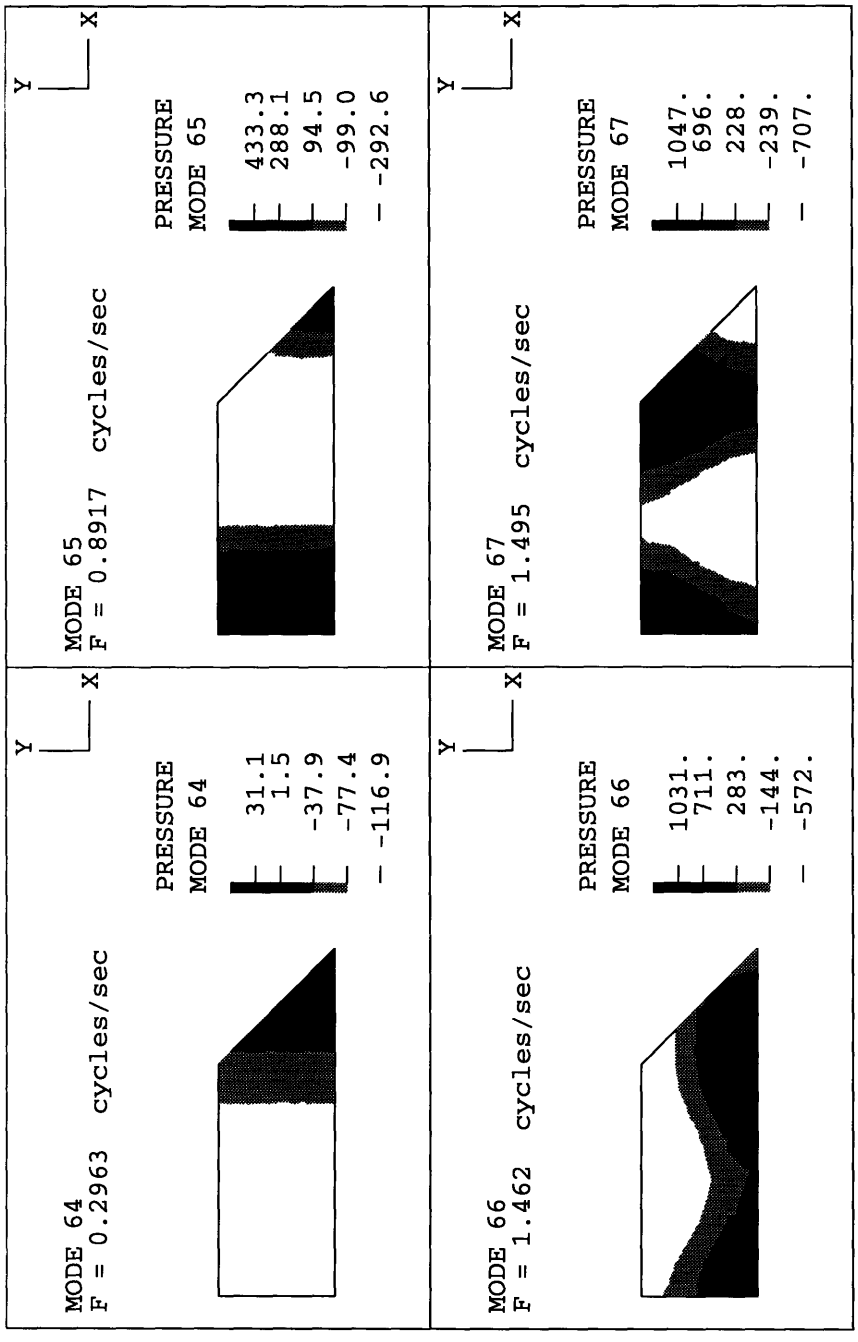

Figure 6-18: Pressure bands of the first four modes of the tilted piston-container problem. (Mesh of thirty-two 9-3-3 elements.)

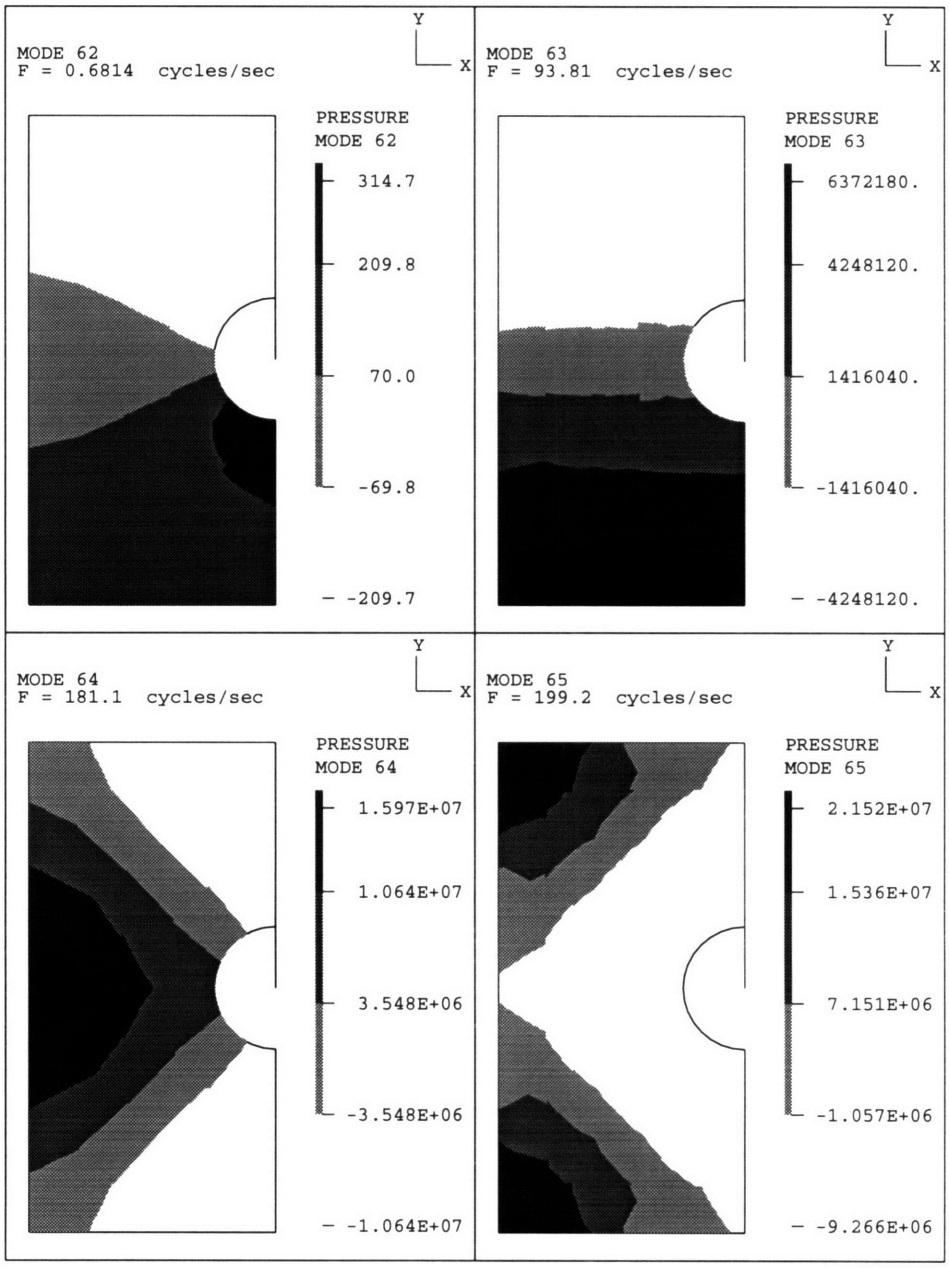

Figure 6-19: Pressure bands of the first four modes of the rigid cylinder problem. (Mesh of thirty-two 9-3-3 elements.)

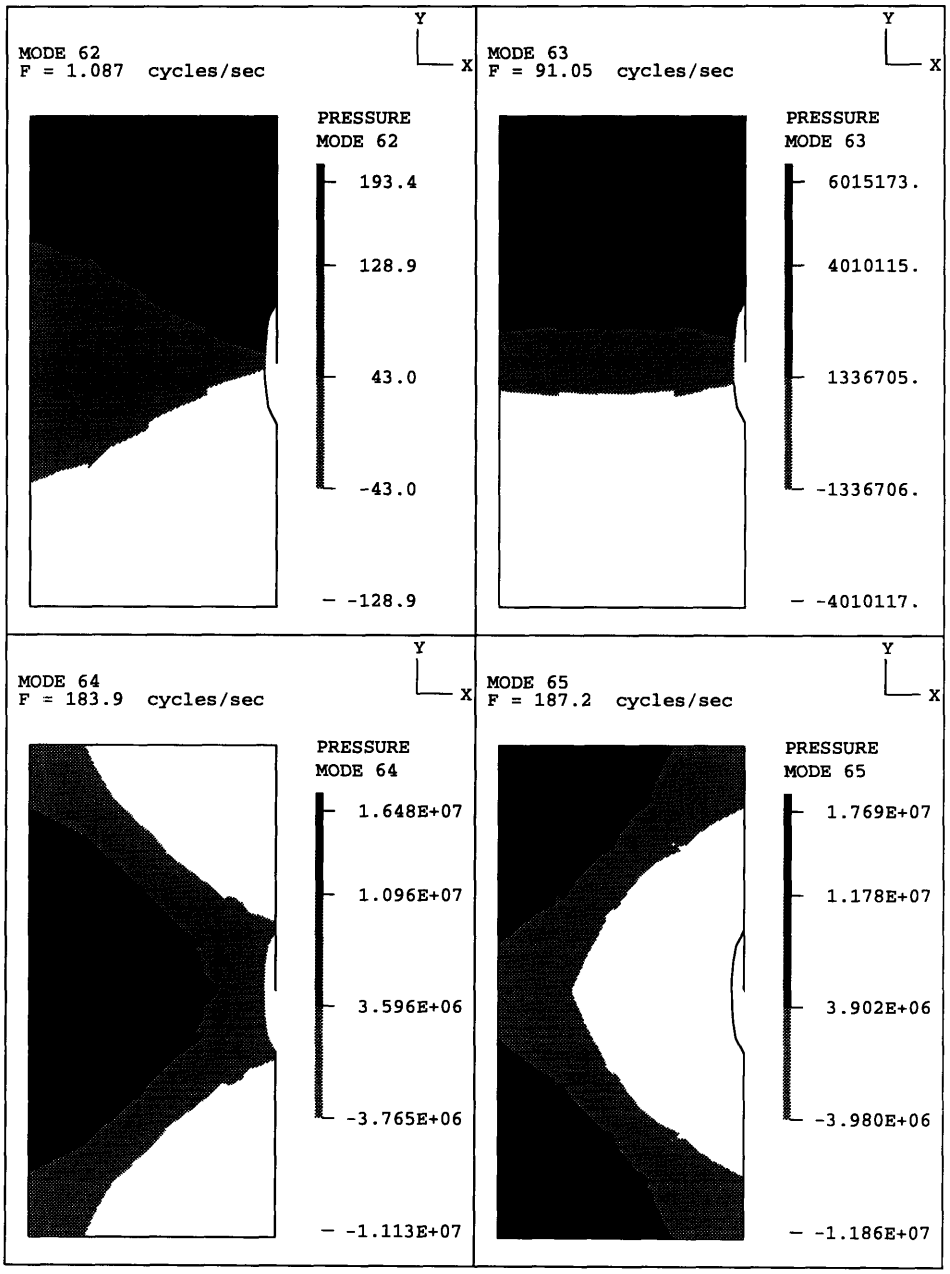

Figure 6-20: Pressure bands of the first four modes of the rigid ellipse problem. (Mesh of thirty-two 9-3-3 elements.)

Test case	Mesh, no. of elements	Frequencies (rad/sec) First	Second	Third	Fourth
Tilted piston problem	32	1.858	5.569	9.116	9.299
Rigid cylinder problem	32	4.269	581.8	1124	1224
Rigid ellipse problem	32	7.071	563.2	1138	1158

Table 6-9: Results obtained using the $\mathbf{u} - \phi$ formulation for analysis of three test problems.

Figs. 6-15, 6-16 and 6-17 show the typical meshes used in these problems. Tab. 6-8 and Tab. 6-7 list the results obtained using the $9-3-3$ element and 9/3 element, and Tab. 6-9 gives the results obtained with the velocity potential (that is $\mathbf{u} - \phi$) formulation [14] which can be considered a very reliable procedure (refer to Chapter 7). The meshes used in this analysis have been derived by starting with coarse meshes and subdividing in each refinement each element into two or four elements.

Figs. 6-18, 6-19 and 6-20 show the pressure band plots of the modes considered in Tab. 6-7. The frequencies from the incompressible fluid model (with added mass effects) are the upper bound of the calculated frequencies in Tab. 6-8 and Tab. 6-7. This matches with the mathematical prediction in [58].

To illustrate the importance of assigning the appropriate tangential displacement directions at the fluid nodal points on the fluid-structure interfaces, we present the results of two test cases.

In the first test case, the very coarse finite element model shown in Fig. 6-21 for the response analysis of the rigid cylinder is considered. The assignment of the correct tangential directions at nodes 10 and 11 is critical. If we use the actual cylinder geometry, the tangential directions are 60 and 120 degrees from the x-axis. However, using Eq. (5.22) we obtain 45 and 135 degrees, respectively. Tab. 6-10 lists some solution results and shows that a spurious non-zero frequency appears when the incorrect tangential directions are assigned.

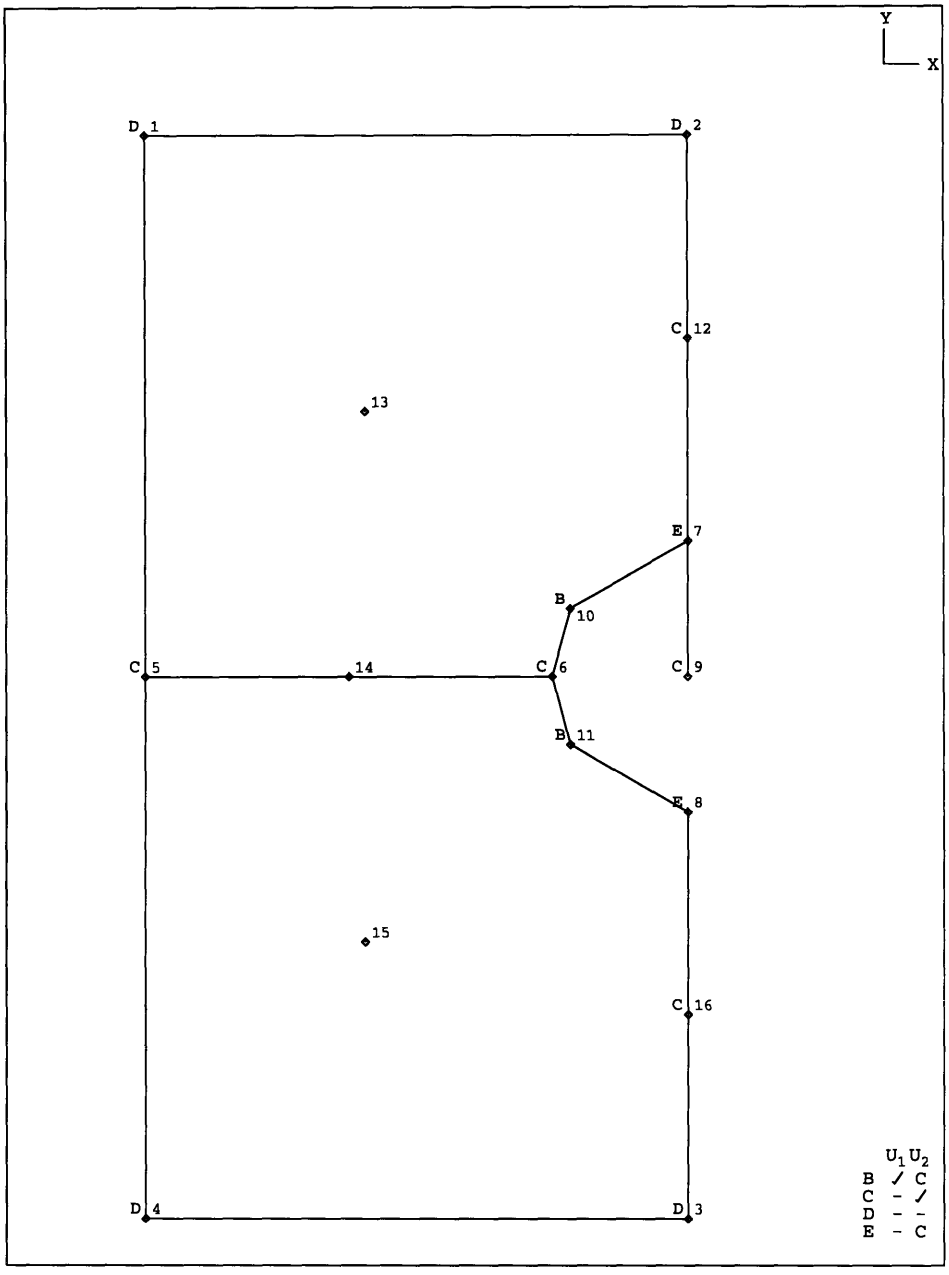

Figure 6-21: Response analysis of rigid cylinder; use of two 9-3-1 elements.

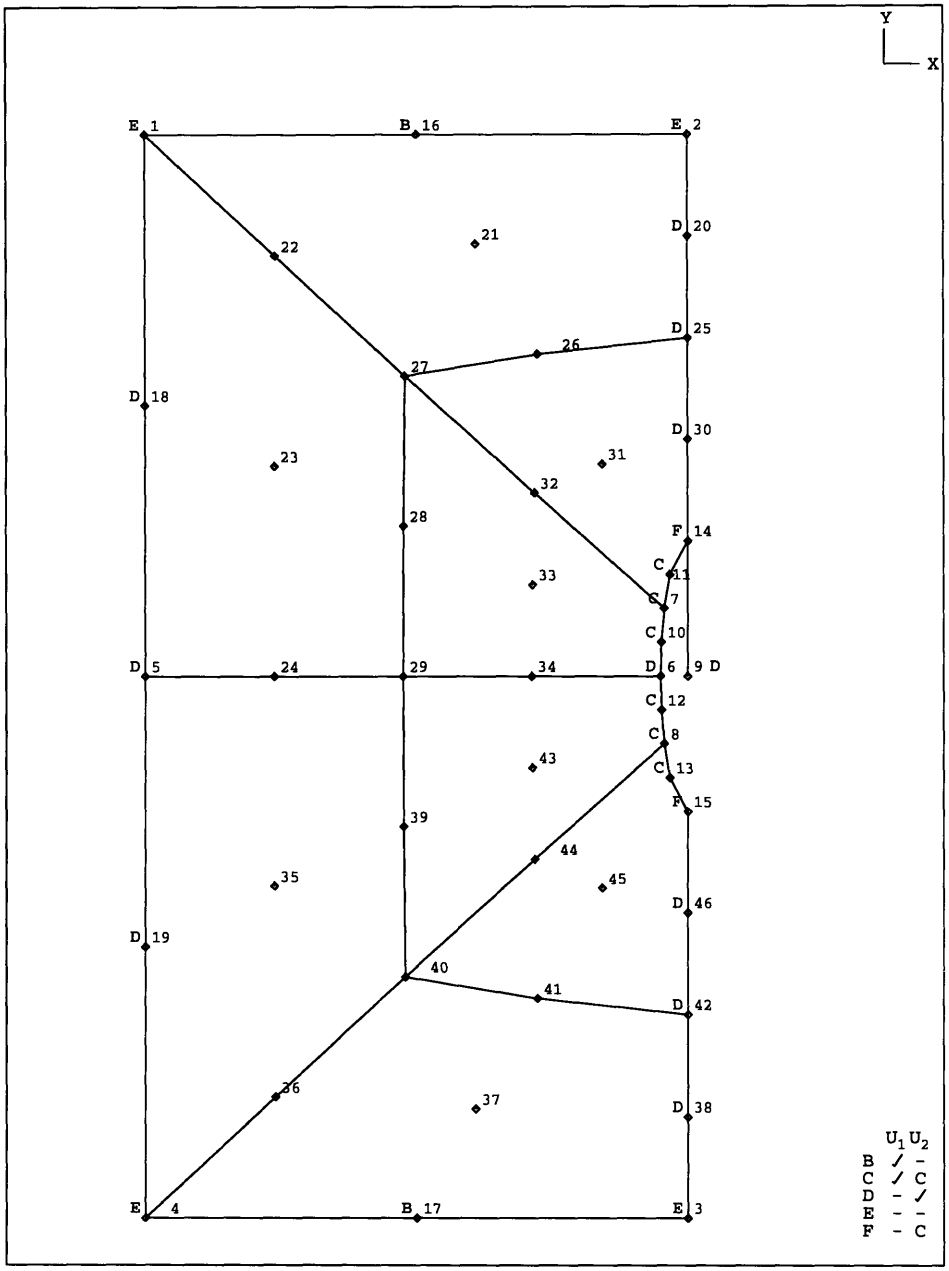

Figure 6-22: Response analysis of rigid ellipse; use of eight 9-3-3 elements.

Test case	Tangent direction	Number of zero frequencies		Frequencies (rad/sec)			
		Theory	Result	First	Second	Third	Fourth
Rigid cylinder	incorrect	≥ 5	4	4.649	86.17*	693.7	1154
model in Fig. 6-21	correct	≥ 5	5	3.861	688.2	1169	1324
Rigid ellipse	incorrect	≥ 13	12	6.719	34.65*	591.4	1213
model in Fig. 6-22	correct	≥ 13	13	6.612	589.1	1220	1232

Table 6-10: Spurious modes (*) due to assignment of incorrect tangential displacement directions at the fluid-structure interfaces.

In the rigid ellipse test case, the finite element model shown in Fig. 6-22 is used for the frequency solution of the rigid ellipse vibrating in the fluid-filled cavity. If we use the tangential directions given by the actual geometry of the ellipse, a non-zero spurious frequency is calculated, whereas if the tangential directions are assigned using Eqs. (5.19) and (5.22), good solution results are obtained, see Tab. 6-10. The comparison of the angles (γ) from the x-axis obtained using Eqs. (5.19) and (5.22) with the angles using the actual geometry is as follows:

$$
\begin{aligned}
&\textit{node}\ \ 10: \quad \text{angle}\ \gamma|_{model} = 86.93^o \quad \text{angle}\ \gamma|_{geometry} = 87.04^o \\
&\textit{node}\ \ 7: \quad \text{angle}\ \gamma|_{model} = 87.40^o \quad \text{angle}\ \gamma|_{geometry} = 83.41^o \\
&\textit{node}\ \ 11: \quad \text{angle}\ \gamma|_{model} = 70.89^o \quad \text{angle}\ \gamma|_{geometry} = 77.22^o
\end{aligned}
$$

It is interesting to note that based on the mass transport requirement the angle γ at node 7 is larger than at node 10, which is an unexpected result based on the actual geometry of the ellipse.

We also show results obtained with the $4-1-1$ element. Since the 4/1 displacement/pressure element (that is, the element with 4 corner nodes for the displacement interpolation and a constant pressure assumption) for incompressible analysis does not satisfy the inf-sup condition, we expect that the $4-1-1$ element will not provide a

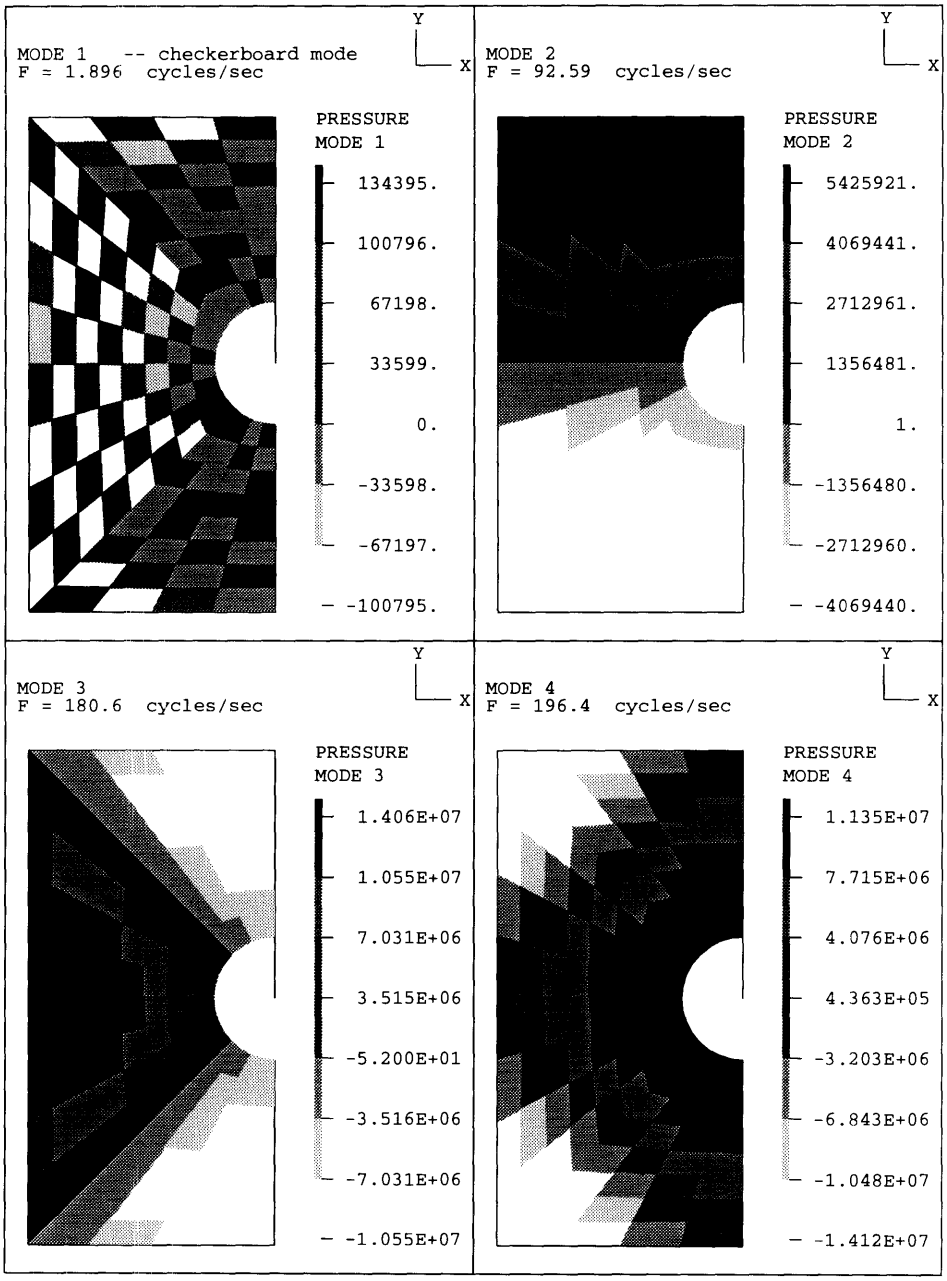

Figure 6-23: Checkerboard pressure band of the rigid cylinder problem with 4-1-1 elements.

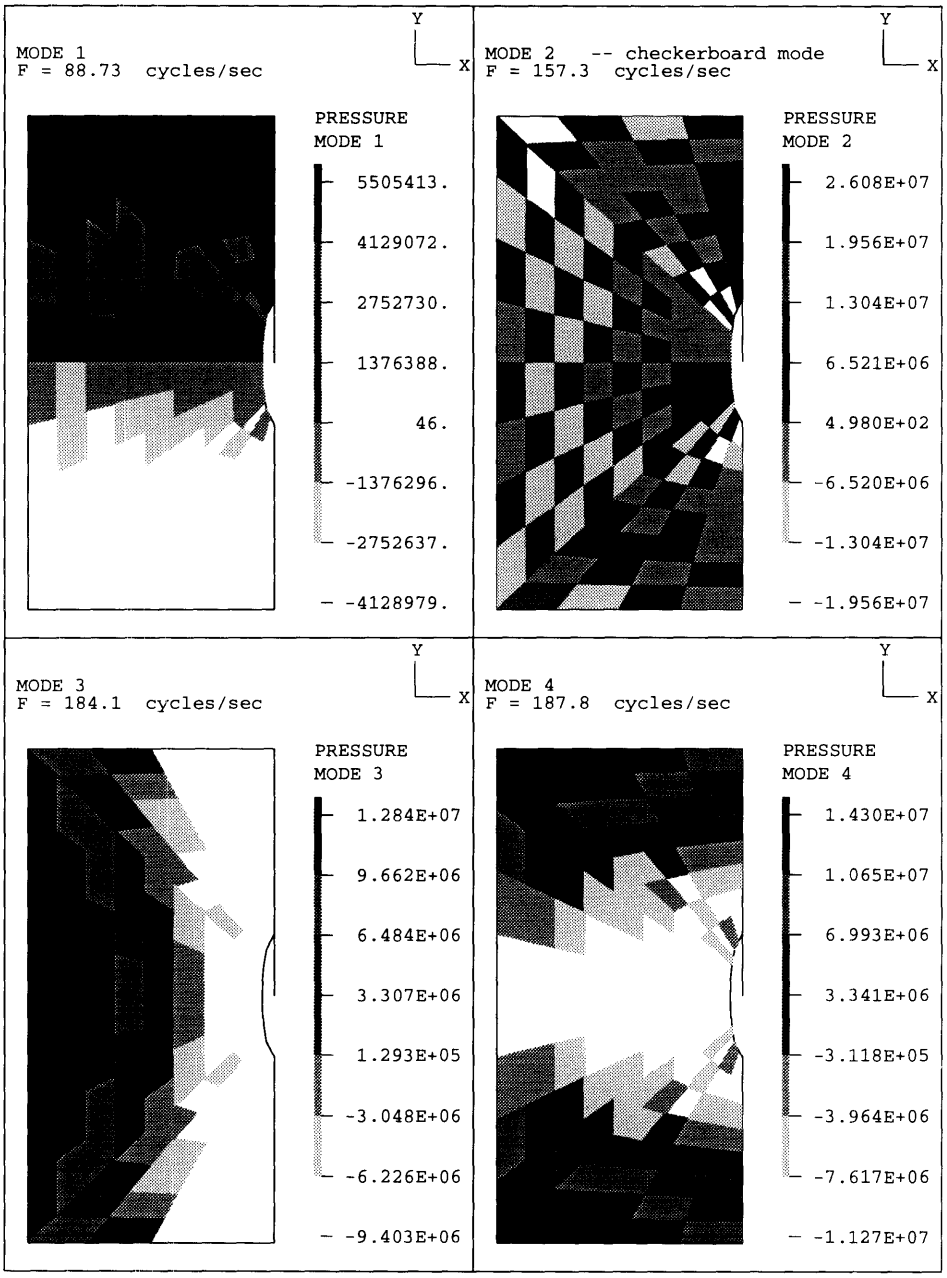

Figure 6-24: Checkerboard pressure band of the rigid ellipse problem with 4-1-1 elements.

Test case	Mesh, no. of elements	Frequencies (rad/sec)			
		First	Second	Third	Fourth
Rigid cylinder problem	128	11.91	581.8	1135	1234
Rigid ellipse problem	128	557.5	988.2	1157	1180

Table 6-11: Solution results using 4-1-1 elements.

Mode #	Type I		Type II	
	(4/1)	(4-1-1)	(4/1)	(4-1-1)
1	6.802	560.8	6.781	559.2
2	575.6	1035	579.0	1155
3	1167	1167	1165	1163
4	1210	1194	1195	1191

Table 6-12: Macroelements with $4-1-1$ and 4/1 elements for the rigid ellipse problem.

stable discretization. Tab. 6-11, Figs. 6-23 and 6-24 show some solution results. These clearly indicate that the $4-1-1$ element is not a reliable element; the predicted lowest frequencies are not accurate and the checkerboard pressure bands obtained here are typical of those observed with the 4/1 element in incompressible analysis.

However, some types of macroelements shown in Fig. 3-2 with 4/1 elements have been proved mathematically to satisfy the inf-sup condition for the $\mathbf{u}/\mathrm{p}$ formulation. As a natural extension, we expected the same macroelements with $4-1-1$ elements will give good results. Surprisingly, we found that for both the rigid ellipse and rigid cylinder problems, the structure modes predicted with type I and II macroelements (shown in Fig. 3-2) in the $\mathbf{u}$-p-$\mathbf{\Lambda}$ formulation are spurious. This indicates that the inf-sup condition for the $\mathbf{u}$-p-$\mathbf{\Lambda}$ formulation is not exactly the same as for the $\mathbf{u}/\mathrm{p}$ formulation regardless of the similarities (refer to Chapter 3).

Mode #	Type I		Type II	
	(4/1)	(4-1-1)	(4/1)	(4-1-1)
1	4.413	254.0	4.466	203.1
2	590.0	583.1	593.2	581.6
3	1157	1149	1156	1142
4	1280	1249	1262	1242

Table 6-13: Macroelements with $4-1-1$ and 4/1 elements for the rigid cylinder problem.

The explanation for this is that $4-1-1$ elements give extra constraints indicated from the mathematical prediction of zero frequency modes, however, no mathematical proof is yet available. As expected, using the 4/1 macroelement in the $\mathbf{u}$/p formulation, we can calculate the structure mode accurately. We come to the conclusion that the inf-sup condition can help to select good elements for both the $\mathbf{u}$/p and $\mathbf{u}$-p-$\mathbf{\Lambda}$ formulations, but for the $\mathbf{u}$-p-$\mathbf{\Lambda}$ formulation, $4-1-1$ element and its macroelements are not recommended.

Fig. 6-25 shows the system involving a submerged structure and the free surface. The submerged 2D plane strain structure has the dimension 0.2×0.0026. Tab. 6-16 lists the first four dry modes. Some preliminary analysis on the similar systems are available in references [5], [59], [60], [61] and [62]. In certain acoustoelastic fluid-structure interaction problems, gravity effects are ignored. However, we will take the gravity effects into account in this example and demonstrate that the $\mathbf{u}$/p formulation can in one finite element analysis obtain the sloshing, structure and acoustic frequencies accurately (results from convergence studies are listed in Tabs. 6-15 and 6-14). Fig. 6-26 shows the typical mesh of this problem. Using the proposed $\mathbf{u}$/p formulation, the computational results of the number of zero frequency modes match with the mathematical prediction in Chapter 3.

Figs. 6-28 and 6-27 show the mode shapes and pressure bands of the first two

Mode	No. of elements		Sequence Number		Frequencies (rad/sec)	
	Structure	Fluid	Theory	Result	First	Second
Sloshing	1	11	≥ 68	68	5.4717	8.8003
	2	38	≥ 250	250	5.3901	8.4892
	4	140	≥ 950	950	5.3696	8.4533
Structure	1	11	≥ 76	76	190.85	6964.3
	2	38	≥ 266	266	150.27	1808.6
	4	140	≥ 982	982	129.07	1105.5
Acoustic	1	11	≥ 78	78	8867.4	12009
	2	38	≥ 268	268	7386.5	9214.8
	4	140	≥ 985	985	7509.3	9366.3

Table 6-14: Analysis of the acoustoelastic/slosh problem using the u/p formulation with $9/4 - c$ elements.

Mode	No. of elements		Sequence Number		Frequencies (rad/sec)	
	Structure	Fluid	Theory	Result	First	Second
Sloshing	1	11	≥ 55	55	5.4717	8.8003
	2	38	≥ 190	190	5.3360	8.6016
	4	140	≥ 700	700	5.3435	8.4673
Structure	1	11	≥ 63	63	190.85	6964.3
	2	38	≥ 206	206	111.07	1800.72
	4	140	≥ 732	732	113.93	1013.29
Acoustic	1	11	≥ 65	65	8867.4	12009
	2	38	≥ 208	208	7381.3	9257.5
	4	140	≥ 735	735	7513.2	9382.8

Table 6-15: Analysis of the acoustoelastic/slosh problem using the u/p formulation with 9/3 elements.

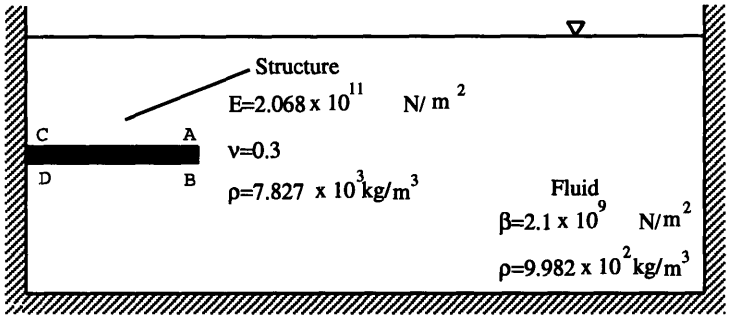

Figure 6-25: Acoustoelastic/slosh problem.

No. of elements	Frequencies (rad/sec)			
	First	Second	Third	Fourth
1	457.432	36851.0	43851.5	155273
2	378.365	3802.02	42256.1	42882.7
4	363.097	2446.82	7852.46	20493.2

Table 6-16: First four dry modes of the submerged structure (plane strain) (with 9-node elements).

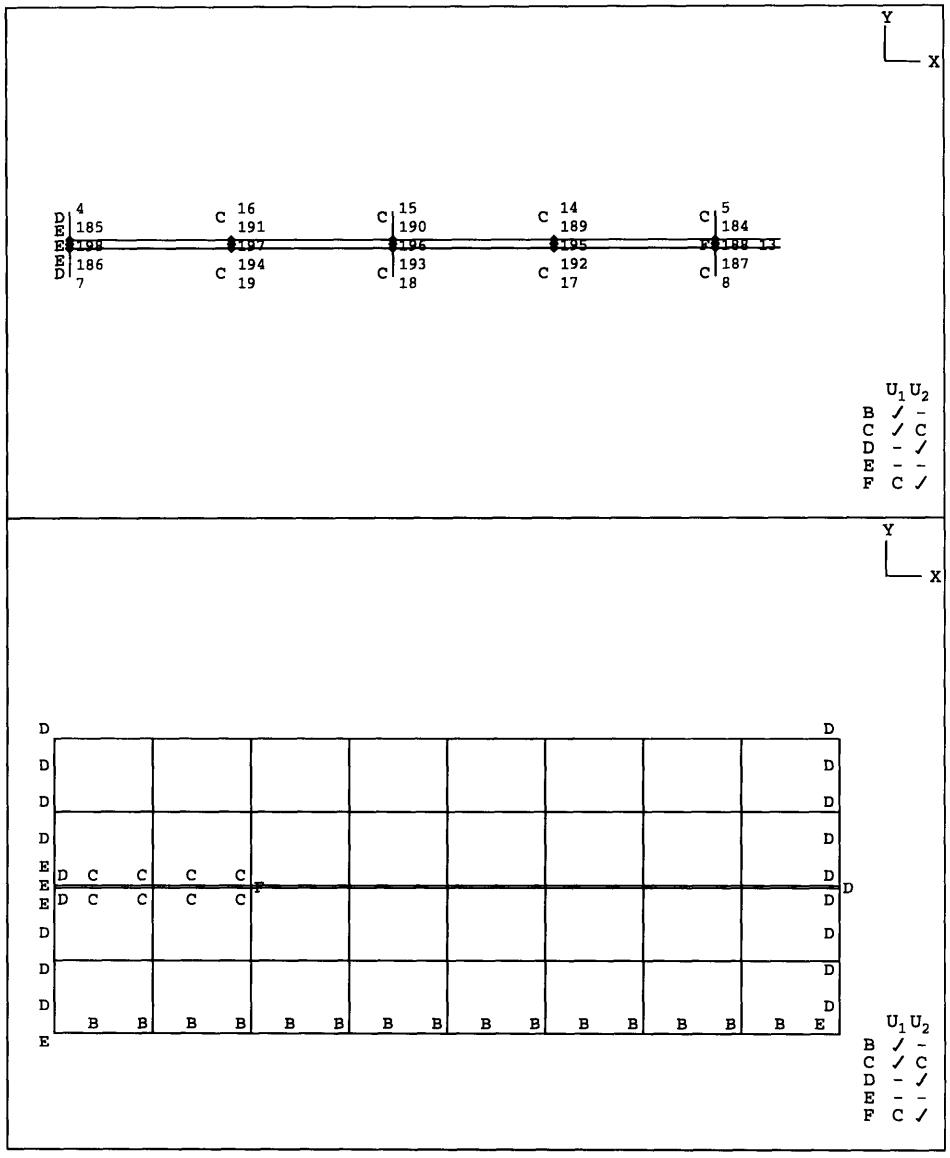

Figure 6-26: Typical mesh of the acoustoelastic/slosh problem.

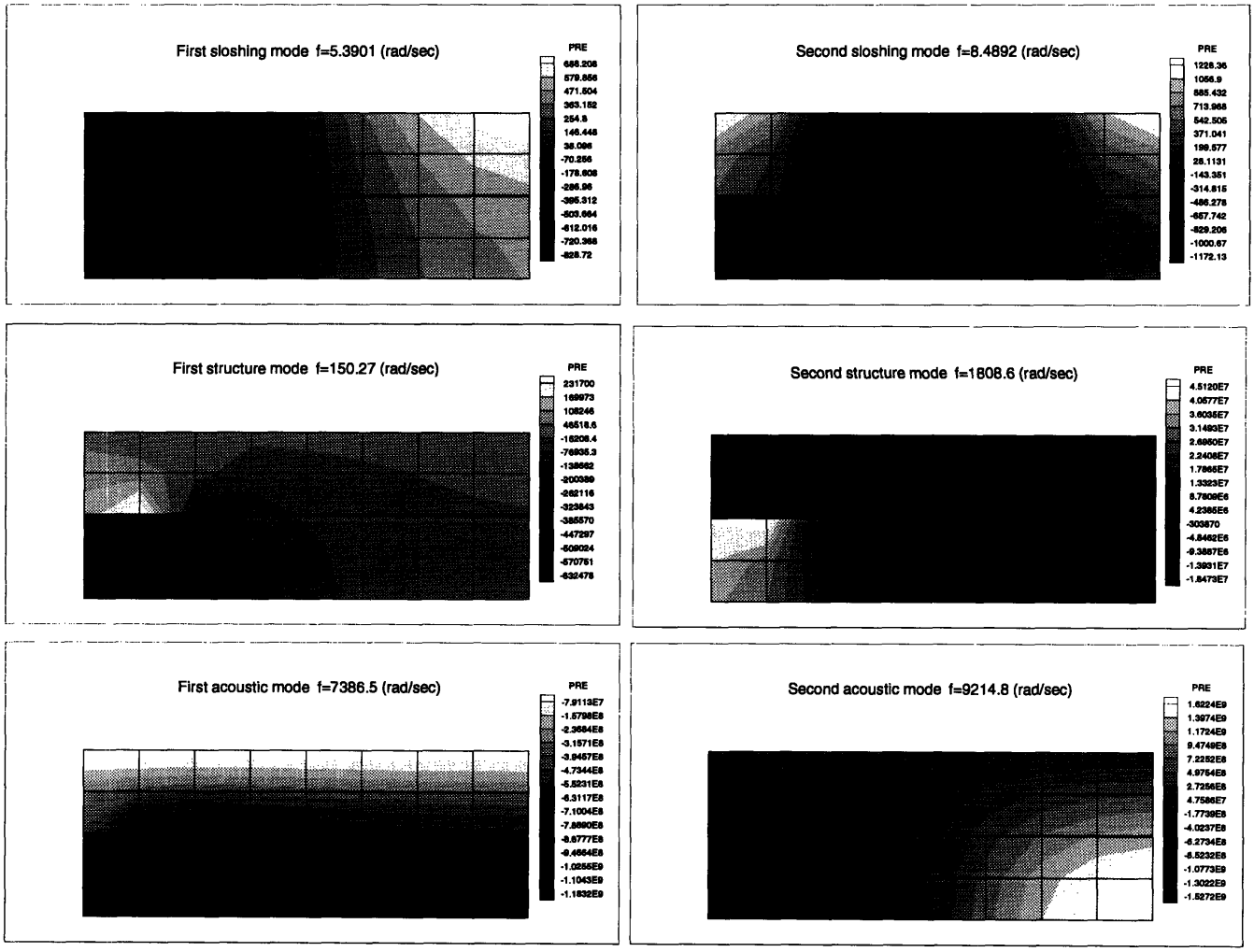

Figure 6-27: Pressure bands of the first two sloshing, structure and acoustic modes of the acoustoelastic/slosh problem.

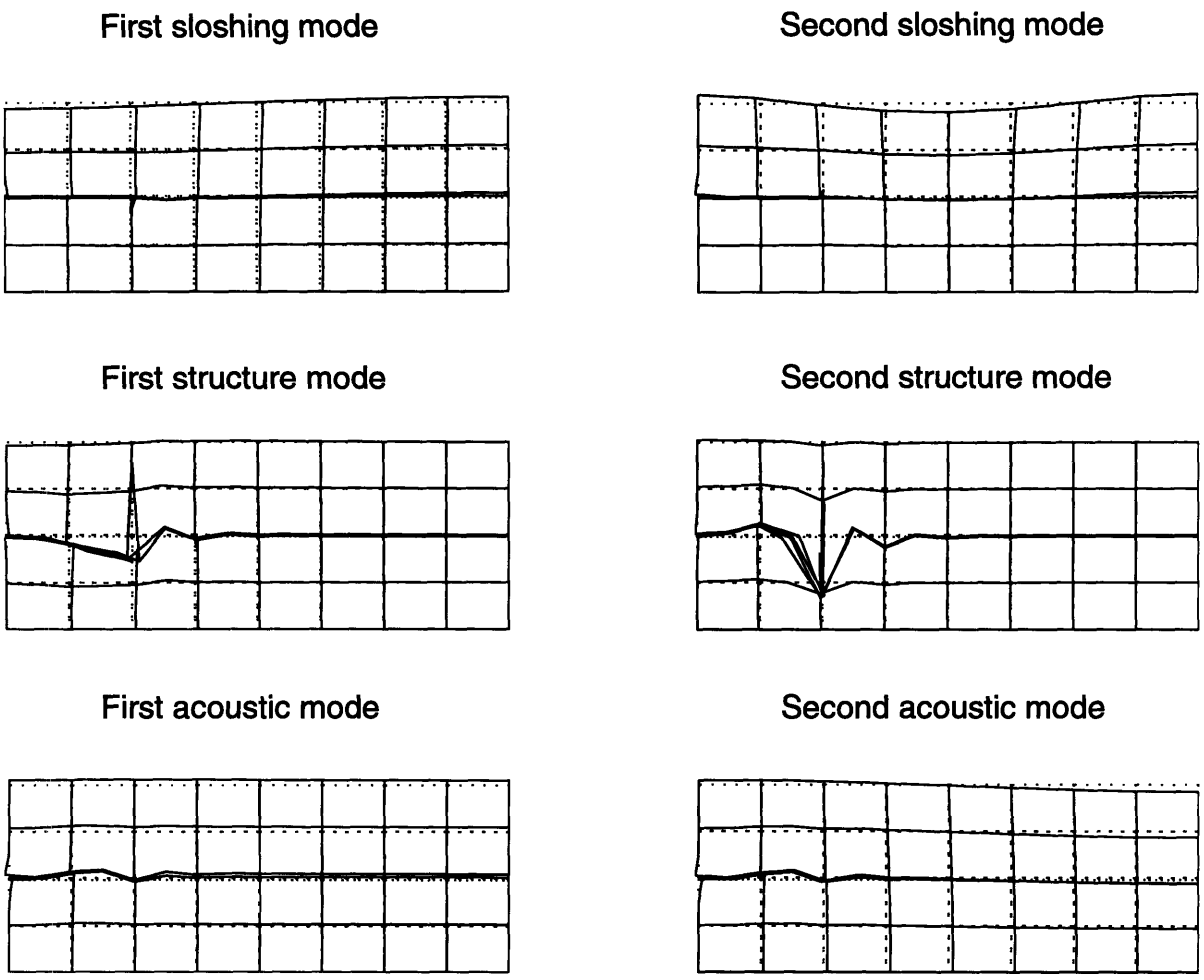

Figure 6-28: First two sloshing, structure and acoustic modes for the acoustoelastic/slosh problem.

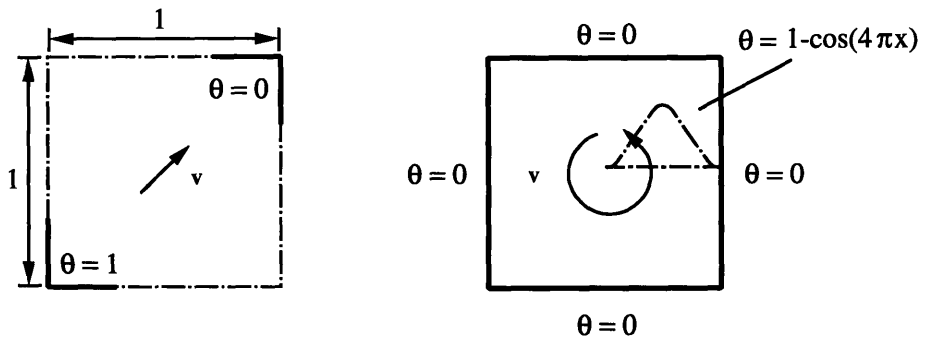

Figure 6-29: Two convection dominated heat transfer problems.

sloshing, structure and acoustic frequencies calculated with forty 9-node elements.

6.2 Upwinding Test Problems

6.2.1 Convection-Diffusion Examples

To test our proposed upwinding formulation for 9-node elements, we analyzed two convection dominated heat transfer examples (Peclet number is 6.25×10^9 for both cases) shown in Fig. 6-29. In the diagonal flow problem, the flow is uniform ($|\mathbf{v}| = 1.0$) in the diagonal direction; while in the rotating cosine hill problem, the flow is rotational ($v_1 = -x_2$ and $v_2 = x_1$). Figs. 6-30 and 6-31 show the results from the standard Galerkin (with 9-node elements), the SUPG formulation (with 4-node elements) and the proposed upwinding formulation (with 9-node elements). Indicated from the results, the SUPG formulation introduces less crosswind diffusion, however, it retains some spatial oscillations around the sharp changing regions. Since the SUPG formulation was originally introduced for 4-node elements, the formulation

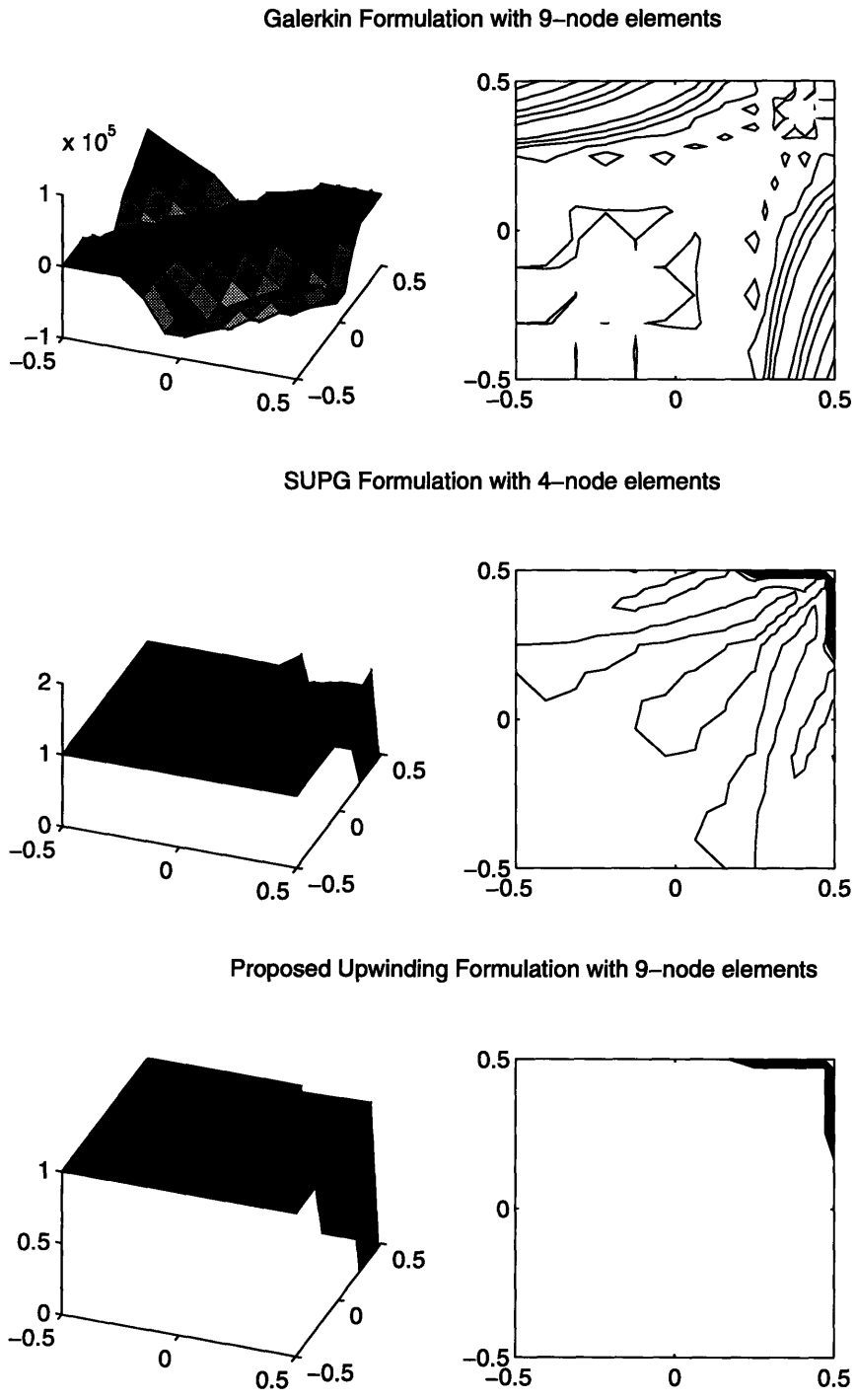

Figure 6-30: The diagonal flow problem with distorted meshes.

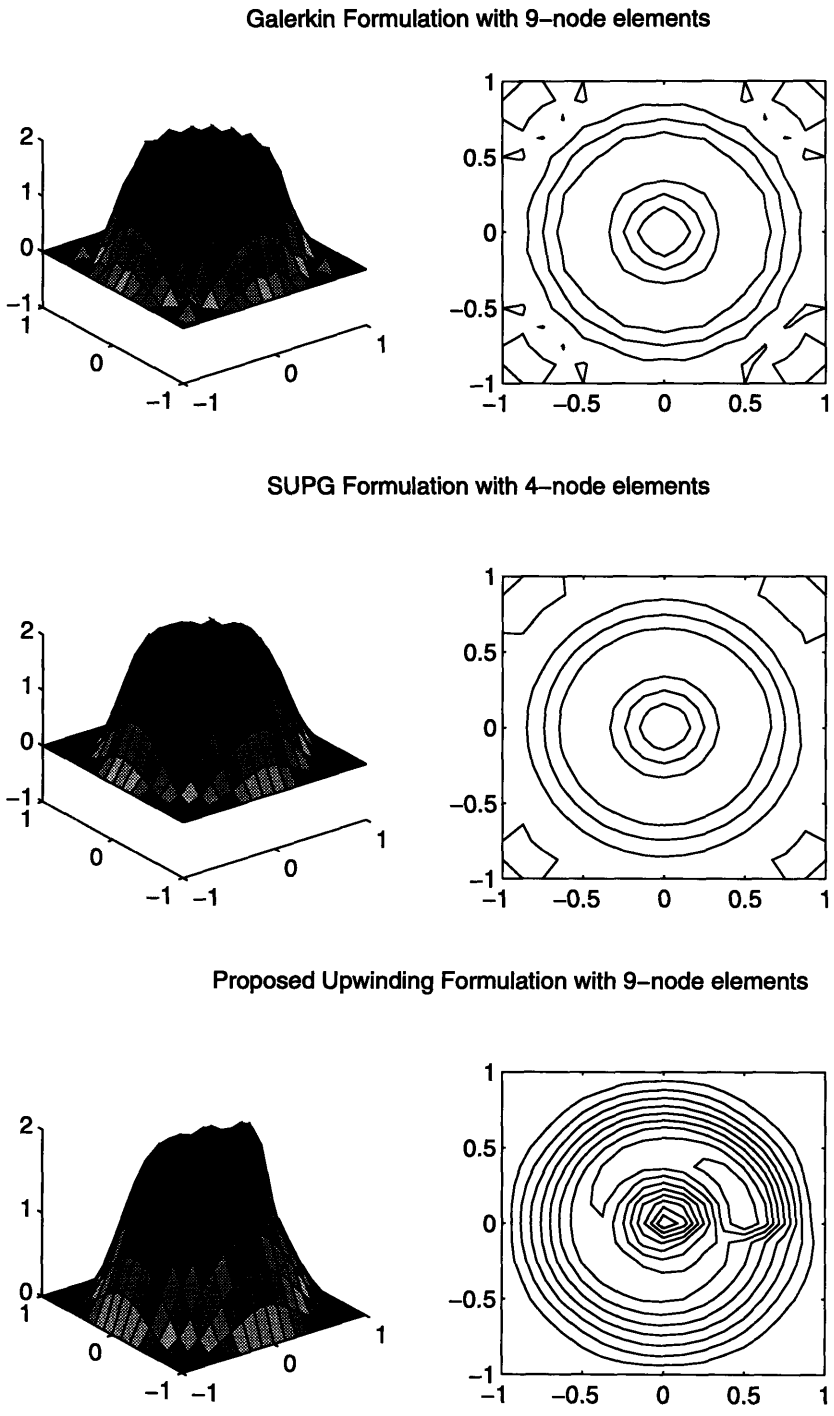

Figure 6-31: The rotating cosine hill problem with uniform meshes.

will be unstable for low Reynolds number flow problems with general 4/1 element meshes. The proposed formulation for 9-node elements works well for the diagonal flow problem even with the distorted mesh, but in the rotating cosine hill problem, there exists some crosswind diffusion. From our numerical tests, we find that the crosswind diffusion will be reduced with the mesh refinement. As a side remark, whether there exists an optimal upwinding scheme which has neither oscillation nor crosswind diffusion needs to be further investigated.

6.2.2 Corner Flow

Fig. 6-32 illustrates the turning flow test problem for the control volume upwinding scheme in convection dominated flow problems. In this test problem, we assign a known corner flow field,

$$u_1 = x_1 \tag{6.7}$$

$$u_2 = -x_2 \tag{6.8}$$

The corresponding pressure distribution is,

$$p = -\frac{\rho}{2}(x_1^2 + x_2^2) \tag{6.9}$$

where the nodal pressure at node A is assigned to be zero.

From the analytic solution, node B should have the pressure -1000.0; using the proposed upwinding formulation with sixteen 9-node elements, the calculated pressure for node B is -717.0. Fig. 6-33 shows that the pressure distribution is not exactly the circular shape as indicated in Eq. (6.9) due to the crosswind diffusion. Nevertheless, with that coarse mesh, the flow field is smooth and accurately predicted.

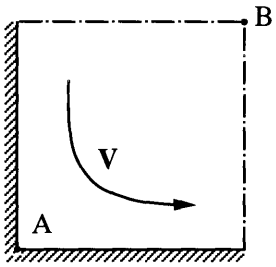

Figure 6-32: Corner flow problem.

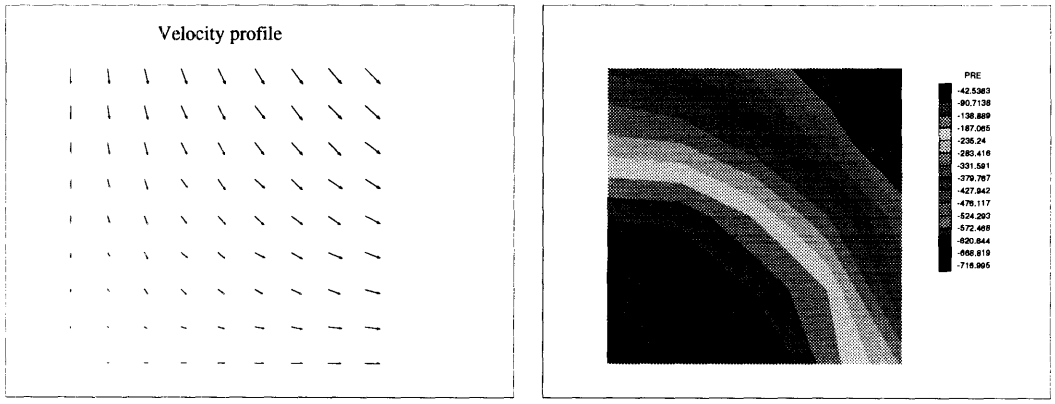

Figure 6-33: Velocity profile and pressure band of the corner flow problem.

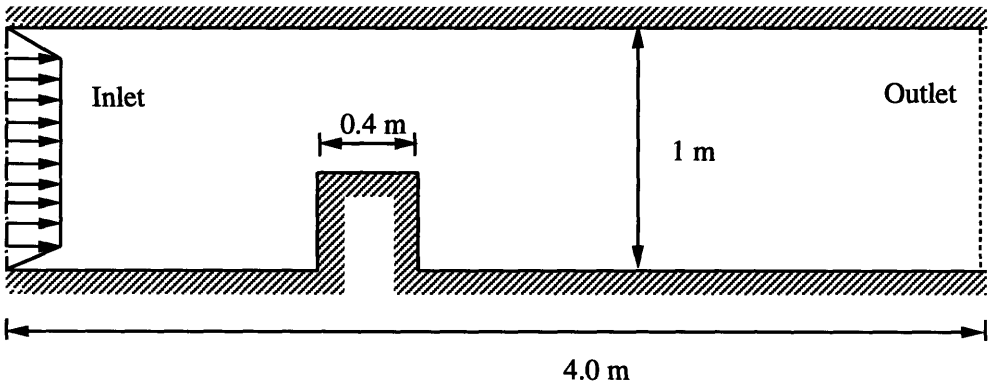

Figure 6-34: Navier-Stokes flow over a step problem.

6.2.3 Navier-Stokes Flow Over a Step

This test problem is used to show the spatial oscillations with the standard Galerkin formulation for the Navier-Stokes equations and demonstrate the capability of the developed upwinding scheme for 9-node elements. The mathematical model is shown in Fig. 6-34. In the reference [51], Hughes, et al analyzed the same problem with a penalty formulation and reduced integration techniques for low order elements. Results of the velocity profiles and pressure distributions for 9-node elements with the standard Galerkin formulation are shown in Figs. 6-36 and 6-35. As is clearly visible, 'wiggles' appear upstream of the step. This confirms that it is inappropriate to use the standard Galerkin formulation for convection dominated problems. With only thirty-eight 9-node mixed elements, the proposed $\mathbf{v}/\mathrm{p}$ formulation and the upwinding technique gave fairly good results shown in Figs. 6-38 and 6-37. The employed data for this problem were: ($Re = 200$, $V_{in} = 0.25$).

6.3 Nonlinear Problems

To demonstrate the capability of the proposed $\mathbf{v}/\mathrm{p}$ formulation with the ALE kinematic description and developed upwinding formulation for 9-node elements, we an-

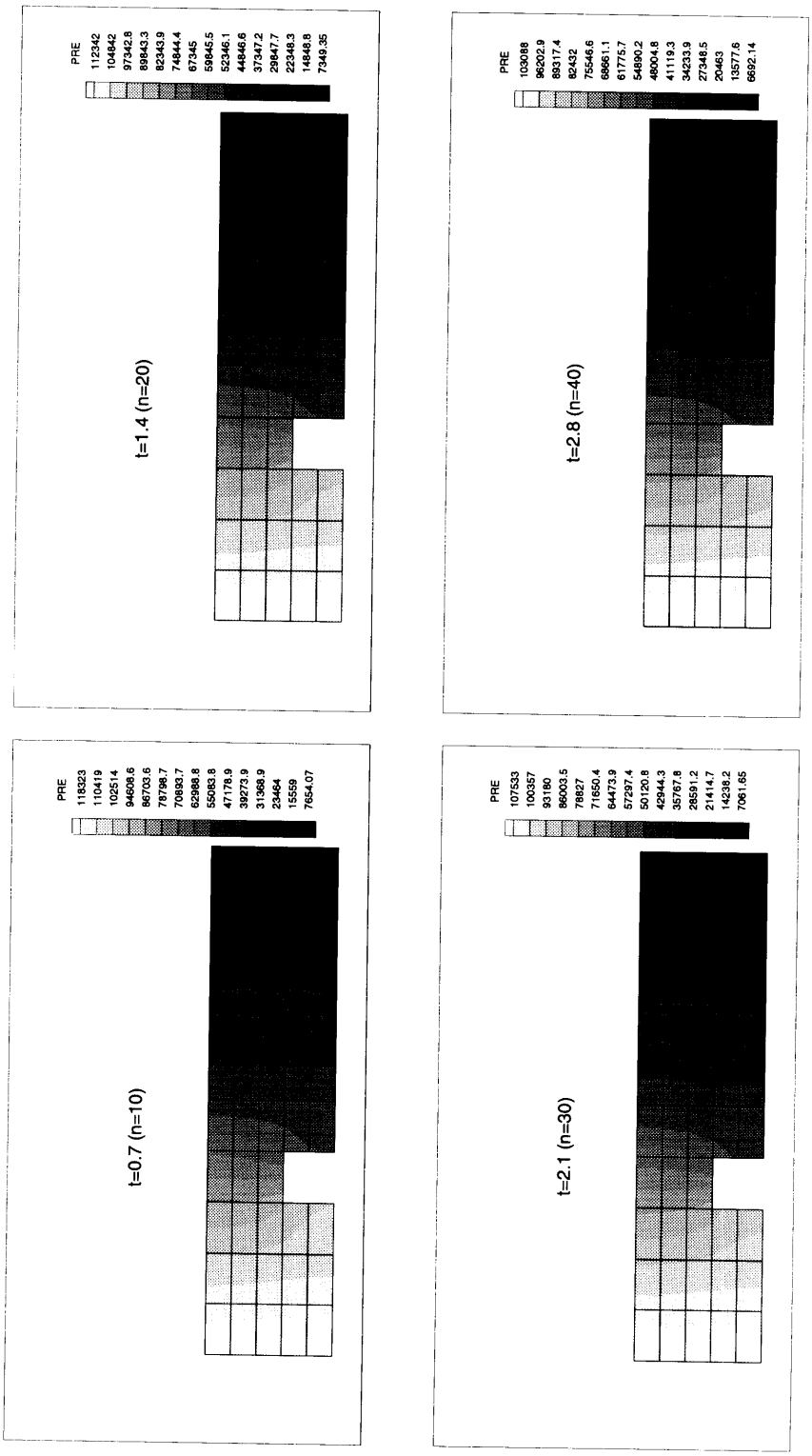

Figure 6-35: Pressure bands of the Navier-Stokes flow over a step problem (the standard Galerkin formulation with thirty-eight 9-node elements).

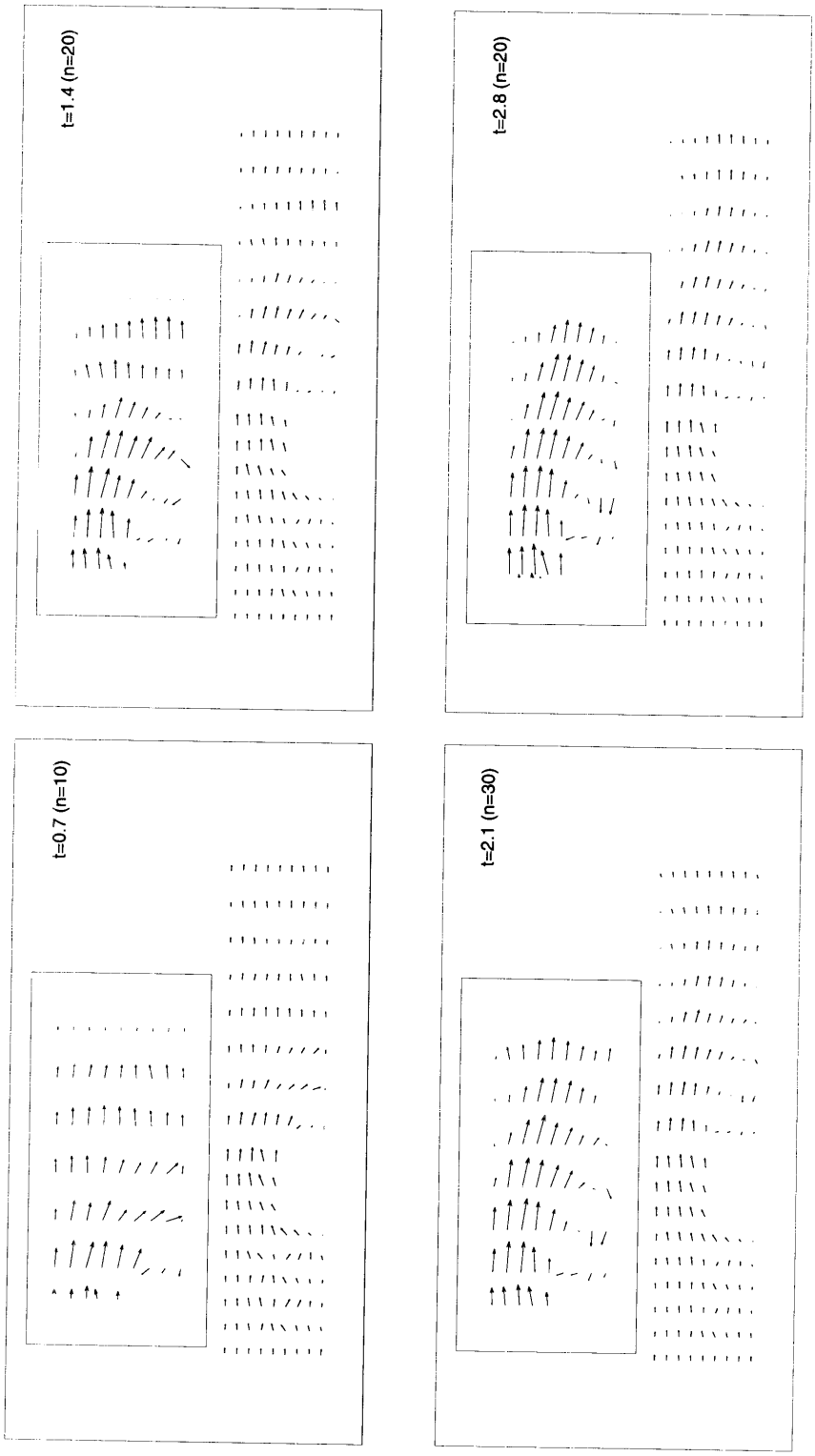

Figure 6-36: Velocity fields of the Navier-Stokes flow over a step problem (the standard Galerkin formulation with thirty-eight 9-node elements).

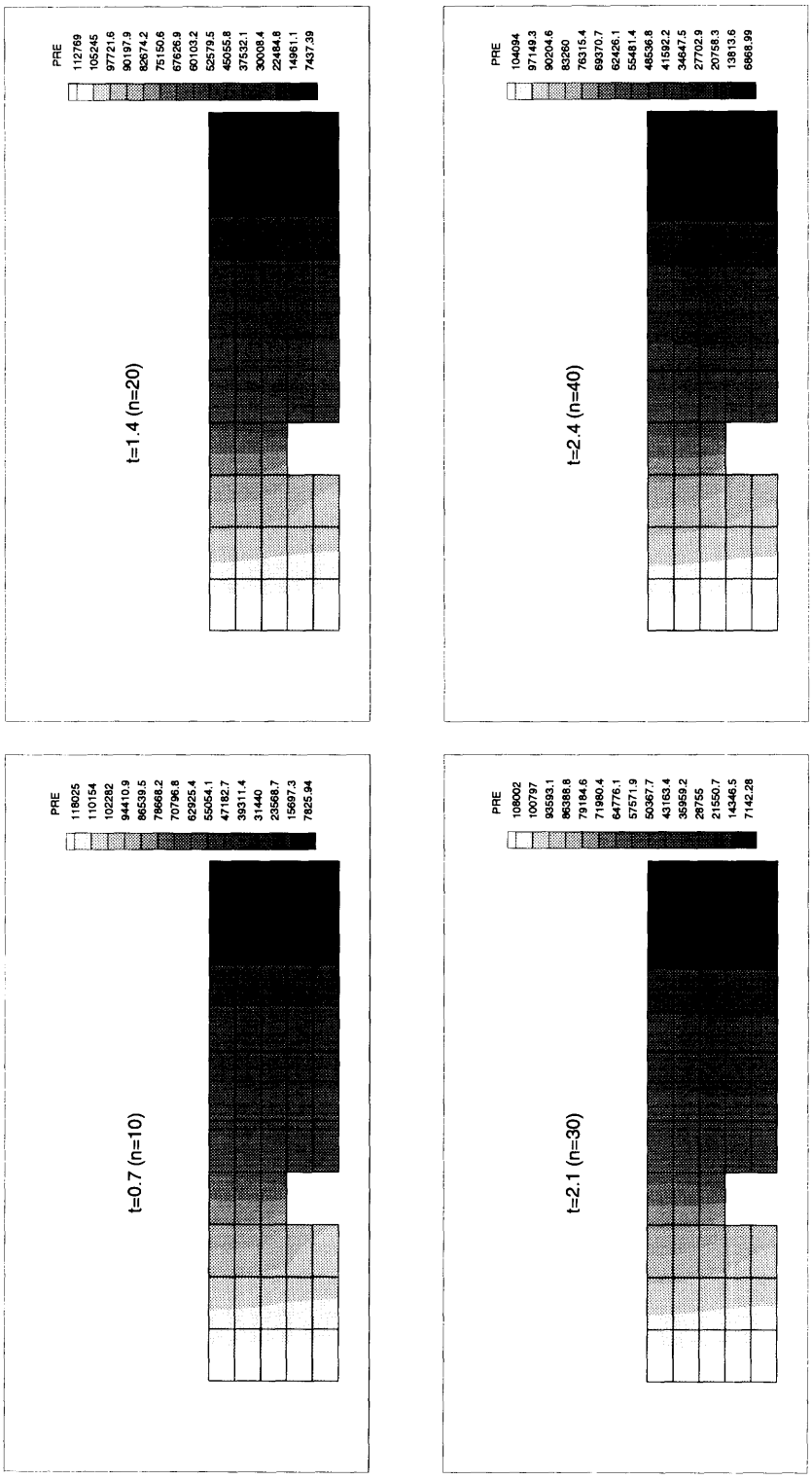

Figure 6-37: Pressure bands of the Navier-Stokes flow over a step problem (the new upwinding formulation with thirty-eight 9-node elements).

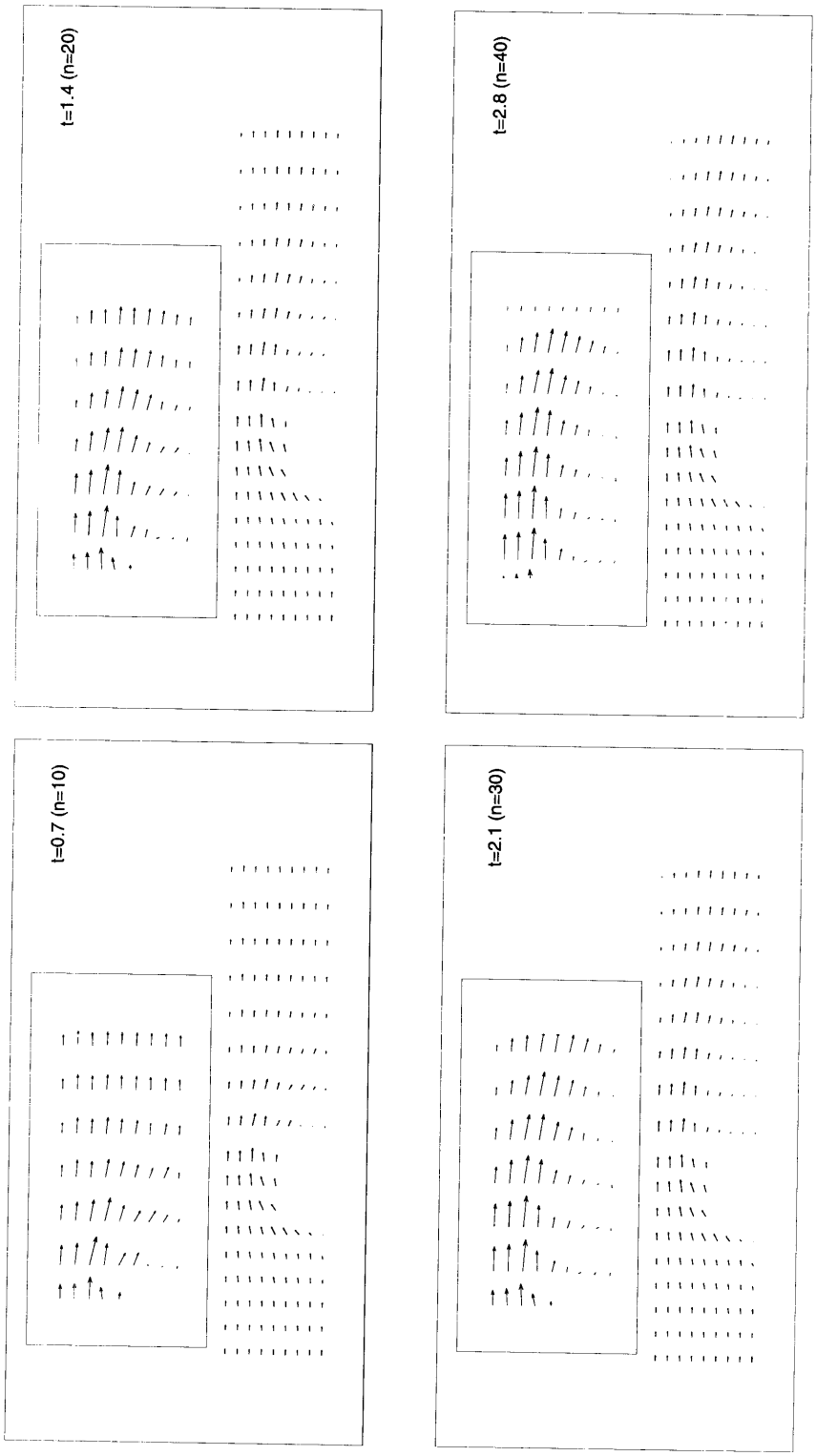

Figure 6-38: Velocity fields of the Navier-Stokes flow over a step problem (the new upwinding formulation with thirty-eight 9-node elements).

alyze a problem involving large free surface motions and a problem of the Navier-Stokes flow interacting with a hyperelastic structure under large displacements and large strains. In the region around the structure and free surfaces, with the help of the ALE description, we can relate the fluid mesh points to the structure nodes or assign additional mesh velocity unknowns in order to regularize the mesh inside the fluid domain. We use 9/3 or $9/4 - c$ elements and apply the developed upwinding formulation.

6.3.1 Large-amplitude Sloshing Problem

The applications of the finite element method with velocity potential formulations for nonlinear free surface waves have been discussed in [63] [64] [65] [66]. In this thesis, we use the proposed v/p formulation with 9-node mixed elements. To avoid the excessive mesh distortion, we apply the ALE description to the v/p formulation.

For the rigid tank with a free sloshing surface shown in Fig. 6-7, we subject it to the horizontal sinusoidal motion $a \sin \omega t$, where $w = 0.89(rad/sec)$ and $a = 0.098g$. The free surface profiles are shown in Fig. 6-39.

Figs. 6-41 and 6-42 show the velocity profiles and the pressure bands. Fig. 6-40 gives amplitudes. In a linear analysis, both downward and upward motions of the sloshing tank will have the same magnitude. However, indicated by nonlinear analysis, the amplitudes of upward displacements and velocities are much higher than the downward ones. Notice that with the influence of viscosities and crosswind diffusion due to the coarse mesh, free surface amplitudes are less than the results with the potential formulation [46].

6.3.2 Hyperelastic Structures Interacting With Viscous Flows

Fig. 6-43 shows the first testing problem. Through this test example, we want to demonstrate that our v/p formulation with the ALE description and newly developed upwinding formulation can be successfully applied to convection dominated problems

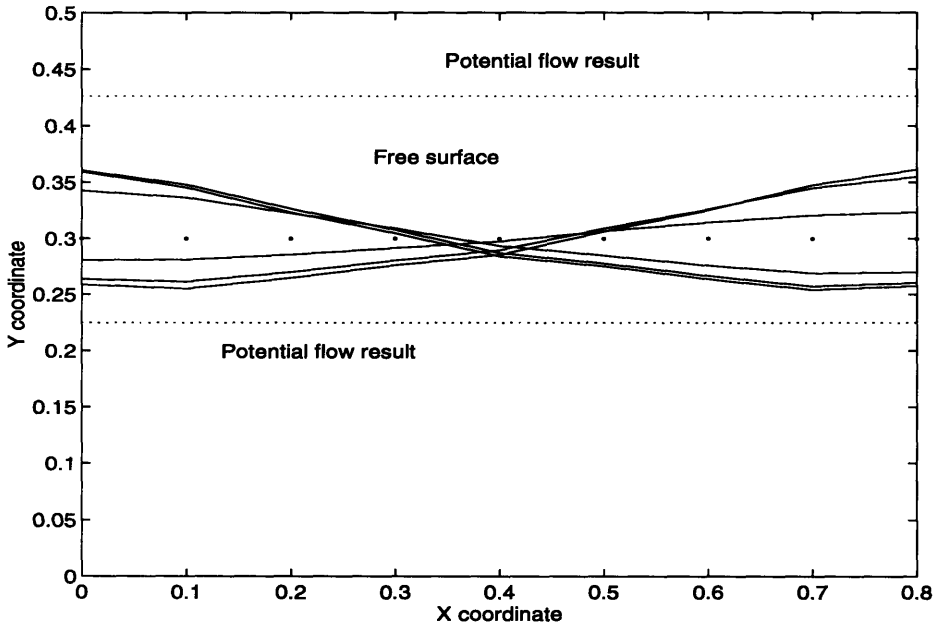

Figure 6-39: Free surface profiles (with eight 9-node elements, $\nu = 0.05$).

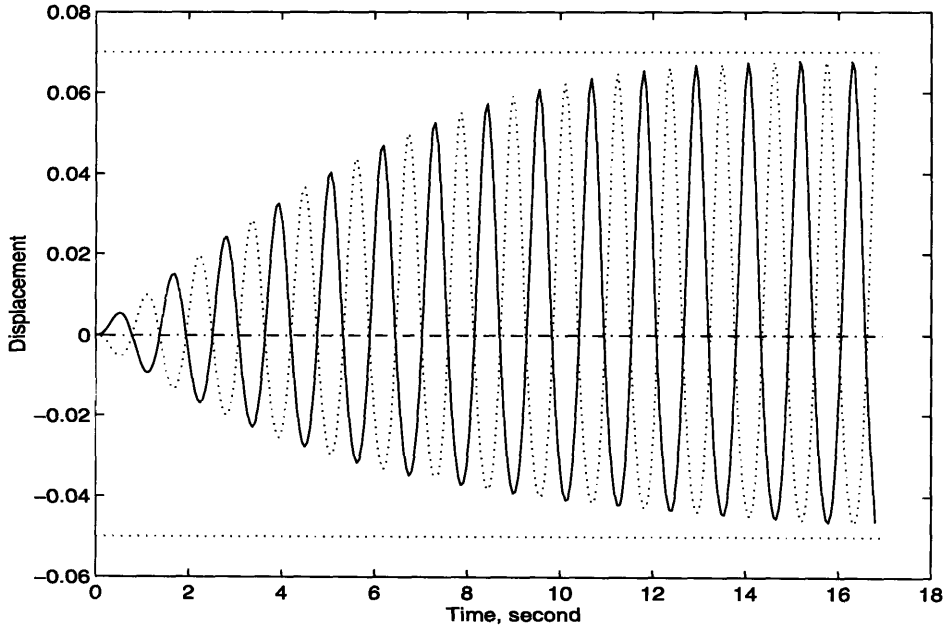

Figure 6-40: Amplitudes of the nonlinear sloshing water tank problem (eight 9-node elements).

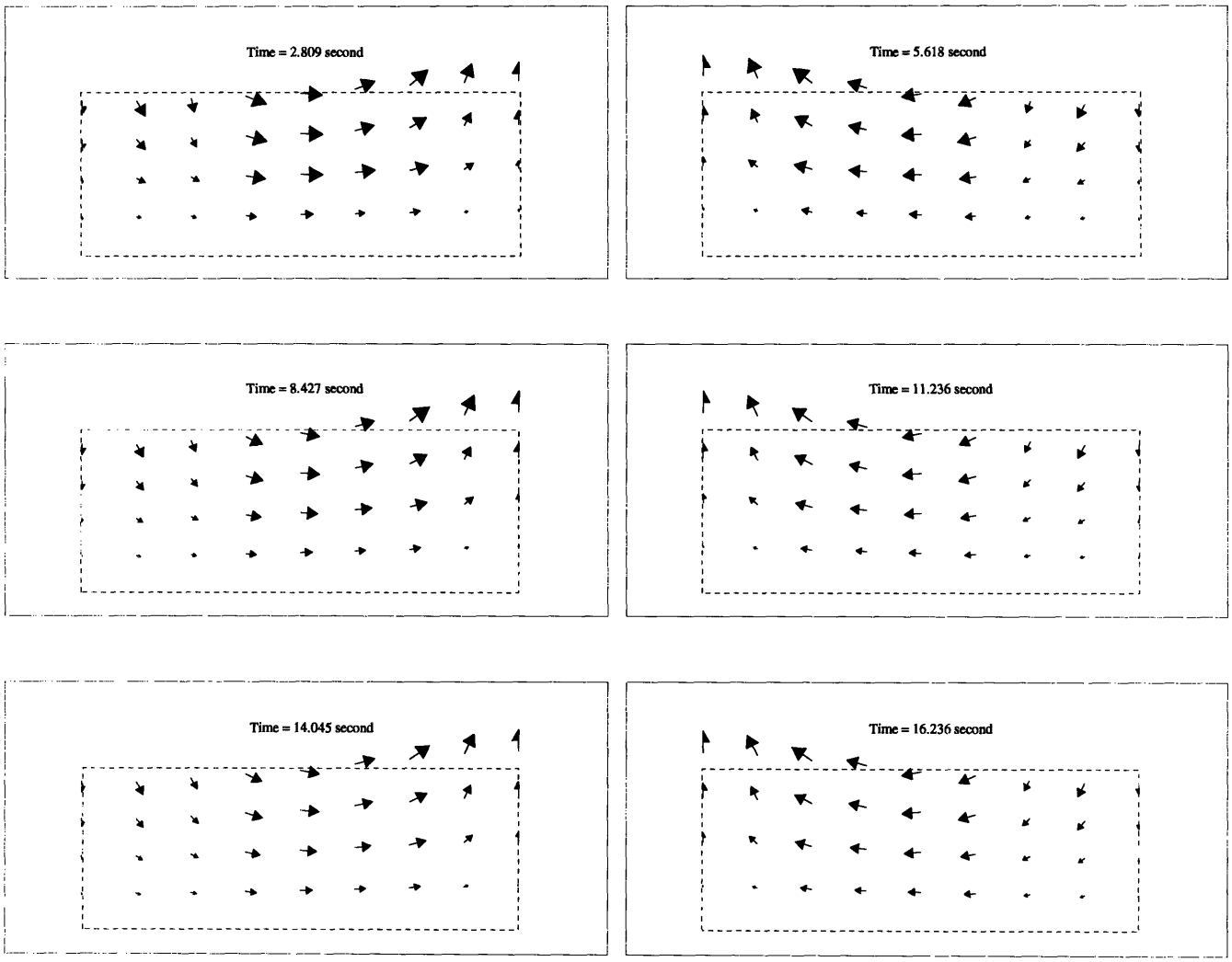

Figure 6-41: Velocity profiles of the nonlinear sloshing water tank problem (eight 9-node elements).

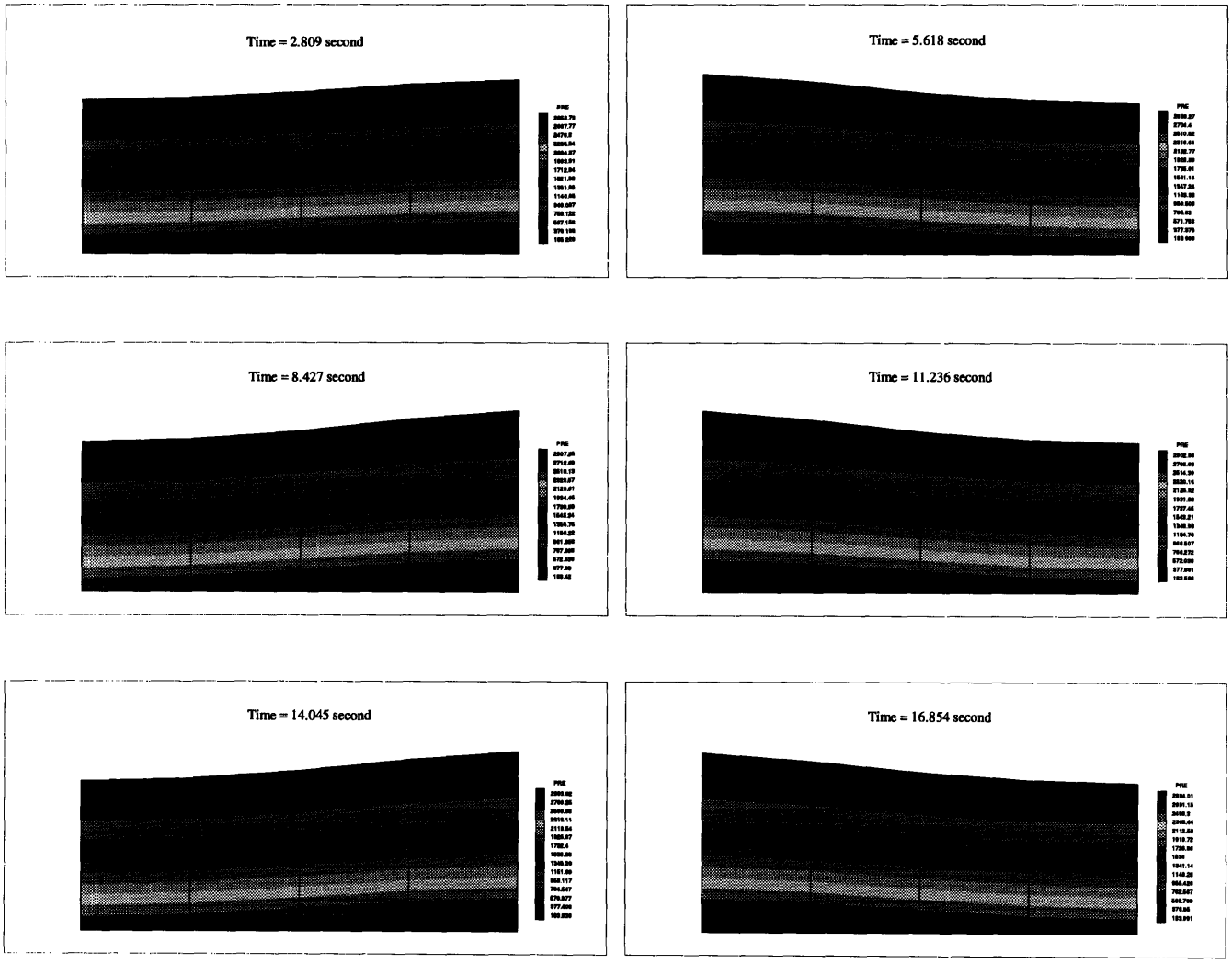

Figure 6-42: Pressure bands of the nonlinear sloshing water tank problem.

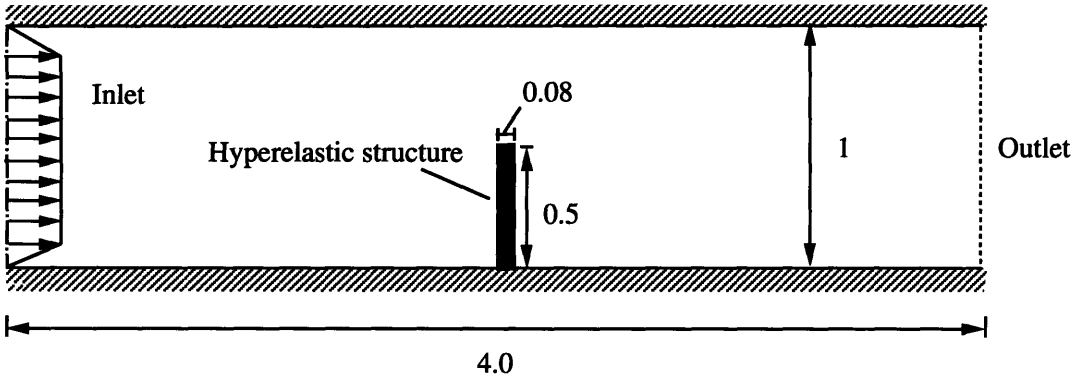

Figure 6-43: Navier-Stokes flow interacting with a hyperelastic structure problem.

involving almost incompressible fluids and solids with large displacements and large strains.

The typical mesh (very coarse one) is given in Fig. 6-44. Figs. 6-45 and 6-46 give the flow fields and the pressure bands. Interestingly, with the coarse mesh used, the developed ALE and upwinding formulation gives the convergence and provides reasonable results with no spatial oscillation and checkerboard pressure modes. In practice, before a large number of finite elements is used, this type of coarse meshes can be applied to get a first estimation of a rather complicated problem.

Fig. 6-47 shows the displacement time history of Node 5.

The results from finer meshes are shown in Figs. 6-48, 6-49, 6-50 and 6-51.

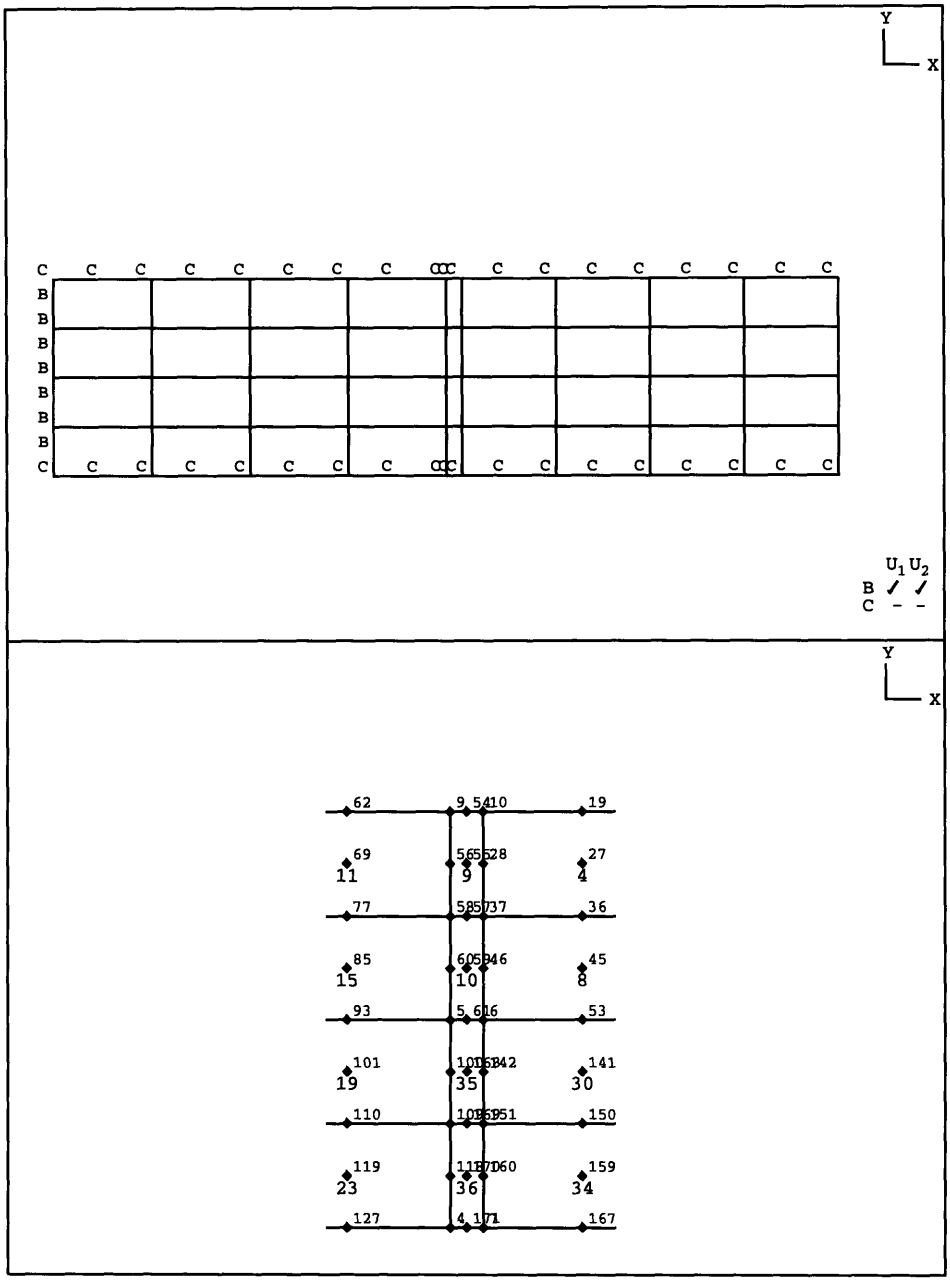

Figure 6-44: Typical mesh of the Navier-Stokes flow interacting with a hyperelastic structure problem.

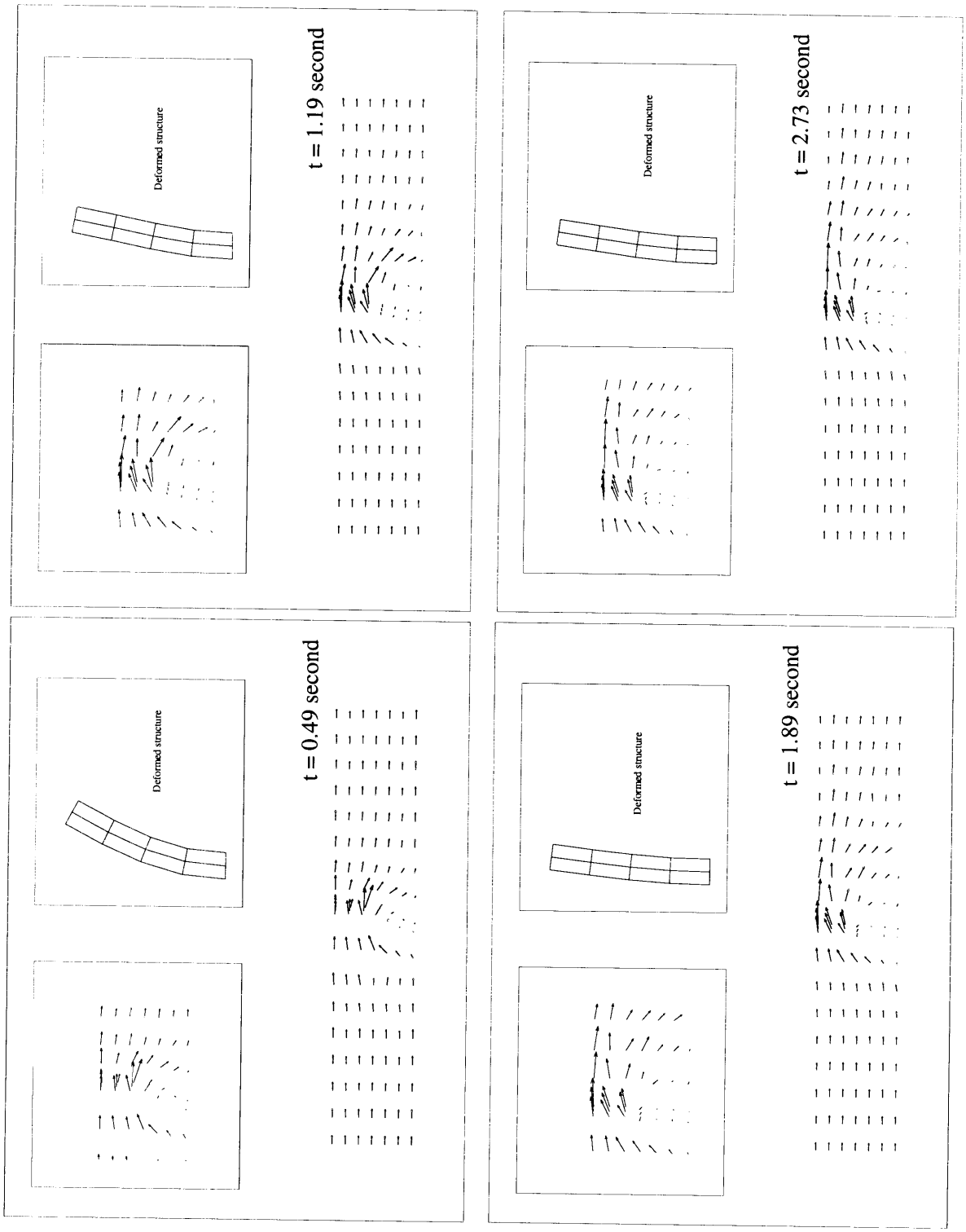

Figure 6-45: Flow fields of the Navier-Stokes flow interacting with a hyperelastic structure problem.

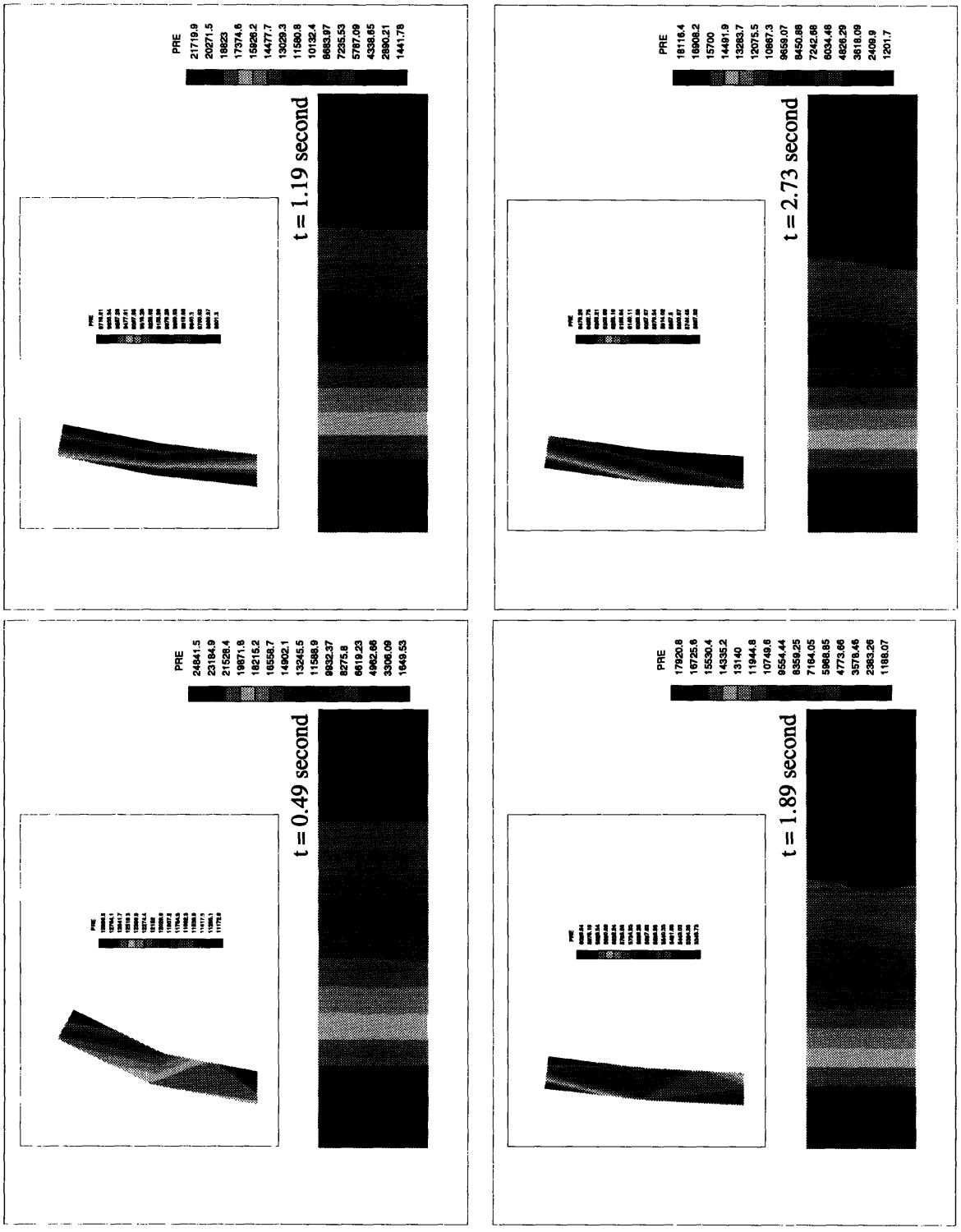

Figure 6-46: Pressure bands of the Navier-Stokes flow interacting with a hyperelastic structure problem.

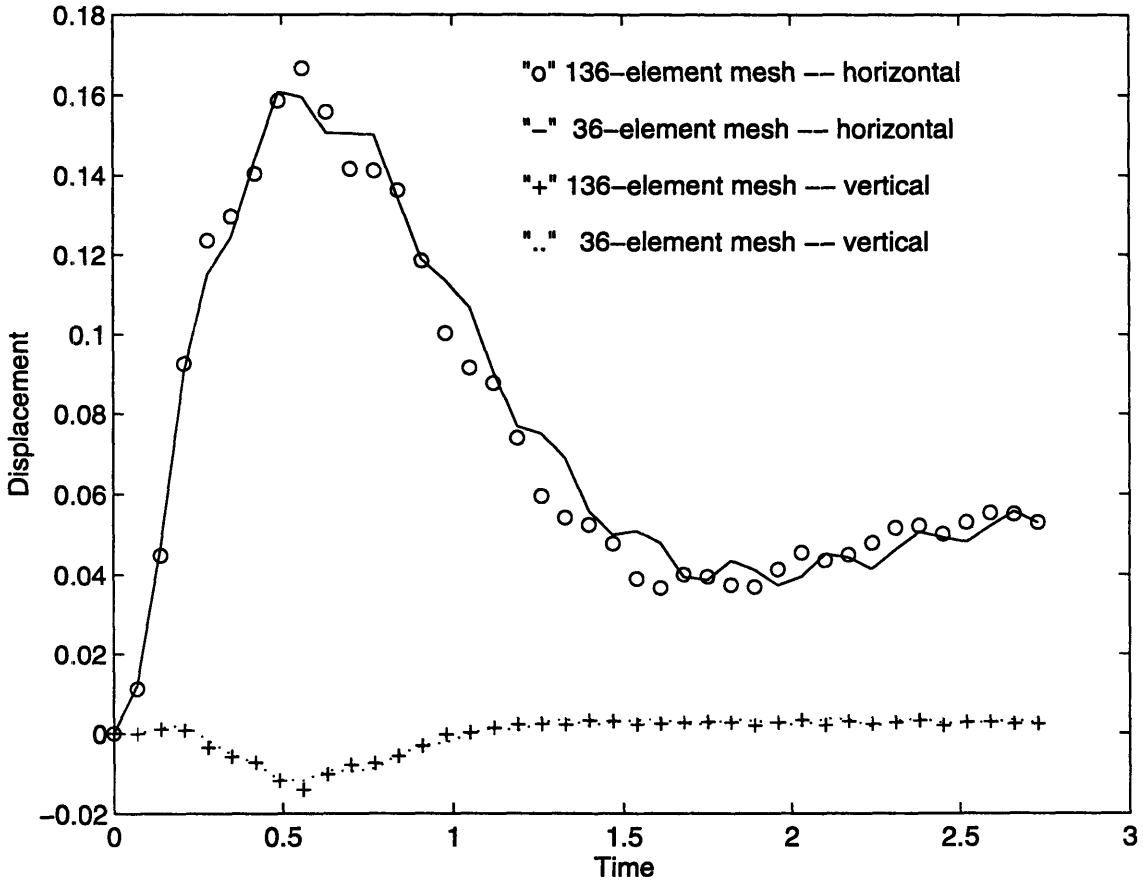

Figure 6-47: Node 5 displacement history of the Navier-Stokes flow interacting with a hyperelastic structure problem.

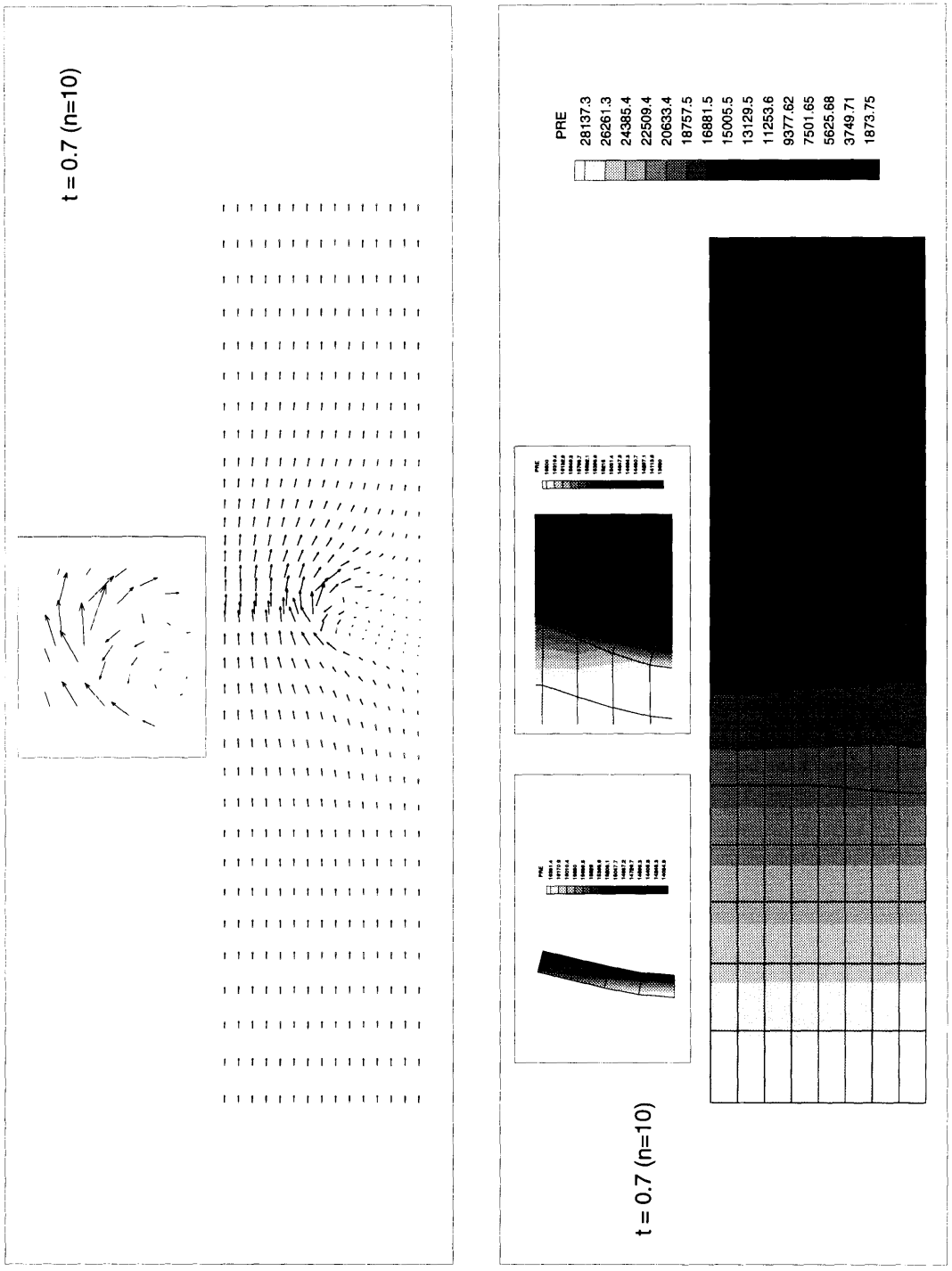

Figure 6-48: Results at time 0.7 of the viscous flows interacting with structures (one hundred and thirty-six 9-node elements).

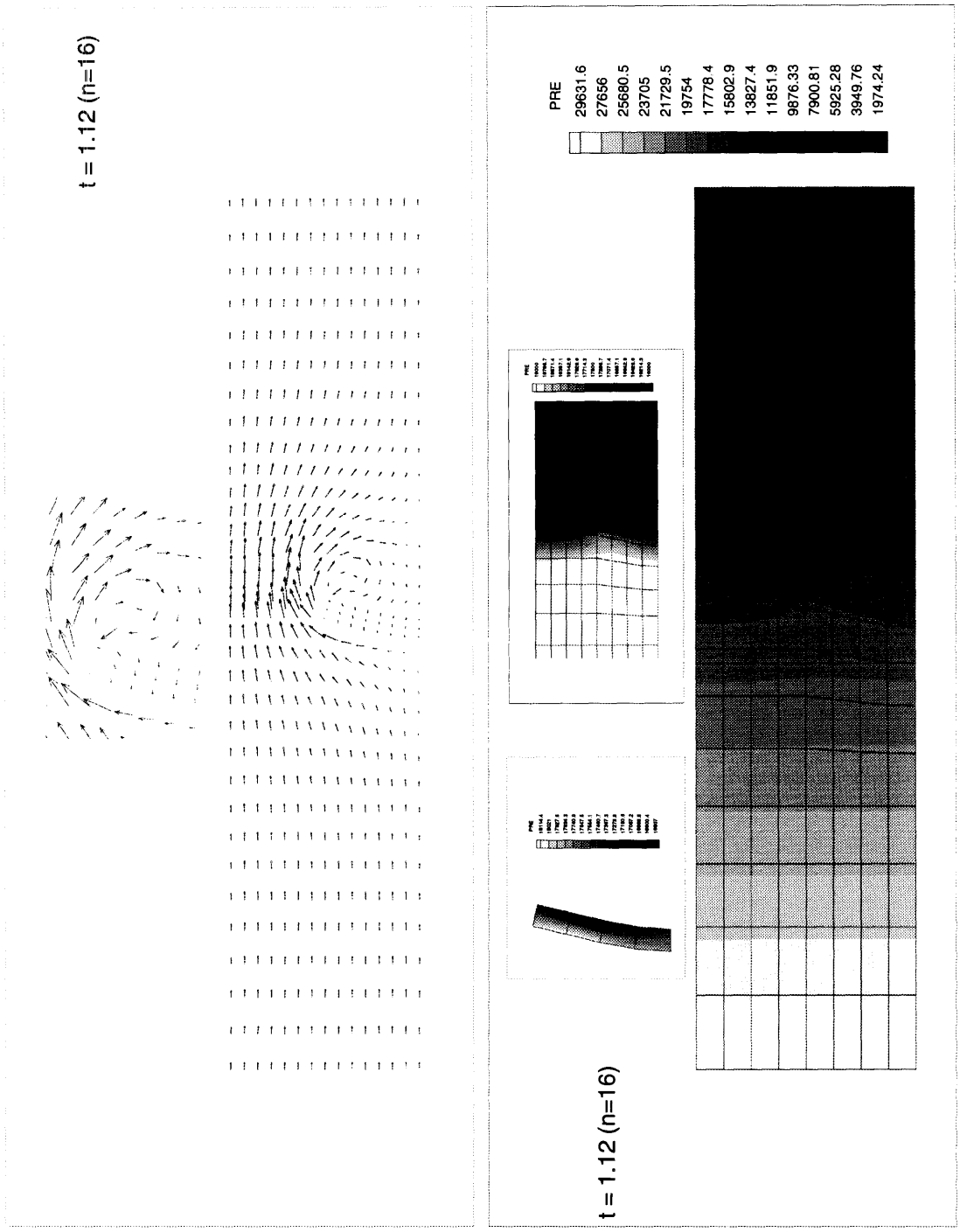

Figure 6-49: Results at time 1.12 of the viscous flows interacting with structures (one hundred and thirty-six 9-node elements).

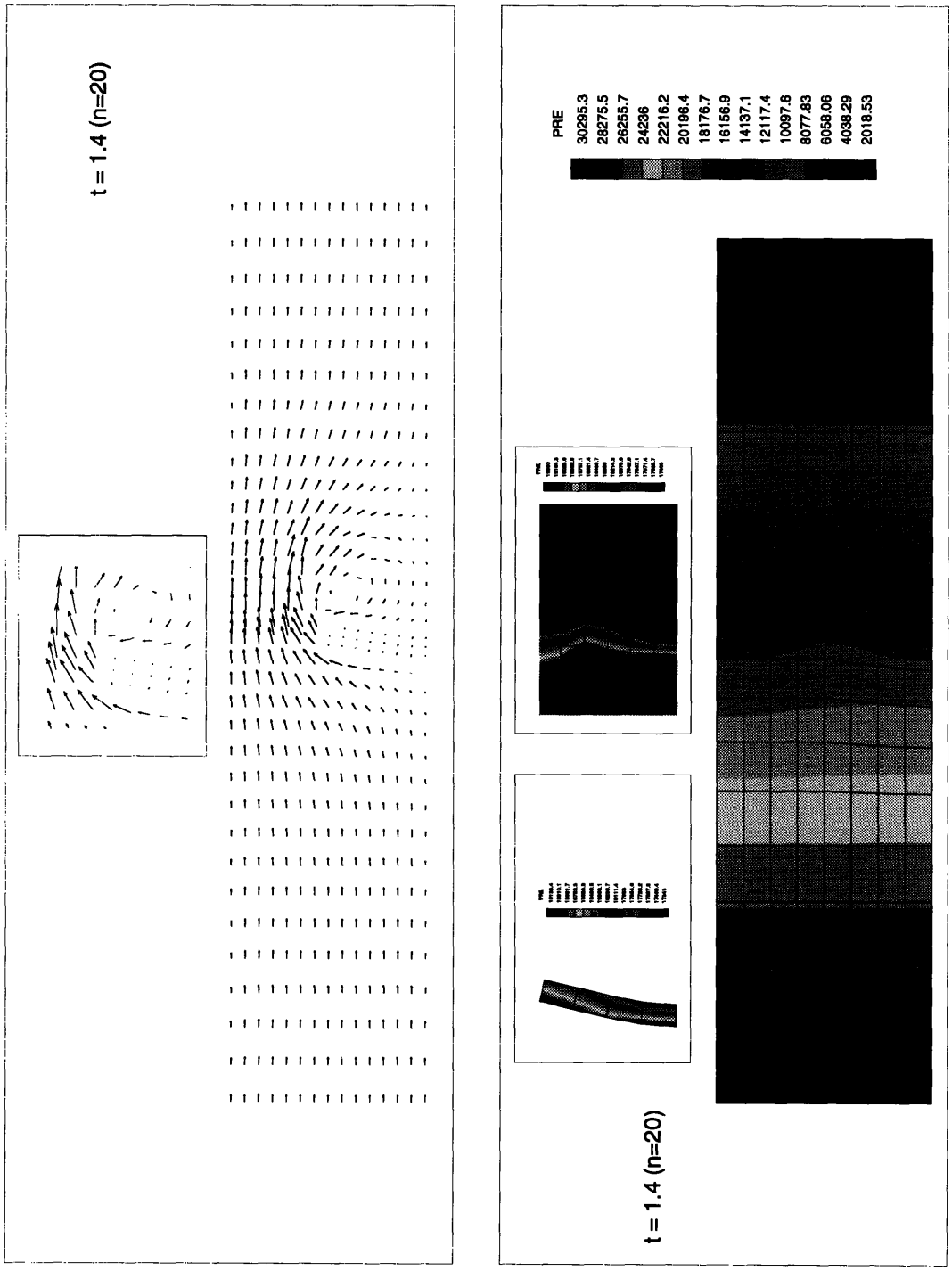

Figure 6-50: Results at time 1.4 of the viscous flows interacting with structures (one hundred and thirty-six 9-node elements).

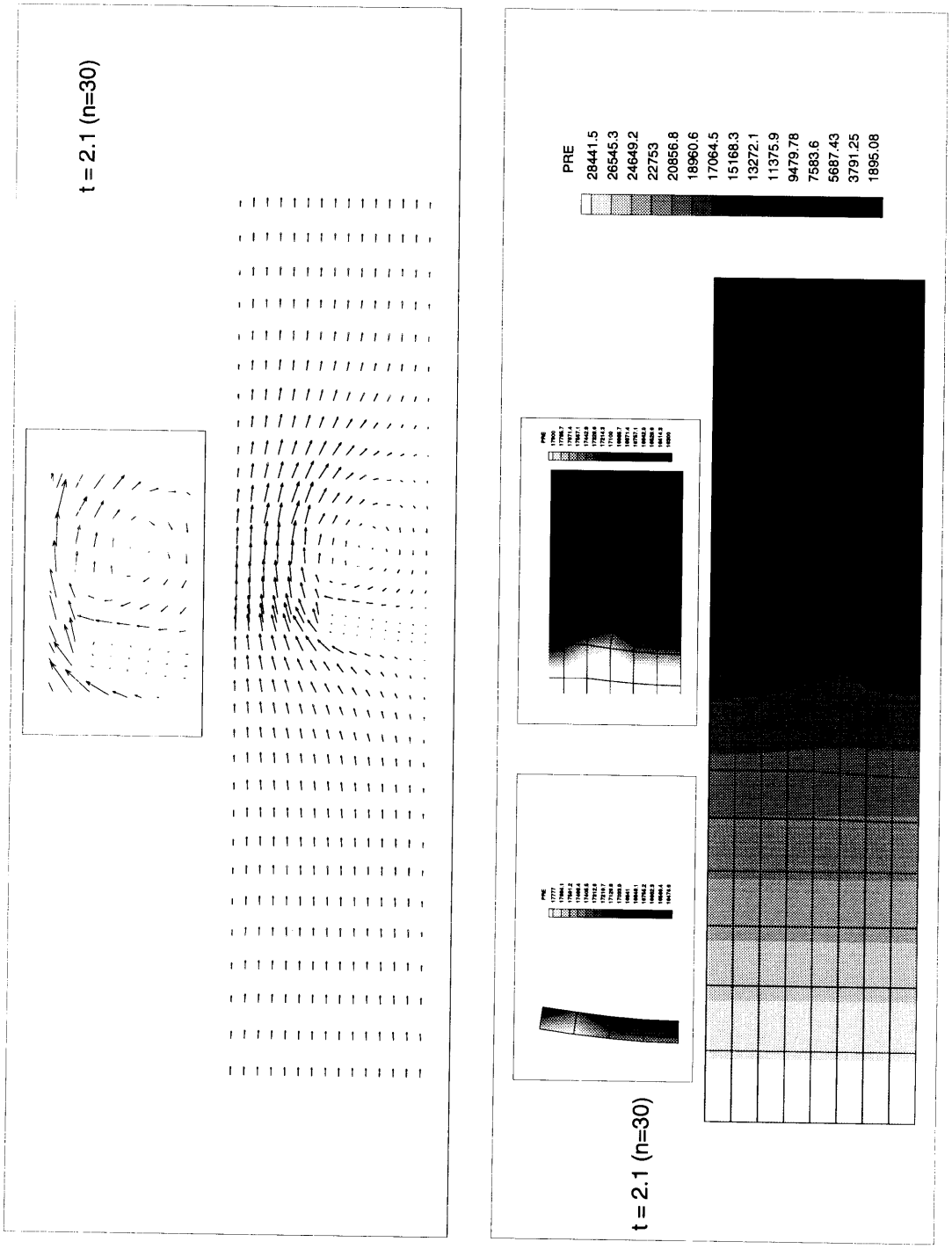

Figure 6-51: Results at time 2.1 of the viscous flows interacting with structures (one hundred and thirty-six 9-node elements).

Chapter 7

Mode Superposition Method For Linear Fluid-structure Interaction

7.1 Introduction

A great deal of research has been performed on finite element methods for fluid-structure systems [1] [3] [10] and mostly direct integration methods are employed [14] [67]. With symmetric $\mathbf{M}, \mathbf{K}$, and $\mathbf{C}$ matrices (for conservative systems, the coupling matrix $\mathbf{C}$ has zero diagonal entries) in $\phi - U$ and $P - \phi - U$ formulations, a mode superposition method can be applied. However, this thesis shows that the procedure is different from the common spectrum analysis we are familiar with in structural dynamics [68] [35].

In this chapter, we will give the spectrum method for both potential-based and displacement-based formulations.

We assume an inviscid, irrotational compressible fluid with small motions and no gravity effects (to introduce the gravity effects in linear analysis, we have to include the surface potential). In the $\phi - U$ formulation, we use the velocity potential as the state variable for fluids and displacements for solids. In the $P - \phi - U$ formulation, we replace one velocity potential unknown with a pressure unknown for each fluid

region. Both potential-based formulations will give the same natural frequencies of the fluid-structure system, except the zero frequency mode.

In the u/p or u-p-Λ formulation, displacements are the state variables for both the structures and fluids, therefore $\mathbf{M}$ and $\mathbf{K}$ matrices are the true physical mass and stiffness matrices. Based on the discussion in Chapter 3 and 4, for general acoustoelastic/slosh fluid-structure interactions, we will have the standard spectrum method as used in structural dynamics.

The treatment of the effect of ground motions is discussed for both types of formulations.

7.2 Potential-based Formulations

7.2.1 Governing Equations

We start with the variational indicators for the structural region and the fluid region. For the solid region:

$$\begin{aligned}(V.I.)_s &= \int_{t_1}^{t_2}\{\frac{1}{2}\int_{V_s}\boldsymbol{\epsilon}^T\mathbf{C}_s\boldsymbol{\epsilon}dV - \frac{1}{2}\int_{V_s}\rho_s\dot{\mathbf{u}}^T\dot{\mathbf{u}}dV \\ &\quad -\int_{S_{fs}}(\mathbf{u}^I)^T\boldsymbol{f}^I dS - \int_{S_f}(\mathbf{u}^{S_f})^T\boldsymbol{f}^s dS - \int_{V_s}\mathbf{u}^T\mathbf{b}_s dV\}dt \end{aligned} \tag{7.1}$$

For the fluid region:

$$\begin{aligned}(V.I.)_f &= \int_{t_1}^{t_2}\{\frac{1}{2}\int_{V_f}\frac{1}{\beta}(P-\rho_f\dot{\phi})^2 dV - \frac{1}{2}\int_{V_f}\rho_f(\nabla\phi)^2 dV \\ &\quad -\int_{S_{fs}}(P-\rho_f\dot{\phi}^I)u_N dS\}dt \end{aligned} \tag{7.2}$$

where V_s, V_f, S_s and S_{fs} refer to structure domains, fluid domains, structure natural boundaries and fluid-structure interaction surfaces respectively. $\mathbf{u}$, ϕ and P are inde-

pendent variables. Note that only one hydrostatic pressure P is used to replace one nodal velocity potential for each fluid region. If we have k separate fluid domains, we should use k independent hydrostatic pressure P.

Using the fact that $\delta\mathcal{F} = 0$ at t_1 and t_2, where $\mathcal{F}$ stands for admissible independent state variables, we get,

$$\int_{V_s} \rho_s \delta\mathbf{u}^T \ddot{\mathbf{u}} dV + \int_{V_s} \delta\boldsymbol{\epsilon}^T \mathbf{C}_s \boldsymbol{\epsilon} dV - \int_{S_{fs}} (\delta\mathbf{u}^I)^T \boldsymbol{f}^I dS - \int_{S_f} (\delta\mathbf{u}^{S_f})^T \boldsymbol{f}^s dS - \int_{V_s} \delta\mathbf{u}^T \mathbf{b}_s dV = 0 \tag{7.3}$$

$$\int_{V_f} \frac{P}{\beta} \delta P dV - \int_{V_f} \frac{\rho_f}{\beta} \dot{\phi} \delta P dV + \int_{V_f} \frac{\dot{P}}{\beta} \rho_f \delta\phi dV - \int_{V_f} \rho_f (\nabla\delta\phi) \cdot (\nabla\phi) dV - \int_{V_f} \frac{{\rho_f}^2}{\beta} \ddot{\phi} \delta\phi dV - \int_{S_{fs}} \mathbf{u}^I \cdot \mathbf{n}\, \delta P dS - \int_{S_{fs}} \rho_f \dot{\mathbf{u}}^I \cdot \mathbf{n} \delta\phi^I dS = 0 \tag{7.4}$$

7.2.2 Finite Element Discretization and Frequency Analysis

The discretized forms of Eqs. (7.3) and (7.4) are,

$$\begin{aligned} \delta\mathbf{U}: \quad & \mathbf{M}_{ss}\ddot{\mathbf{U}} + \mathbf{C}_{fs}^T \dot{\boldsymbol{\Phi}} + \mathbf{K}_{ss}\mathbf{U} + \mathbf{K}_{ps}^T \mathbf{P} &&= \mathbf{R}_s \\ \delta P: \quad & \mathbf{C}_{pf}\dot{\boldsymbol{\Phi}} + \mathbf{K}_{pp}\mathbf{P} + \mathbf{K}_{ps}\mathbf{U} &&= \mathbf{0} \\ \delta\phi: \quad & -\mathbf{M}_{ff}\ddot{\boldsymbol{\Phi}} + \mathbf{C}_{fs}\dot{\mathbf{U}} + \mathbf{C}_{pf}^T \dot{\mathbf{P}} - \mathbf{K}_{ff}\boldsymbol{\Phi} &&= \mathbf{0} \end{aligned} \tag{7.5}$$

We use the standard isoparametric elements for both fluid domains and structure domains [14] [35]. A typical N-node solid element has the following discretization relations,

$$\begin{aligned} x &= \mathbf{h}\,\mathbf{X}, \qquad y = \mathbf{h}\,\mathbf{Y}, \qquad z = \mathbf{h}\,\mathbf{Z} \\ \mathbf{u} &= \mathbf{H}\,\mathbf{U}, \qquad \mathbf{u}^I\mathbf{n} = \mathbf{b}\,\mathbf{U} \end{aligned} \tag{7.6}$$

where

$$\mathbf{h} = [h_1 \;\; h_2 \;\; h_3 \;\; ... \;\; h_N], \qquad \mathbf{X}^T = [x_1 \;\; x_2 \;\; x_3 \;\; ... \;\; x_N]$$
$$\mathbf{Y}^T = [y_1 \;\; y_2 \;\; y_3 \;\; ... \;\; y_N], \qquad \mathbf{Z}^T = [z_1 \;\; z_2 \;\; z_3 \;\; ... \;\; z_N]$$

$$\mathbf{H} = \begin{bmatrix} h_1 & 0 & 0 & h_2 & 0 & 0 & h_3 & 0 & 0 & ... & h_N & 0 & 0 \\ 0 & h_1 & 0 & 0 & h_2 & 0 & 0 & h_3 & 0 & 0 & ... & h_N & 0 \\ 0 & 0 & h_1 & 0 & 0 & h_2 & 0 & 0 & h_3 & 0 & 0 & ... & h_N \end{bmatrix}$$

$$\mathbf{U}^T = [u_1 \;\; v_1 \;\; w_1 \;\; u_2 \;\; v_2 \;\; w_2 \;\; ... \;\; u_N \;\; v_N \;\; w_N]$$

Then on the solid element level, we have,

$$\mathbf{K}_{ss} = \int \mathbf{B}^T \mathbf{C}_s \mathbf{B} \, dV, \quad \mathbf{M}_{ss} = \int \rho_s \mathbf{H}^T \mathbf{H} \, dV \tag{7.7}$$

where $\mathbf{C}_s$ is the elasticity matrix, and

$$\mathbf{R}_s = \int \mathbf{H}^T \mathbf{b}_s \, dV + \int \mathbf{H}^{S_f T} \boldsymbol{f}^s \, dS$$

For a typical fluid element (without replacement of one velocity potential unknown by the pressure unknown), we have the following discretization relations,

$$\phi = \mathbf{h}\,\boldsymbol{\Phi}, \qquad \nabla\phi = \mathbf{D}\,\boldsymbol{\Phi}, \qquad \phi^I = \mathbf{a}\,\boldsymbol{\Phi} \tag{7.8}$$

where

$$\boldsymbol{\Phi}^T = [\phi_1 \;\; \phi_2 \;\; \phi_3 \;\; ... \;\; \phi_N]$$

$$\mathbf{D} = \begin{bmatrix} \frac{\partial h_1}{\partial x} & \frac{\partial h_2}{\partial x} & \frac{\partial h_3}{\partial x} & \cdots & \frac{\partial h_N}{\partial x} \\ \frac{\partial h_1}{\partial y} & \frac{\partial h_2}{\partial y} & \frac{\partial h_3}{\partial y} & \cdots & \frac{\partial h_N}{\partial y} \\ \frac{\partial h_1}{\partial z} & \frac{\partial h_2}{\partial z} & \frac{\partial h_3}{\partial z} & \cdots & \frac{\partial h_N}{\partial z} \end{bmatrix}$$

Therefore, on the fluid element level, we have,

$$\mathbf{M}_{ff} = \int \frac{\rho_f^2}{\beta} \mathbf{h}^T \mathbf{h} dV, \quad \mathbf{K}_{ff} = \int \rho_f \mathbf{D}^T \mathbf{D} \, dV \tag{7.9}$$

For the fluid element in which one velocity potential unknown is replaced by the pressure unknown, the discretization relations are the following (without loss of generality, we assume the N-th nodal velocity potential unknown is replaced by a pressure unknown),

$$\phi = \mathbf{h}' \boldsymbol{\Phi}, \quad \nabla\phi = \mathbf{D}' \boldsymbol{\Phi}, \quad \phi^I = \mathbf{a}' \boldsymbol{\Phi} \tag{7.10}$$

where

$$\boldsymbol{\Phi}^T = [\phi_1 \quad \phi_2 \quad \phi_3 \quad \cdots \quad \phi_{N-1}]$$

$$\mathbf{D}' = \begin{bmatrix} \frac{\partial h_1}{\partial x} & \frac{\partial h_2}{\partial x} & \frac{\partial h_3}{\partial x} & \cdots & \frac{\partial h_{N-1}}{\partial x} \\ \frac{\partial h_1}{\partial y} & \frac{\partial h_2}{\partial y} & \frac{\partial h_3}{\partial y} & \cdots & \frac{\partial h_{N-1}}{\partial y} \\ \frac{\partial h_1}{\partial z} & \frac{\partial h_2}{\partial z} & \frac{\partial h_3}{\partial z} & \cdots & \frac{\partial h_{N-1}}{\partial z} \end{bmatrix}$$

For these types of elements, we have,

$$\begin{aligned}
\mathbf{C}_{pf} &= \int \frac{\rho_f}{\beta}\mathbf{h}'\, dV, & \mathbf{C}_{fs}^T &= -\int \rho_f \mathbf{b}^T\mathbf{a}'\, dS \\
\mathbf{M}_{ff} &= \int \frac{\rho_f^2}{\beta}\mathbf{h}'^T\mathbf{h}' dV, & \mathbf{K}_{ff} &= \int \rho_f \mathbf{D}'^T\mathbf{D}'\, dV \\
\mathbf{K}_{pp} &= -\int \frac{1}{\beta} dV, & \mathbf{K}_{ps}^T &= \int \mathbf{b}^T dS
\end{aligned} \tag{7.11}$$

Note that the three equations in (7.5) have the units of force, volume and mass flow rate respectively. Combining the units from their corresponding variations, they all have the unit of energy.

The matrix form of (7.5) is,

$$\begin{bmatrix} \mathbf{M}_{ss} & \mathbf{0} & \mathbf{0} \\ \mathbf{0} & \mathbf{0} & \mathbf{0} \\ \mathbf{0} & \mathbf{0} & -\mathbf{M}_{ff} \end{bmatrix} \begin{Bmatrix} \ddot{\mathbf{U}} \\ \ddot{\mathbf{P}} \\ \ddot{\boldsymbol{\Phi}} \end{Bmatrix} + \begin{bmatrix} \mathbf{0} & \mathbf{0} & \mathbf{C}_{fs}^T \\ \mathbf{0} & \mathbf{0} & \mathbf{C}_{pf} \\ \mathbf{C}_{fs} & \mathbf{C}_{pf}^T & \mathbf{0} \end{bmatrix} \begin{Bmatrix} \dot{\mathbf{U}} \\ \dot{\mathbf{P}} \\ \dot{\boldsymbol{\Phi}} \end{Bmatrix}$$

$$+ \begin{bmatrix} \mathbf{K}_{ss} & \mathbf{K}_{ps}^T & \mathbf{0} \\ \mathbf{K}_{ps} & \mathbf{K}_{pp} & \mathbf{0} \\ \mathbf{0} & \mathbf{0} & -\mathbf{K}_{ff} \end{bmatrix} \begin{Bmatrix} \mathbf{U} \\ \mathbf{P} \\ \boldsymbol{\Phi} \end{Bmatrix} = \begin{Bmatrix} \mathbf{R}_s \\ \mathbf{0} \\ \mathbf{0} \end{Bmatrix} \tag{7.12}$$

If we change the sign of the second equation in (7.5), we get the new matrix form as,

$$\begin{bmatrix} \mathbf{M}_{ss} & \mathbf{0} & \mathbf{0} \\ \mathbf{0} & \mathbf{0} & \mathbf{0} \\ \mathbf{0} & \mathbf{0} & -\mathbf{M}_{ff} \end{bmatrix} \begin{Bmatrix} \ddot{\mathbf{U}} \\ \ddot{\mathbf{P}} \\ \ddot{\boldsymbol{\Phi}} \end{Bmatrix} + \begin{bmatrix} \mathbf{0} & \mathbf{0} & \mathbf{C}_{fs}^T \\ \mathbf{0} & \mathbf{0} & -\mathbf{C}_{pf} \\ \mathbf{C}_{fs} & \mathbf{C}_{pf}^T & \mathbf{0} \end{bmatrix} \begin{Bmatrix} \dot{\mathbf{U}} \\ \dot{\mathbf{P}} \\ \dot{\boldsymbol{\Phi}} \end{Bmatrix}$$

$$+ \begin{bmatrix} \mathbf{K}_{ss} & \mathbf{K}_{ps}^T & \mathbf{0} \\ -\mathbf{K}_{ps} & -\mathbf{K}_{pp} & \mathbf{0} \\ \mathbf{0} & \mathbf{0} & -\mathbf{K}_{ff} \end{bmatrix} \begin{Bmatrix} \mathbf{U} \\ \mathbf{P} \\ \boldsymbol{\Phi} \end{Bmatrix} = \begin{Bmatrix} \mathbf{R}_s \\ \mathbf{0} \\ \mathbf{0} \end{Bmatrix} \tag{7.13}$$

Both Eqs. (7.12) and (7.13) represent the same fluid-structure interaction problem and should have the same eigenvalues and eigenvectors. From the kinematic boundary conditions along the fluid-structure interface, we find that physically $\mathbf{\Phi}$ has a $\pi/2$ phase shift from $\mathbf{U}$. Therefore we assign the m-th eigenvector as $\mathbf{X}_m^T = (\mathbf{U}_m^T\ \mathbf{P}_m^T\ i\mathbf{\Phi}_m^T)$ where $\mathbf{U}_m$,$\mathbf{P}_m$ and $\mathbf{\Phi}_m$ are real values.

Let the m-th eigensolution be $\mathbf{X} = \mathbf{X}_m e^{\lambda_m t}$; from Eqs. (7.13) and (7.12), we get,

$$a_m' \lambda_m^2 + b_m' \lambda_m + c_m' = 0 \tag{7.14}$$

$$a_m \lambda_m^2 + b_m \lambda_m + c_m = 0 \tag{7.15}$$

where

$$\begin{aligned} a_m' &= \mathbf{U}_m^T \mathbf{M}_{ss} \mathbf{U}_m + \mathbf{\Phi}_m^T \mathbf{M}_{ff} \mathbf{\Phi}_m \\ b_m' &= 2i \mathbf{U}_m^T \mathbf{C}_{fs}^T \mathbf{\Phi}_m \\ c_m' &= \mathbf{U}_m^T \mathbf{K}_{ss} \mathbf{U}_m + \mathbf{\Phi}_m^T \mathbf{K}_{ff} \mathbf{\Phi}_m + \mathbf{P}_m^T (-\mathbf{K}_{pp}) \mathbf{P}_m \end{aligned}$$

and

$$\begin{aligned} a_m &= \mathbf{U}_m^T \mathbf{M}_{ss} \mathbf{U}_m + \mathbf{\Phi}_m^T \mathbf{M}_{ff} \mathbf{\Phi}_m \\ b_m &= 2i(\mathbf{U}_m^T \mathbf{C}_{fs}^T \mathbf{\Phi}_m + \mathbf{P}_m^T \mathbf{C}_{pf} \mathbf{\Phi}_m) \\ c_m &= \mathbf{U}_m^T \mathbf{K}_{ss} \mathbf{U}_m + \mathbf{\Phi}_m^T \mathbf{K}_{ff} \mathbf{\Phi}_m + \mathbf{P}_m^T \mathbf{K}_{pp} \mathbf{P}_m + 2\mathbf{P}_m^T \mathbf{K}_{ps} \mathbf{U}_m \end{aligned}$$

Since $\mathbf{M}_{ss}$, $\mathbf{M}_{ff}$,$-\mathbf{K}_{pp}$ and $\mathbf{K}_{ss}$ are positive definite matrices, a_m' and c_m' should be positive. Furthermore, Eq. (7.14) gives pure imaginary eigenvalues of the coupled fluid-structure system. Assign $\lambda_m = i\omega_m$, $m = 1, 2, ..., n$, n is the total number of degrees of freedom and substitute eigensolution $\mathbf{X}_m e^{i\omega_m t}$ into the left side of equation (7.12), we get

$$\begin{aligned} -\omega_m^2 \mathbf{M}_{ss}\mathbf{U}_m - \omega_m \mathbf{C}_{fs}^T \boldsymbol{\Phi}_m + \mathbf{K}_{ss}\mathbf{U}_m + \mathbf{K}_{ps}^T \mathbf{P}_m &= \mathbf{0} \\ -\omega_m \mathbf{C}_{pf}\boldsymbol{\Phi}_m + \mathbf{K}_{ps}\mathbf{U}_m + \mathbf{K}_{pp}\mathbf{P}_m &= \mathbf{0} \\ \omega_m^2 \mathbf{M}_{ff}\boldsymbol{\Phi}_m + \omega_m \mathbf{C}_{fs}\mathbf{U}_m + \omega_m \mathbf{C}_{pf}^T \mathbf{P}_m - \mathbf{K}_{ff}\boldsymbol{\Phi}_m &= \mathbf{0} \end{aligned} \tag{7.16}$$

with matrix form,

$$-\omega_m^2 \begin{bmatrix} \mathbf{M}_{ss} & \mathbf{0} & \mathbf{0} \\ \mathbf{0} & \mathbf{0} & \mathbf{0} \\ \mathbf{0} & \mathbf{0} & \mathbf{M}_{ff} \end{bmatrix} \begin{Bmatrix} \mathbf{U}_m \\ \mathbf{P}_m \\ \boldsymbol{\Phi}_m \end{Bmatrix} - \omega_m \begin{bmatrix} \mathbf{0} & \mathbf{0} & \mathbf{C}_{fs}^T \\ \mathbf{0} & \mathbf{0} & \mathbf{C}_{pf} \\ \mathbf{C}_{fs} & \mathbf{C}_{pf}^T & \mathbf{0} \end{bmatrix} \begin{Bmatrix} \mathbf{U}_m \\ \mathbf{P}_m \\ \boldsymbol{\Phi}_m \end{Bmatrix}$$

$$+ \begin{bmatrix} \mathbf{K}_{ss} & \mathbf{K}_{ps}^T & \mathbf{0} \\ \mathbf{K}_{ps} & \mathbf{K}_{pp} & \mathbf{0} \\ \mathbf{0} & \mathbf{0} & \mathbf{K}_{ff} \end{bmatrix} \begin{Bmatrix} \mathbf{U}_m \\ \mathbf{P}_m \\ \boldsymbol{\Phi}_m \end{Bmatrix} = \begin{Bmatrix} \mathbf{0} \\ \mathbf{0} \\ \mathbf{0} \end{Bmatrix} \tag{7.17}$$

In the $\phi - U$ formulation, we get the similar equation as Eq. (7.12),

$$\begin{bmatrix} \mathbf{M}_{ss} & \mathbf{0} & \mathbf{0} \\ \mathbf{0} & -\mathbf{M}_{ff} & -\mathbf{M}_{af}^T \\ \mathbf{0} & -\mathbf{M}_{af} & -\mathbf{M}_{aa} \end{bmatrix} \begin{Bmatrix} \ddot{\mathbf{U}} \\ \ddot{\boldsymbol{\Phi}} \\ \ddot{\boldsymbol{\Phi}}_a \end{Bmatrix} + \begin{bmatrix} \mathbf{0} & \mathbf{C}_{fs}^T & \mathbf{C}_{as}^T \\ \mathbf{C}_{fs} & \mathbf{0} & \mathbf{0} \\ \mathbf{C}_{as} & \mathbf{0} & \mathbf{0} \end{bmatrix} \begin{Bmatrix} \dot{\mathbf{U}} \\ \dot{\boldsymbol{\Phi}} \\ \dot{\boldsymbol{\Phi}}_a \end{Bmatrix}$$

$$+ \begin{bmatrix} \mathbf{K}_{ss} & \mathbf{0} & \mathbf{0} \\ \mathbf{0} & -\mathbf{K}_{ff} & -\mathbf{K}_{af}^T \\ \mathbf{0} & -\mathbf{K}_{af} & -\mathbf{K}_{ff} \end{bmatrix} \begin{Bmatrix} \mathbf{U} \\ \boldsymbol{\Phi} \\ \boldsymbol{\Phi}_a \end{Bmatrix} = \begin{Bmatrix} \mathbf{R}_s \\ \mathbf{0} \\ \mathbf{0} \end{Bmatrix} \tag{7.18}$$

where $\boldsymbol{\Phi}_a$ denotes the velocity potentials which will be replaced by pressure unknowns. Eq. (7.18) has the same eigenvalues as Eq. (7.12) except for the zero energy mode. From the same reasoning, the m-th eigensolution of Eq. (7.18) is in the form $\mathbf{X} =$

$\mathbf{X}_m e^{\lambda_m t}$, where $\mathbf{X}_m^T = (\mathbf{U}_m^T \; i\boldsymbol{\Phi}_m^{'T} \; i(\boldsymbol{\Phi}_a)_m^T)$. Assign $\lambda_m = i\omega_m$, then we have,

$$-\omega_m^2 \begin{bmatrix} \mathbf{M}_{ss} & \mathbf{0} & \mathbf{0} \\ \mathbf{0} & \mathbf{M}_{ff} & \mathbf{M}_{af}^T \\ \mathbf{0} & \mathbf{M}_{af} & \mathbf{M}_{aa} \end{bmatrix} \begin{Bmatrix} \mathbf{U}_m \\ \boldsymbol{\Phi}_m^{'} \\ (\boldsymbol{\Phi}_a)_m \end{Bmatrix} - \omega_m \begin{bmatrix} \mathbf{0} & \mathbf{C}_{fs}^T & \mathbf{C}_{as}^T \\ \mathbf{C}_{fs} & \mathbf{0} & \mathbf{0} \\ \mathbf{C}_{as} & \mathbf{0} & \mathbf{0} \end{bmatrix} \begin{Bmatrix} \mathbf{U}_m \\ \boldsymbol{\Phi}_m^{'} \\ (\boldsymbol{\Phi}_a)_m \end{Bmatrix}$$

$$+ \begin{bmatrix} \mathbf{K}_{ss} & \mathbf{0} & \mathbf{0} \\ \mathbf{0} & \mathbf{K}_{ff} & \mathbf{K}_{af}^T \\ \mathbf{0} & \mathbf{K}_{af} & \mathbf{K}_{aa} \end{bmatrix} \begin{Bmatrix} \mathbf{U}_m \\ \boldsymbol{\Phi}_m^{'} \\ (\boldsymbol{\Phi}_a)_m \end{Bmatrix} = \begin{Bmatrix} \mathbf{0} \\ \mathbf{0} \\ \mathbf{0} \end{Bmatrix} \tag{7.19}$$

7.2.3 Mode Superposition Method

A determinant search method can be used to find the needed real eigenvalues ω_m from Eq. (7.17), where $m = 1, ..., p$. Note that the number of negative elements in the matrix $\mathbf{D}$ of the $\mathbf{L}\,\mathbf{D}\,\mathbf{L}^T$ factorization of $\mathbf{K} - \omega_i\mathbf{C} - \omega_i^2\mathbf{M}$ is the number of eigenvalues below ω_i [35] [2].

Rewrite Eq. (7.12) in the following form,

$$\mathbf{A}\,\mathbf{Y} + \mathbf{B}\,\dot{\mathbf{Y}} = \boldsymbol{\mathcal{F}} \tag{7.20}$$

where $\mathbf{X}^T = (\mathbf{U}^T \; \mathbf{P}^T \; \boldsymbol{\Phi}^T)$, $\mathbf{F}^T = (\mathbf{R}_s^T \; \mathbf{0}^T \; \mathbf{0}^T)$ and

$$\mathbf{A} = \begin{bmatrix} \mathbf{K} & \mathbf{0} \\ \mathbf{0} & -\mathbf{M} \end{bmatrix} \qquad \mathbf{Y} = \begin{pmatrix} \mathbf{X} \\ \dot{\mathbf{X}} \end{pmatrix}$$

$$\mathbf{B} = \begin{bmatrix} \mathbf{C} & \mathbf{M} \\ \mathbf{M} & \mathbf{0} \end{bmatrix} \qquad \boldsymbol{\mathcal{F}} = \begin{pmatrix} \mathbf{F} \\ \mathbf{0} \end{pmatrix}$$

Without loss of generality, we assume the system has distinct eigenvalues. The following orthogonal relationships hold,

$$\mathbf{Y}_m^T \mathbf{B}\ \mathbf{Y}_k = \begin{cases} 0 & \text{if } m \neq k \\ b_m + 2a_m\lambda_m & \text{if } m = k \end{cases} \tag{7.21}$$

$$\mathbf{Y}_m^T \mathbf{A}\ \mathbf{Y}_k = \begin{cases} 0 & \text{if } m \neq k \\ c_m - a_m\lambda_m^2 & \text{if } m = k \end{cases} \tag{7.22}$$

If we have multiple eigenvalues, we can construct independent eigenvector pairs which still have the orthogonality properties [35].

Assign $\mathbf{Y}(t) = \mathbf{YQ}(t)$, where $\mathbf{Y} = (\mathbf{Y}_1\ \mathbf{Y}_2\ ...\ \mathbf{Y}_{2n})$ are the mode shapes, $\mathbf{Q}^T(t) = (q_1\ q_2\ ...\ q_{2n})$ is the generalized coordinate vector. Using the orthogonality relations, we have,

$$\dot{q}_i + p_i q_i = h_i \tag{7.23}$$

where $i = 1, 2, ..., 2n$ and

$$\begin{aligned} p_i &= \frac{c_i - a_i\lambda_i^2}{b_i + 2a_i\lambda_i} \\ h_i &= \frac{\mathbf{Y}_i^T\ \mathbf{F}}{b_i + 2a_i\lambda_i} \end{aligned} \tag{7.24}$$

The initial conditions for Eq. (7.20) are,

$$q_i(0) = \frac{\mathbf{Y}_i^T \mathbf{B}\ \mathbf{Y}_0}{b_i + 2a_i\lambda_i} \tag{7.25}$$

Note that $\mathbf{Y}_0^T = (\mathbf{U}_0\ \ \mathbf{P}_0\ \ \boldsymbol{\Phi}_0\ \ \dot{\mathbf{U}}_0\ \ \dot{\mathbf{P}}_0\ \ \dot{\boldsymbol{\Phi}}_0)$ has to satisfy the second equation of Eqs. (7.5).

Define

$$
\begin{aligned}
\alpha_m &= \left[\mathbf{U}_m^T \mathbf{V}_o^{(u)} + \mathbf{P}_m^T \mathbf{V}_o^{(p)} - \omega_m \boldsymbol{\Phi}_m^T \mathbf{V}_o^{(\dot{\Phi})}\right] \\
\beta_m &= \left[\boldsymbol{\Phi}_m^T \mathbf{V}_o^{(\phi)} + \omega_m \mathbf{U}_m^T \mathbf{V}_o^{(\dot{u})} + \omega_m \mathbf{P}_m^T \mathbf{V}_o^{(\dot{p})}\right] \\
\gamma_m &= 2\left[\boldsymbol{\Phi}_m^T \mathbf{C}_{fs} \mathbf{U}_m + \boldsymbol{\Phi}_m^T \mathbf{C}_{pf}^T \mathbf{P}_m\right] \\
\xi_m &= 2\omega_m \left[\mathbf{U}_m^T \mathbf{M}_{ss} \mathbf{U}_m + \boldsymbol{\Phi}_m^T \mathbf{M}_{ff} \boldsymbol{\Phi}_m\right]
\end{aligned}
$$

with

$$
\mathbf{V}_o = \mathbf{B}\,\mathbf{Y}_o = \begin{Bmatrix} \mathbf{V}_o^{(u)} \\ \mathbf{V}_o^{(p)} \\ \mathbf{V}_o^{(\phi)} \\ \mathbf{V}_o^{(\dot{u})} \\ \mathbf{V}_o^{(\dot{p})} \\ \mathbf{V}_o^{(\dot{\phi})} \end{Bmatrix}
$$

Therefore we will have,

$$
q_{(2m-1)}(0) = \frac{\mathbf{Y}_{(2m-1)}^T \mathbf{V}_o}{b_m + 2\lambda_m a_m} = \frac{\alpha_m + \beta_m i}{(\gamma_m + \xi_m) i} = A_m + B_m i
$$

$$
q_{(2m)}(0) = -\frac{\mathbf{Y}_{2m}^T \mathbf{V}_o}{b_m + 2\lambda_m a_m} = \frac{-\alpha_m + \beta_m i}{(\gamma_m + \xi_m) i} = A_m - B_m i
$$

where

$$
A_m = \frac{\beta_m}{\gamma_m + \xi_m}, \quad B_m = -\frac{\alpha_m}{\gamma_m + \xi_m}
$$

Eqs. (7.24) give us,

$$
h_{(2m-1)} = C_m + D_m i
$$

$$h_{2m} = C_m - D_m i$$

where

$$D_m = \frac{-\mathbf{U}_m^T \mathbf{F}^{(u)} - \mathbf{P}_m^T \mathbf{F}^{(p)} + \omega_m \boldsymbol{\Phi}_m^T \mathbf{F}^{(\dot{\phi})}}{\gamma_m + \xi_m}$$

$$C_m = \frac{\boldsymbol{\Phi}_m^T \mathbf{F}^{(\phi)} - \omega_m \mathbf{U}_m^T \mathbf{F}^{(\dot{u})} - \omega_m \mathbf{P}_m^T \mathbf{F}^{(\dot{p})}}{\gamma_m + \xi_m}$$

and

$$\mathbf{F} = \mathbf{B}\,\mathbf{Y}_o = \begin{Bmatrix} \mathbf{F}^{(u)} \\ \mathbf{F}^{(p)} \\ \mathbf{F}^{(\phi)} \\ \mathbf{F}^{(\dot{u})} \\ \mathbf{F}^{(\dot{p})} \\ \mathbf{F}^{(\dot{\phi})} \end{Bmatrix}$$

The solution to Eq. (7.23) is,

$$q_i(t) = \int_0^T e^{p_i(\tau - t)} h_i(\tau) d\tau + q_i(0) e^{-p_i t} \tag{7.26}$$

Eq. (7.20) has the solution,

$$\mathbf{Y}(t) = \mathbf{YQ}(t) = \sum_{m=1}^{2n} \mathbf{Y}_m q_m(t) \tag{7.27}$$

Based on the discussion before, we reconstruct the complex eigenvector and eigenvalue couples as follows,

$$\begin{aligned}
\mathbf{Y}_{2m-1}^T &= (\mathbf{U}_m^T \quad \mathbf{P}_m^T \quad i\boldsymbol{\Phi}_m^T \quad i\omega_m\mathbf{U}_m^T \quad i\omega_m\mathbf{P}_m^T \quad -\omega_m\boldsymbol{\Phi}_m^T) \\
\mathbf{Y}_{2m}^T &= (\mathbf{U}_m^T \quad \mathbf{P}_m^T \quad -i\boldsymbol{\Phi}_m^T \quad -i\omega_m\mathbf{U}_m^T \quad -i\omega_m\mathbf{P}_m^T \quad -\omega_m\boldsymbol{\Phi}_m^T)
\end{aligned} \tag{7.28}$$

The final form of the mode superposition solution is,

$$\begin{Bmatrix} \mathbf{U} \\ \mathbf{P} \\ \boldsymbol{\Phi} \\ \dot{\mathbf{U}} \\ \dot{\mathbf{P}} \\ \dot{\boldsymbol{\Phi}} \end{Bmatrix} = \sum_{m=1}^{p} \begin{Bmatrix} \mathbf{U}_m & \{ \; F_m^u(t) + 2A_m \cos\omega_m t - 2B_m \sin\omega_m t \; \} \\ \mathbf{P}_m & \{ \; F_m^p(t) + 2A_m \cos\omega_m t - 2B_m \sin\omega_m t \; \} \\ \boldsymbol{\Phi}_m & \{ \; F_m^\phi(t) - 2A_m \sin\omega_m t - 2B_m \cos\omega_m t \; \} \\ \omega_m\mathbf{U}_m & \{ \; F_m^{\dot{u}}(t) - 2A_m \sin\omega_m t - 2B_m \cos\omega_m t \; \} \\ \omega_m\mathbf{P}_m & \{ \; F_m^{\dot{p}}(t) - 2A_m \sin\omega_m t - 2B_m \cos\omega_m t \; \} \\ \omega_m\boldsymbol{\Phi}_m & \{ \; F_m^{\dot{\phi}}(t) - 2A_m \cos\omega_m t + 2B_m \sin\omega_m t \; \} \end{Bmatrix} \tag{7.29}$$

where p denotes the number of real eigenvalues we are interested in and,

$$\begin{aligned}
F_m^u(t) &= \int_0^T [2C_m(\tau)\cos\omega_m(\tau - t) + 2D_m(\tau)\sin\omega_m(\tau - t)]\, d\tau \\
F_m^p(t) &= \int_0^T [2C_m(\tau)\cos\omega_m(\tau - t) + 2D_m(\tau)\sin\omega_m(\tau - t)]\, d\tau \\
F_m^\phi(t) &= \int_0^T [2C_m(\tau)\sin\omega_m(\tau - t) - 2D_m(\tau)\cos\omega_m(\tau - t)]\, d\tau \\
F_m^{\dot{u}}(t) &= \int_0^T [2C_m(\tau)\sin\omega_m(\tau - t) - 2D_m(\tau)\cos\omega_m(\tau - t)]\, d\tau \\
F_m^{\dot{p}}(t) &= \int_0^T [2C_m(\tau)\sin\omega_m(\tau - t) - 2D_m(\tau)\cos\omega_m(\tau - t)]\, d\tau \\
F_m^{\dot{\phi}}(t) &= \int_0^T [-2C_m(\tau)\cos\omega_m(\tau - t) - 2D_m(\tau)\sin\omega_m(\tau - t)]\, d\tau
\end{aligned} \tag{7.30}$$

7.2.4 Ground Motion Effects

To incorporate ground motion effects is an important part of many dynamic analyses of fluid-structure systems. It is obvious that the fluid kinetic energy will include the ground motion as well as the relative fluid motion in the system. The change of the variational indicator for fluids is as follows,

$$(V.I.)_f = \int_{t_1}^{t_2} \{\frac{1}{2}\int_{V_f} \frac{1}{\beta}(P - \rho_f \dot{\phi})^2 dV - \frac{1}{2}\int_{V_f} \rho_f (\nabla\phi + \dot{\mathbf{u}}_g)^2 dV - \int_{S_{fs}} (P - \rho_f \dot{\phi}^I) u_N dS\} dt \tag{7.31}$$

Note that the displacement $\mathbf{u}$ and potential ϕ represent the relative motion and $\dot{\mathbf{u}}_g$ is a known quantity. From a similar approach to the structure, we obtain the final dynamic equations of the fluid-structure system,

$$\begin{bmatrix} \mathbf{M}_{ss} & \mathbf{0} & \mathbf{0} \\ \mathbf{0} & \mathbf{0} & \mathbf{0} \\ \mathbf{0} & \mathbf{0} & -\mathbf{M}_{ff} \end{bmatrix} \begin{Bmatrix} \ddot{\mathbf{U}} \\ \ddot{\mathbf{P}} \\ \ddot{\boldsymbol{\Phi}} \end{Bmatrix} + \begin{bmatrix} \mathbf{0} & \mathbf{0} & \mathbf{C}_{fs}^T \\ \mathbf{0} & \mathbf{0} & \mathbf{C}_{pf} \\ \mathbf{C}_{fs} & \mathbf{C}_{pf}^T & \mathbf{0} \end{bmatrix} \begin{Bmatrix} \dot{\mathbf{U}} \\ \dot{\mathbf{P}} \\ \dot{\boldsymbol{\Phi}} \end{Bmatrix}$$

$$+ \begin{bmatrix} \mathbf{K}_{ss} & \mathbf{K}_{ps}^T & \mathbf{0} \\ \mathbf{K}_{ps} & \mathbf{K}_{pp} & \mathbf{0} \\ \mathbf{0} & \mathbf{0} & -\mathbf{K}_{ff} \end{bmatrix} \begin{Bmatrix} \mathbf{U} \\ \mathbf{P} \\ \boldsymbol{\Phi} \end{Bmatrix} = \begin{Bmatrix} \mathbf{R}_s - \mathbf{M}_{ss}\ddot{\mathbf{U}}_g \\ \mathbf{0} \\ \mathbf{G}\dot{\mathbf{u}}_g \end{Bmatrix} \tag{7.32}$$

where

$$\mathbf{G} = \int \rho_f \mathbf{D}^T \, dV$$

7.3 Displacement-based Formulations

In Chapters 3 and 4, the **u**/p and **u**-p-$\boldsymbol{\Lambda}$ formulations are discussed in detail. After we condense out the pressure and vorticity moment unknowns, we will have,

$$\mathbf{M}\ddot{\mathbf{U}} + \mathbf{K}^*\mathbf{U} = \mathbf{R}(t) \tag{7.33}$$

where $\mathbf{M}$ is the positive definite mass (true physical mass) matrix, $\mathbf{K}^*$ is the stiffness

(true physical stiffness) matrix, $\mathbf{U}$ is the nodal displacement unknowns and $\mathbf{R}(t)$ is the discretized oscillatory force term. As discussed in Chapters 3 and 4, $\mathbf{K}^*$ is not necessarily a positive definite matrix and

$$\begin{aligned} \mathbf{K}^* &= \mathbf{K} - \mathbf{L}\mathbf{A}^{-1}\mathbf{L}^T && \text{for the } \mathbf{u}/\text{p formulation} \\ \mathbf{K}^* &= -\mathbf{L}\mathbf{A}^{-1}\mathbf{L}^T - \mathbf{Q}\mathbf{G}^{-1}\mathbf{Q}^T && \text{for the } \mathbf{u}\text{-p-}\mathbf{\Lambda} \text{ formulation} \end{aligned}$$

where we assume the total degrees of the freedom is n and the rank of $\mathbf{K}^*$ matrix is k. The mode superposition method for Eq. (7.33) is the standard one for structure dynamcis as discussed in [35].

Chapter 8

Conclusions and Discussions

In this thesis, we conclude that to have a reliable finite element procedure for both linear and nonlinear fluid-structure interaction analyses, the $\mathbf{u}/\mathrm{p}$ or $\mathbf{v}/\mathrm{p}$ formulations with mixed elements satisfying the inf-sup condition are to be highly recommended. The developed primitive variable formulations in this thesis can be used for general acoustoelastic/slosh problems, incompressible (or almost incompressible) flows (including large free surface motions) and their interactions with linear and nonlinear solids. In these formulations, displacements (or velocities) and pressure are used as independent variables. It is effective that the pressure is associated with element internal variables and is statically condensed out at the element level. Then the only nodal point variables used in the assemblage of elements are those corresponding to the displacements (or velocities). This enables the direct coupling of the fluid elements with the structural elements. Of course, in principle, we could also employ element nodal pressures that provide for continuity in pressure (hence cannot be statically condensed out at the element level).

We point out that the inviscid fluid model is not a requirement for acoustic fluid-structure interactions as long as the mesh is proper and the viscosity (or shear modulus) is assigned $O(\frac{1}{\beta})$. However, it is important to satisfy the requirements of both mass and momentum conservation around the fluid boundaries and fluid-structure

interfaces. We also conclude that in frequency analysis, the historically reported non-zero frequency spurious modes were caused either by the pure displacement formulation (and its penalty formulations) or the improper treatment of the boundary conditions. Therefore, the proper way of eliminating the non-zero frequency spurious modes is to use the $\mathbf{u}/\mathrm{p}$ formulations with mixed elements satisfying the inf-sup condition. A new effective three-field mixed finite element formulation ($\mathbf{u}$-p-$\mathbf{\Lambda}$) for the analyses of acoustic fluids and their interactions with structures is also presented in this thesis.

The developed upwinding scheme with both the standard Galerkin and the control volume finite element formulations is successfully used with the ALE kinematic description and high order mixed elements satisfying the inf-sup condition. This approach is the first attempt to incorporate both the need of upwinding techniques and the inf-sup condition for 9-node elements.

We have tested the formulations on some simple but well-chosen analysis problems, which heretofore we could not solve with displacement (or velocity)-based finite element formulations (or formulations derived therefrom). As indicated from the numerical results, the proposed upwinding formulation provides good solutions even for very coarse meshes. The new formulations have performed well in all linear and nonlinear analysis cases.

The results of our numerical experiments confirm that $9/3$ and $9/4-c$ elements for the $\mathbf{u}/\mathrm{p}$ and $\mathbf{v}/\mathrm{p}$ formulations; and $9-3-3$ and $9-4c-4c$ elements for the $\mathbf{u}$-p-$\mathbf{\Lambda}$ formulation are reliable. However, the use of $4/1$ elements with general meshes is not recommended for practical applications. It is shown that the $\mathbf{u}/\mathrm{p}$ formulation can be applied with $4/1$ macroelements which satisfy the inf-sup condition. The results of some numerical experiments on the use of $4/1$ elements with general meshes and inappropriate boundary tangential directions have been included in order to illustrate the importance of our recommendations.

In linear analysis, general acoustoelastic/slosh fluid-structure interactions can be

solved reliably with the developed primitive variable based mixed finite element formulations. In nonlinear analysis, the proposed upwinding formulation along with ALE descriptions for 9-node mixed elements provides a better option for the solution of the Navier-Stokes flows and their interactions with structures. Nevertheless, considerable research remains to be done. In particular, we look forward to:

- a better upwinding technique for convection dominated problems and the fundamental mathematical criterion (if there is one);
- a more comprehensive formulation involving thermal coupling and turbulence effects;
- ALE formulations for elastoplastic analysis;
- more feasible mesh adaptive procedures.

Appendix A

Constant Pressure Mode

Further insight into the inf-sup condition is obtained by studying the governing algebraic finite element equations [35]. Let us consider the case of the following matrix,

$$\begin{bmatrix} (\mathbf{K}_{uu})_h & (\mathbf{K}_{up})_h \\ (\mathbf{K}_{up})_h^T & (\mathbf{K}_{pp})_h \end{bmatrix} \begin{Bmatrix} \widehat{\mathbf{U}}_h \\ \widehat{\mathbf{P}}_h \end{Bmatrix} = \begin{Bmatrix} \mathbf{R}_h \\ \mathbf{0} \end{Bmatrix} \tag{A.1}$$

where $\widehat{\mathbf{U}}_h$ lists all the unknown nodal point displacements and $\widehat{\mathbf{P}}_h$ lists the unknown pressure variables. The number of displacement and pressure unknowns are n and m. The right side matrix of Eq. (A.1) is denoted as $\mathbf{K}_h$. The mathematical analysis of the formulation resulting in Eq. (A.1) consists of a study of the solvability and the stability of the equations (i.e. the structure of $\mathbf{K}_h$); where the stability of the equations implies their solvability [35].

From the discretized formulation, we have,

$$\delta\widehat{\mathbf{U}}_h^T (\mathbf{K}_{up})_h \widehat{\mathbf{P}}_h = \int_V p \nabla \cdot \mathbf{v}_h dV \tag{A.2}$$

where $\mathbf{v}_h$ can be any arbitrary admissible displacements and $\delta\widehat{\mathbf{U}}_h$ contains n independent admissible vectors.

Assuming that $(\mathbf{K}_{uu})_h$ is a positive definite matrix (i.e. the ellipticity condition

is satisfied), if we have,

$$\int_V p_o \nabla \cdot \mathbf{v}_h dV = p_o \int_S \mathbf{v}_h \cdot \mathbf{n} dS = 0 \qquad \forall \mathbf{v}_h \in V_h \tag{A.3}$$

where p_o is a constant pressure, and $(\mathbf{K}_{pp})_h = \mathbf{0}$ (incompressible case); we can add an arbitrary constant pressure p_o to any proposed solution of Eq. (A.1) [35].

In fact, Eq. (A.3) is equivalent to the following condition,

$$\sum_{j=1}^{m} (K_{up})_h^{ij} = 0 \qquad i = 1, ..., n \tag{A.4}$$

where $(K_{up})_h^{ij}$ is the ij'th element of $(\mathbf{K}_{up})_h$. Therefore, for the incompressible case, Eq. (A.3) implies that the rank of $\mathbf{K}_h$ is at most $n+m-1$, and the mode corresponding to the zero eigenvalue contains the constant pressure mode $\widehat{\mathbf{P}}_h^T = p_o(1, 1, ..., 1)$.

For almost incompressible fluid models discussed in this thesis, we will have the following stiffness matrix for the **u**/p formulation (refer to Chapter 3),

$$\mathbf{K}_h = \begin{bmatrix} \mathbf{0} & \mathbf{L}_h \\ \mathbf{L}_h^T & \mathbf{A}_h \end{bmatrix} \tag{A.5}$$

where the artificial shear modulus G is taken as zero in the limit case. Since we are using the Galerkin formulation, for almost incompressible fluids, $\mathbf{A}_h$ is a negative definite matrix. Therefore, we have

$$\mathbf{K}_h^* = -\mathbf{L}_h \mathbf{A}_h^{-1} \mathbf{L}_h^T \tag{A.6}$$

If Eq. (A.3) holds, from Eq. (A.4), it is clear that the rank of $\mathbf{L}_h$ is at most $m - 1$. From the discussion in Chapter 3, we conclude that the rank of $\mathbf{K}_h^*$ is also at most $m - 1$. In actuality, to have a non-zero pressure p_o, Eq. (A.3) requires that the *discretized* boundary tangential directions satisfy Eqs. (5.19) and (5.22) (refer to Chapter 5). That is the fundamental reason why spurious modes can be produced

when Eqs. (5.19) and (5.22) are violated for inviscid acoustic fluids.

In the proposed **u**-p-$\mathbf{\Lambda}$ formulation, we have,

$$\mathbf{K}_h = \begin{bmatrix} \mathbf{0} & \mathbf{L}_h & \mathbf{Q}_h \\ \mathbf{L}_h^T & \mathbf{A}_h & \mathbf{0} \\ \mathbf{Q}_h^T & \mathbf{0} & \mathbf{G}_h \end{bmatrix} \tag{A.7}$$

for which the comparable analysis holds. The corresponding mode contains the constant pressure $\widehat{\mathbf{P}}_h^T = p_o(1, 1, ..., 1)$ along with the zero vorticity moment mode $\widehat{\mathbf{\Lambda}}_h^T = (0, 0, ..., 0)$

References

[1] O.C. Zienkiewicz and P. Bettess. Fluid-structure dynamics interaction and wave forces. An introduction to numerical treatment. *International Journal for Numerical Methods in Engineering*, 13:1–16, 1978.

[2] L.G. Olson. *Finite element analysis of fluid-structure interactions.* PhD thesis, Massachusetts Institute of Technology, 77 Massachusetts Avenue, Cambridge, MA 02139, June 1985.

[3] T. Belytschko. Fluid-structure interaction. *Computers & Structures*, 12:459–469, 1980.

[4] L.D. Flippen, Jr. An overview of the common fluid models used in fluid-structure interactions. *Naval Research Laboratory Memorandum Report*, 6841, 1991.

[5] M.K. Hakala. Application of the finite element method to fluid-structure interaction in ship vibration. *Technical Research Center of Finland, Research Report*, 433, 1986.

[6] C.A. Felippa and R. Ohayon. Mixed variational formulation of finite element analysis of acoustoelastic/slosh fluid-structure interaction. *Journal of Fluids and Structures*, 4:35–57, 1990.

[7] K.J. Bathe and W.F. Hahn. On transient analysis of fluid-structure systems. *Computers & Structures*, 10:383–391, 1979.

[8] N. Akkas, H.U. Akay, and C. Yilmaz. Applicability of general-purpose finite element programs in solid-fluid interaction problems. *Computers & Structures*, 10:773–783, 1979.

[9] M.A. Hamdi, Y. Ousset, and G. Verchery. A displacement method for the analysis of vibrations of coupled fluid-structure systems. *International Journal for Numerical Methods in Engineering*, 13:139–150, 1978.

[10] T.B. Belytschko and J.M. Kennedy. A fluid-structure finite element method for the analysis of reactor safety problems. *Nuclear Engineering and Design*, 38:71–81, 1976.

[11] L.G. Olson and K.J. Bathe. A study of displacement-based fluid finite elements for calculating frequencies of fluid and fluid-structure systems. *Nuclear Engineering and Design*, 76:137–151, 1983.

[12] H. Morand and R. Ohayon. Substructure variational analysis of the vibrations of coupled fluid-structure systems. Finite element results. *International Journal for Numerical Methods in Engineering*, 14:741–755, 1979.

[13] G.C. Everstine. A symmetric potential formulation for fluid-structure interaction. *Journal of Sound and Vibration*, 79(1):157–160, 1981.

[14] L.G. Olson and K.J. Bathe. Analysis of fluid-structure interactions. A direct symmetric coupled formulation based on the fluid velocity potential. *Computers & Structures*, 21(1/2):21–32, 1985.

[15] L. Kiefling and G.C. Feng. Fluid-structure finite element vibrational analysis. *AIAA Journal*, 14(2):199–203, 1976.

[16] H.C. Chen and R.L. Taylor. Vibration analysis of fluid-solid systems using a finite element displacement formulation. *International Journal for Numerical Methods in Engineering*, 29:683–698, 1990.

[17] A. Huerta and W.K. Liu. Viscous flow with large free surface motion. *Computer Methods in Applied Mechanics and Engineering*, 69:277–324, 1988.

[18] T. Nomura and T.J.R. Hughes. An arbitrary Lagrangian-Eulerian finite element method for interaction of fluid and a rigid body. *Computer Methods in Applied Mechanics and Engineering*, 95:115–138, 1992.

[19] P.A.B.de Sampaio, P.R.M. Lyra, K. Morgan, and N.P. Weatherill. Petrov-Galerkin solutions of the incompressible Navier-Stokes equations in primitive variables with adaptive remeshing. *Computer Methods in Applied Mechanics and Engineering*, 106:143–178, 1993.

[20] T.J.R. Hughes, L.P. Franca, and M. Balestra. A new finite element formulation for computational fluid dynamics: V. Circumventing the Babuška-Brezzi condition: A stable Petrov-Galerkin formulation of the Stokes problem accommodating equal-order interpolations. *Computer Methods in Applied Mechanics and Engineering*, 59:85–99, 1986.

[21] I. Babuška. The finite element method with lagrangian multipliers. *Numer. Math.*, 20:179–192, 1973.

[22] F. Brezzi. On the existence, uniqueness, and approximation of saddle point problems arising from lagrangian multipliers. *RAIRO, Anal. Numer.*, 2:129–151, 1974.

[23] D. Pelletier, A. Fortin, and R. Camarero. Are FEM solutions of incompressible flows really incompressible? (or How simple flows can cause headaches!). *International Journal for Numerical Methods in Fluids*, 9:99–112, 1989.

[24] D.S. Malkus. Eigenproblems associated with the discrete LBB condition for incompressible finite elements. *Int. J. Engng Sci.*, 19:1299–1310, 1981.

[25] F. Brezzi and M. Fortin. *Mixed and Hybrid Finite Element Methods.* Springer-Verlag, 1991.

[26] T.J.R. Hughes, W.K. Liu, and T.K. Zimmermann. Lagrangian-Eulerian finite element formulation for incompressible viscous flows. *Computer Methods in Applied Mechanics and Engineering*, 29:329–349, 1981.

[27] B.P. Leonard and S. Mokhtari. Beyond first-order upwinding: The ultra-sharp alternative for non-oscillatory steady-state simulation of convection. *International Journal for Numerical Methods in Engineering*, 30:729–766, 1990.

[28] T.J.R. Hughes and A. Brooks. A theoretical framework for Petrov-Galerkin methods with discontinuous weighting functions: Application to the streamline-upwind procedure. *Finite Elements in Fluids*, 4:47–65, 1982.

[29] D. Hendriana. *On finite element and control volume upwinding methods for high Peclet number flows.* MS thesis, Massachusetts Institute of Technology, 77 Massachusetts Avenue, Cambridge, MA 02139, May 1994.

[30] E.L. Wilson and M. Khalvati. Finite elements for the dynamic analysis of fluid-solid systems. *International Journal for Numerical Methods in Engineering*, 19:1657–1668, 1983.

[31] G.E. Schneider and M.J. Raw. A skewed, positive influence coefficient upwinding procedure for control-volume-based finite-element convection-diffusion computation. *Numerical Heat Transfer*, 9:1–26, 1986.

[32] Y.C. Fung. *Foundations of Solid Mechanics.* Prentice Hall, Englewood Cliffs, N.J., 1965.

[33] K.J. Bathe, E. Ramm, and E.L. Wilson. Finite element formulations for large deformation dynamic analysis. *International Journal for Numerical Methods in Engineering*, 9:353–386, 1975.

[34] T. Sussman and K.J. Bathe. A finite element formulation for nonlinear incompressible elastic and inelastic analysis. *Computers & Structures*, 26(1/2):357–409, 1987.

[35] K.J. Bathe. *Finite Element Procedures.* Prentice Hall, Englewood Cliffs, N.J., 1995.

[36] O.C. Zienkiewicz and R.E. Newton. Coupled vibrations of a structure submerged in a compressible fluid. *Proc. Symp. Finite Element Techniques*, pages 359–379, 1969. University of Stuttgart, Germany.

[37] B.M. Irons. Role of part inversion in fluid-structure problems with mixed variables. *AIAA Journal*, 8(3):568, 1970.

[38] A.J. Chorin. A numerical method for solving incompressible viscous flow problems. *Journal of Computational Physics*, 2:12–26, 1967.

[39] J. Sundqvist. An application of ADINA to the solution of fluid-structure interaction problems. *Computers & Structures*, 17(5–6):793–807, 1983.

[40] W.K. Liu and R.A. Uras. Variational approach to fluid-structure interaction with sloshing. *Nuclear Engineering and Design*, 106:69–85, 1988.

[41] P.G. Ciarlet. *The Finite Element Method for Elliptic Problems.* North Holland, Amsterdam, 1978.

[42] D. Chapelle and K.J. Bathe. The inf-sup test. *Computers & Structures*, 47(4/5):537–545, 1993.

[43] D. Pantuso and K.J. Bathe. A four-node quadrilateral mixed-interpolated element for solids and fluids. *Mathematical Models & Methods in Applied Sciences*, 1995. To appear.

[44] P. Le Tallec and V. Ruas. On the convergence of the bilinear-velocity constant pressure finite element method in viscous flow. *Computer Methods in Applied Mechanics and Engineering*, 54:235–243, 1986.

[45] N. Jacobson. *Basic Algebra I.* W.H. Freeman and Company, New York, 1985.

[46] C. Nitikitpaiboon. *Finite element formulations for fluid-structure interaction.* PhD thesis, Massachusetts Institute of Technology, 77 Massachusetts Avenue, Cambridge, MA 02139, February 1993.

[47] K.J. Bathe and V. Sonnad. On effective implicit time integration in analysis of fluid-structure problems. *International Journal for Numerical Methods in Engineering*, 15(6):943–948, 1980.

[48] C.R. Swaminathan, V.R.Voller, and S.V.Patankar. A streamline upwind control volume finite element method for modeling fluid flow and heat transfer problems. *Finite Elements in Analysis and Design*, 13:169–184, 1993.

[49] C.R. Swaminathan and V.R.Voller. Streamline upwind scheme for control-volume finite elements, Part I. Formulations. *Numerical Heat Transfer, Part B*, 22:95–107, 1992.

[50] C.R. Swaminathan and V.R.Voller. Streamline upwind scheme for control-volume finite elements, Part II. Implementation and comparison with the SUPG finite-element scheme. *Numerical Heat Transfer, Part B*, 22:109–124, 1992.

[51] T.J.R. Hughes, W.K. Liu, and A. Brooks. Finite element analysis of incompressible viscous flows by the penalty function formulation. *Journal of Computational Physics*, 30:1–60, 1979.

[52] A.N. Brooks and T.J.R. Hughes. Streamline upwind/Petrov-Galerkin formulations for convection dominated flows with particular emphasis on the incompressible Navier-Stokes equations. *Computer Methods in Applied Mechanics and Engineering*, 32:199–259, 1982.

[53] N.S. Lee. *Adaptive Procedures for Nonlinear Elastic and Elasto-Plastic Finite Element Analysis.* PhD thesis, Massachusetts Institute of Technology, 77 Massachusetts Avenue, Cambridge, MA 02139, May 1993.

[54] K.J. Bathe, J. Walczak, and H. Zhang. Some recent advances for practical finite element analysis. *Computers & Structures*, 47(4/5):511–521, 1993.

[55] K.J. Bathe, H. Zhang, and M.H. Wang. Finite element analysis of incompressible and compressible fluid flows with free surfaces and structural interactions. *Computers & Structures*, 56, 1995.

[56] J. Donea, S. Giuliani, and J.P. Halleux. An arbitrary Lagrangian-Eulerian finite element method for transient dynamic fluid-structure interactions. *Computer Methods in Applied Mechanics and Engineering*, 33:689–723, 1982.

[57] T. Hino, L. Martinelli, and A. Jameson. A finite-volume method with unstructured grid for free surface flow simulations. In V.C. Patel and F. Stern, editors, *Sixth International Conference on Numerical Ship Hydrodynamics*, pages (4)18–37, 1994.

[58] W.C. Müller. Simplified analysis of linear fluid-structure interaction. *International Journal for Numerical Methods in Engineering*, 17:113–121, 1981.

[59] M.S. Marcus. A finite-element method applied to the vibration of submerged plates. *Journal of Ship Research*, 22(2):94–99, 1978.

[60] G. Muthuveerappan, N. Ganesan, and M.A. Veluswami. Vibration of square cantilever plate immersed in water. *Journal of Sound and Vibration*, 61(3):467–470, 1978.

[61] P. Kaleff. A hydroelastic approach to ship vibration problems. *Journal of Ship Research*, 27(2):103–112, 1983.

[62] S.M. Soedel and W. Soedel. On the free and forced vibration of a plate supporting a freely sloshing surface liquid. *Journal of Sound and Vibration*, 171(2):159–171, 1994.

[63] M. Kawahara and T. Miwa. Finite element analysis of wave motion. *International Journal for Numerical Methods in Engineering*, 20:1193–1210, 1984.

[64] B. Ramaswamy and M. Kawahara. Arbitrary Lagrangian-Eulerian finite element method for unsteady, convective, incompressible viscous free surface fluid flow. *International Journal for Numerical Methods in Fluids*, 7:1053–1075, 1987.

[65] B. Ramaswamy, M. Kawahara, and T. Nakayama. Lagrangian finite element method for the analysis of two-dimensional sloshing problems. *International Journal for Numerical Methods in Fluids*, 6:659–670, 1986.

[66] L.C. Wellford, Jr. and T.H. Ganaba. A finite element method with a hybrid Lagrange line for fluid mechanics problems involving large free surface motion. *International Journal for Numerical Methods in Engineering*, 17:1201–1231, 1981.

[67] E. Kock and L. Olson. Fluid-structure interaction analysis by the finite element method - A variational approach. *International Journal for Numerical Methods in Engineering*, 31:463–491, 1991.

[68] L. Meirovitch. *Methods of Analytical Dynamics*. McGraw-Hill, 1979.